

User-Level Reliability and Quality Monitoring in Satellite-Based Personal Navigation

Heidi Kuusniemi
Institute of Digital and Computer Systems
Tampere University of Technology
Finland

11th June 2005

ABSTRACT

High sensitivity receiver technology is necessary to ensure sufficient observation availability of satellite navigation in degraded signal environments. However, high sensitivity processing in the deteriorated line-of-sight conditions is susceptible to bringing about severely erroneous navigation observations. Therefore, when using a satellite navigation system, such as the Global Positioning System (GPS) or the future European Galileo in poor signal conditions, monitoring the reliability and the quality of the obtained user navigation solution is of great importance.

This thesis assesses reliability testing and quality control procedures at the user-level in Global Navigation Satellite Systems (GNSS) with the aim of enhancing accuracy and reliability in poor signal conditions with failure detection and exclusion techniques. Reliability testing, namely receiver autonomous integrity monitoring (RAIM) and fault detection and exclusion (FDE), traditionally rely on statistical tests in order to isolate one erroneous measurement from position estimation. In this thesis, a slightly wider point of view is taken to the quality monitoring problem of both user position and velocity, and observation weighting, navigation geometry and accuracy estimation aspects, and statistical reliability theory with applications to personal satellite navigation are assessed. The principal focus of this thesis includes developing and analyzing different FDE schemes based on recursive statistical testing intended for challenging signal environments. The operating environment for the monitoring functions is therefore different from traditional safety-critical navigation, where the usual problem is the failure of only one satellite, and where the error is not necessarily due to obstructions in the propagation path as is the case in urban areas.

The results of applying the developed FDE and quality control methods to high-sensitivity GPS data from indoor and urban tests and simulated GPS/Galileo data demonstrate that reliability and quality monitoring yield a significant improvement in accuracy and are essential in enhancing the user navigation solution reliability.

PREFACE

This research work has been carried out during the years 2002-2005 at the Institute of Digital and Computer Systems at Tampere University of Technology, Tampere, Finland, as a part of a project in Advanced Techniques for Mobile Positioning. The doctoral research included also a valuable ten-month research visit to the Department of Geomatics Engineering, University of Calgary, Canada.

First, I would like to express my deep appreciation to my supervisors Prof. Jarmo Takala and Prof. Gérard Lachapelle for their guidance and for providing excellent research opportunities during my doctoral studies. Prof. Ruizhi Chen and Prof. Bernhard Hofmann-Wellenhof are acknowledged for reviewing the manuscript.

Then, I would like to thank my colleagues with whom I had the pleasure of working with both at Tampere University of Technology and University of Calgary: Jussi Collin, Helena Leppäkoski, Hanna Sairo, Diep Dao, Oleg Mezentsev, Andreas Wieser, Glenn MacGougan, Mark Petovello, and all the rest of the students and staff of the PLAN group in Calgary and of DCS in Tampere. Without the great working atmospheres rich of research ideas my journey towards the doctoral thesis would have been much more difficult. I would also like to thank Dr. Jari Syrjärinne for initially bringing the great research ideas about personal positioning and RAIM to my attention.

This dissertation work has financially been supported by the Graduate School in Electronics, Telecommunications, and Automation (GETA), the National Technology Agency (TEKES), the Nokia Foundation, the Jenny and Antti Wihuri Foundation, the Foundation for Advancement of Technology (TES), and the Tuula and Yrjö Neuvo Foundation, which are all gratefully acknowledged.

Finally, I would like to express my gratitude to my parents Pirjo and Kjell Sandström, all of my dear friends, and my dear husband Tuomas for their encouragement, love, and support during these years of studying towards the doctorate.

TABLE OF CONTENTS

<i>Abstract</i>	i
<i>Preface</i>	iii
<i>Table of Contents</i>	v
<i>List of Publications</i>	ix
<i>List of Figures</i>	xi
<i>List of Tables</i>	xix
<i>Abbreviations</i>	xxi
<i>Symbols</i>	xxvii
<i>1. Introduction</i>	1
1.1 Motivation - Satellite-Based Personal Navigation and Reliability	1
1.2 Research Objectives	4
1.3 Main Contributions	5
1.4 Author's Contribution	7
1.5 Thesis Outline	7
<i>2. Global Navigation Satellite Systems</i>	9
2.1 Overview of GPS	9
2.1.1 System	9
2.1.2 Satellite Signal Structure	11
2.1.3 Receiver Operation	13
2.1.4 GPS Modernization	16

2.1.5	High Sensitivity GPS	20
2.2	Overview of Future Galileo	23
2.2.1	System	24
2.2.2	Services	25
2.2.3	Signal Structure	26
2.3	Overview of GLONASS	28
2.4	Satellite Augmentation Systems	29
2.4.1	Local Area Ground-Based Augmentation Systems	30
2.4.2	Wide Area Satellite-Based Augmentation Systems	30
2.5	Assisting Personal Satellite Navigation	32
2.5.1	Cellular Networks	32
2.5.2	Self-Contained Inertial Sensors	33
3.	<i>Navigation Observables and Error Sources</i>	35
3.1	Observables	35
3.1.1	Code Pseudorange Measurement	35
3.1.2	Carrier Phase Measurement	36
3.1.3	Doppler Measurement	37
3.2	Error Sources	38
3.2.1	Satellite-Based Range Errors	39
3.2.2	Signal Propagation Errors	41
3.2.3	Receiver-Based Range Errors	48
3.3	Signal Strength and Interference	49
3.4	User Error Budgets	50
3.5	Real-Life Estimated Pseudorange and Pseudorange Rate Errors	51
3.5.1	Good Signal Conditions	51

3.5.2	Lightly Degraded Signal Conditions	54
3.5.3	Heavily Degraded Signal Conditions	55
4.	<i>GNSS Navigation Solution Estimation</i>	59
4.1	User Position, Velocity, and Time Solution	59
4.2	Least Squares Navigation Solution	62
4.3	Kalman Filtering in Navigation	65
4.4	Robust Estimation Techniques in Navigation	65
4.5	Geometrical Aspects	66
4.6	Accuracy Estimation	68
5.	<i>Reliability Theory</i>	71
5.1	Reliability Testing	73
5.1.1	Global Test	75
5.1.2	Local Test	76
5.2	Statistical Reliability	78
5.2.1	Internal Reliability	79
5.2.2	External Reliability	79
6.	<i>Fault Detection and Exclusion</i>	81
6.1	Traditional RAIM for Safety Critical Applications	82
6.1.1	Screening Out Poor Geometries	83
6.1.2	Least-Squares-Residuals RAIM Method	84
6.1.3	Parity RAIM Method	84
6.1.4	Range Comparison RAIM Method	85
6.1.5	Maximum Residual RAIM Algorithm	86
6.2	Developed FDE for Personal Satellite Navigation Applications	87
6.2.1	Observation Subset Testing	87

6.2.2	Forward-Backward FDE	88
6.2.3	Iterative Reweighted Estimation - The Danish Method	89
6.3	Quality Control	92
6.4	Observation Weighting Based on Carrier-to-Noise Ratio	94
6.4.1	Variance Models for Lightly Degraded Signal Environments	94
6.4.2	Variance Models for Heavily Degraded Signal Environments	100
7.	<i>Results - Testing and Analysis</i>	107
7.1	Real-Life High-Sensitivity GPS Tests and Reliability Analysis	107
7.1.1	Static HSGPS Tests	107
7.1.2	Kinematic HSGPS Tests	131
7.2	Integrated GPS/Galileo Simulation and Reliability Analysis	148
7.2.1	Degraded Signal-Environment Simulation	149
8.	<i>Conclusions</i>	163
8.1	Main Results	165
8.2	Future Development	166

LIST OF PUBLICATIONS

This thesis is a monograph, but some ideas presented in the thesis have already been published in international journals and conferences or are submitted and currently subject to review. The following published articles form the basis of the research topics discussed in the thesis:

- [P1] H. Kuusniemi, G. Lachapelle, and J. Takala. Position and Velocity Reliability Testing in Degraded GPS Signal Environments. *GPS Solutions*, 8(4): 226 – 237, Dec. 2004.
- [P2] G. Lachapelle, H. Kuusniemi, D.T.H Dao, G. MacGougan, and M.E. Cannon. HSGPS Signal Analysis and Performance Under Various Indoor Conditions. *Navigation, Journal of the Institute of Navigation*, 51(1): 29 – 43, Spring 2004.
- [P3] H. Kuusniemi, G. Lachapelle, and J. Takala. Reliability in Personal Positioning. In *Proc. European Navigation Conference 2004*, 14 pages, Rotterdam, The Netherlands, May 16-19 2004.
- [P4] O. Mezentsev, J. Collin, H. Kuusniemi, and G. Lachapelle. Accuracy Assessment of a High Sensitivity GPS Based Pedestrian Navigation System Aided by Low-Cost Sensors. In *Proc. 11th Saint Petersburg International Conference on Integrated Navigation Systems*, pages 156 – 164, Saint Petersburg, Russia, May 24-26 2004.
- [P5] H. Kuusniemi and G. Lachapelle. GNSS Signal Reliability Testing in Urban and Indoor Environments. In *Proc. ION NTM 2004*, pages 210 – 224, San Diego, CA, Jan. 26-28 2004.
- [P6] J. Collin, H. Kuusniemi, O. Mezentsev, G. MacGougan, and G. Lachapelle. HSGPS under Heavy Signal Masking - Accuracy and Availability Ana-

lysis. In *Proc. 6th Nordic Radio Navigation Conference and Exhibition*, 11 pages, Stockholm-Helsinki, Sweden-Finland, Dec. 2-4 2003.

- [P7] H. Sairo, H. Kuusniemi, and J. Takala. Combined Performance of FDI and KDOP Analysis for User-Level Integrity Monitoring in Personal Satellite Navigation. In *Proc. IAIN World Congress 2003*, 14 pages, Berlin, Germany, Oct. 21-24 2003.

LIST OF FIGURES

1	GPS Receiver - Block Diagram.	15
2	Modernized GPS Signal Evolution	18
3	Allocation of GPS, Galileo, and GLONASS Frequency Bands.	29
4	Ephemeris Error Components.	40
5	Modes of Degradation in Urban Environments: Attenuation and Multipath Propagation.	46
6	Pseudorange Multipath Formulation.	47
7	Outdoor Roof: Multistorey Building.	52
8	Outdoor Roof: Pseudorange and Pseudorange Rate Errors vs. Carrier-to-Noise Ratios.	52
9	Outdoor Roof: Histograms of Pseudorange and Pseudorange Rate Errors.	53
10	Outdoor Roof: Empirical Cumulative Distribution Functions of Absolute Pseudorange and Pseudorange Rate Errors.	53
11	Indoor: Residential Garage.	54
12	Indoor: Pseudorange and Pseudorange Rate Errors vs. Carrier-to-Noise Ratios.	55
13	Indoor: Histograms of Pseudorange and Pseudorange Rate Errors.	55
14	Indoor: Empirical Cumulative Distribution Functions of Pseudorange and Pseudorange Rate Errors.	56
15	Urban Canyon: Parking Lot.	56

16	Urban Canyon: Pseudorange and Pseudorange Rate Errors vs. Carrier-to-Noise Ratios.	57
17	Urban Canyon: Histograms of Pseudorange and Pseudorange Rate Errors.	57
18	Urban Canyon: Empirical Cumulative Distribution Functions of Pseudorange and Pseudorange Rate Errors.	58
19	Relative Geometry and Dilution of Precision.	67
20	Type I Error α and Type II Error β in an One-Tailed Test.	74
21	Central and Non-Central χ^2 Density Functions in Global Testing	76
22	Density Functions of the Unbiased and Biased Normal Distributions in the Local Test.	77
23	FDE by Observation Subset Testing.	88
24	Forward-Backward FDE Procedure.	90
25	FDE by the Danish Method.	92
26	Quality Control of a Navigation Solution.	93
27	Lightly Degraded Signal Environment: Pseudorange Error.	95
28	Lightly Degraded Signal Environment: Absolute Pseudorange Error and the Standard Deviation.	96
29	Lightly Degraded Signal Environment: Normal Probability Plots of Pseudorange Misclosure Data	97
30	Lightly Degraded Signal Environment: Pseudorange Rate Error.	98
31	Lightly Degraded Signal Environment: Absolute Pseudorange Rate Error and the Standard Deviation.	99
32	Lightly Degraded Signal Environment: Normal Probability Plots of Pseudorange Rate Misclosure Data.	100
33	Heavily Degraded Signal Environment: Pseudorange Error.	101
34	Heavily Degraded Signal Environment: Absolute Pseudorange Error and the Standard Deviation.	102

35	Heavily Degraded Signal Environment: Normal Probability Plots of Pseudorange Misclosure Data.	103
36	Heavily Degraded Signal Environment: Pseudorange Rate Error. . .	104
37	Heavily Degraded Signal Environment: Absolute Pseudorange Rate Error and the Standard Deviation.	105
38	Heavily Degraded Signal Environment: Normal Probability Plots of Pseudorange Rate Misclosure Data.	105
39	Residential Garage as the Setting of the Static Indoor HSGPS Test. .	108
40	Garage: Number of Available Satellites.	109
41	Garage: Horizontal Position Errors with Unweighted and Weighted Least Squares.	110
42	Garage: Horizontal Speed Errors with Unweighted and Weighted Least Squares.	110
43	Garage: Horizontal Position Errors when Three Different Fault Detection and Exclusion Methods Applied.	111
44	Garage: Horizontal Speed Errors when Three Different Fault Detection and Exclusion Methods Applied.	112
45	Garage: Empirical Distribution Functions of Horizontal Position Errors.	113
46	Garage: Number of Exclusions of Pseudorange Observations.	114
47	Garage: Empirical Distribution Functions of Horizontal Speed Errors.	115
48	Garage: Number of Exclusions of Pseudorange Rate Observations. .	115
49	Garage: HPE Values.	116
50	Garage: Empirical Distribution of HPE.	117
51	Garage: Empirical Distribution of the Ratio Between Horizontal Position Error and HPE.	117
52	Garage: Horizontal Position Errors and DRMS Error Estimates when Three Different Fault Detection and Exclusion Methods Applied. . .	119

53	Garage: Empirical Distribution of the Ratio Between Horizontal Position Error and DRMS Error Estimate.	119
54	Urban Environment Parking Lot as the Setting of the Static Outdoor HSGPS Test.	120
55	Parking Lot: Number of Available Satellites.	121
56	Parking Lot: Horizontal Position Errors with Unweighted and Weighted Least Squares.	122
57	Parking Lot: Horizontal Speed Errors with Unweighted and Weighted Least Squares.	123
58	Parking Lot: Horizontal Position Errors when Three Different Fault Detection and Exclusion Methods Applied.	124
59	Parking Lot: Horizontal Speed Errors when Three Different Fault Detection and Exclusion Methods Applied.	125
60	Parking Lot: Empirical Distribution Functions of Horizontal Position Errors.	125
61	Parking Lot: Number of Exclusions of Pseudorange Observations.	126
62	Parking Lot: Empirical Distribution Functions of Horizontal Speed Errors.	127
63	Parking Lot: Number of Exclusions of Pseudorange Rate Observations.	127
64	Parking Lot: HPE Values.	128
65	Parking Lot: Empirical Distribution of HPE.	129
66	Parking Lot: Empirical Distribution of the Ratio Between 2D Position Error and HPE.	129
67	Parking Lot: Horizontal Position Errors and DRMS Error Estimates when Three Different Fault Detection and Exclusion Methods Applied.	130
68	Parking Lot: Empirical Distribution of the Ratio Between Horizontal Position Error and DRMS Error Estimate.	131
69	Trajectories of the Urban Environment Kinematic HSGPS Tests.	132

70	Surroundings of the Pedestrian HSGPS Experiment.	132
71	Surroundings of the Vehicular HSGPS Experiment.	133
72	Pedestrian Test: Available Satellites and Their C/N_0 Values.	134
73	Pedestrian Test: Horizontal Position with Unweighted and Weighted Least Squares.	135
74	Pedestrian Test: Horizontal Speed with Unweighted and Weighted Least Squares.	135
75	Pedestrian Test: Horizontal Position when Three Different Fault Detection and Exclusion Methods Applied.	136
76	Pedestrian Test: Number of Exclusions of Pseudorange Observations.	137
77	Pedestrian Test: Horizontal Speed when Three Different Fault Detection and Exclusion Methods Applied.	138
78	Pedestrian Test: Number of Exclusions of Pseudorange Rate Observations.	139
79	Pedestrian Test: HPE Values.	139
80	Pedestrian Test: Empirical Distribution of HPE.	140
81	Pedestrian Test: DRMS Error Estimates when Three Different Fault Detection and Exclusion Methods Applied.	141
82	Vehicular Test: Available Satellites and Their C/N_0 Values.	142
83	Vehicular Test: Horizontal Position with Unweighted and Weighted Least Squares.	142
84	Vehicular Test: Horizontal Speed with Unweighted and Weighted Least Squares.	143
85	Vehicular Test: Horizontal Position when Three Different Fault Detection and Exclusion Methods Applied.	144
86	Vehicular Test: Number of Exclusions of Pseudorange Observations.	145
87	Vehicular Test: Horizontal Speed when Three Different Fault Detection and Exclusion Methods Applied.	146

88	Vehicular Test: Number of Exclusions of Pseudorange Rate Observations.	146
89	Vehicular Test: HPE Values.	147
90	Vehicular Test: Empirical Distribution of HPE.	147
91	Vehicular Test: DRMS Error Estimates when Three Different Fault Detection and Exclusion Methods Applied.	148
92	Simulation: Simulated GPS/Galileo Constellation.	150
93	Simulation: Available Satellites.	151
94	Simulation: Simulated Pseudorange Errors vs. Elevations.	152
95	Simulation: Histogram of Simulated Pseudorange Errors.	152
96	Simulation: Empirical Cumulative Distribution Function of Simulated Pseudorange Errors.	153
97	Simulation: Number of Outlying Pseudorange Observation Errors.	153
98	Simulation: Horizontal Position with Unweighted Least Squares.	154
99	Simulation: Horizontal Position with Forward-Backward FDE and the Danish Method.	155
100	Simulation: Empirical Distribution Functions of the Horizontal Position Errors with Least Squares Estimation, Forward-Backward FDE, and the Danish Method.	156
101	Simulation: Exclusions Performed with Forward-Backward FDE and the Danish Method.	157
102	Simulation: Number of Outlying Measurements Minus the Exclusions Performed.	158
103	Simulation: HPE Values.	158
104	Simulation: Empirical Distribution of HPE.	159
105	Simulation: Empirical Distribution of the Ratio Between 2D Position Error and HPE.	159

106	Simulation: Horizontal Position Errors and DRMS Error Estimate when Two Different Fault Detection and Exclusion Methods Applied.	160
107	Simulation: Empirical Distribution of the Ratio Between Horizontal Position Error of the Forward-Backward FDE and DRMS Error Estimate.	161

LIST OF TABLES

1	GPS Signal Structures.	12
2	Expected Generations of Satellites in GPS Modernization.	19
3	GPS Signal Power Budget.	21
4	Statistical Testing of a Null Hypothesis against an Alternative Hypothesis.	74
5	Garage: Horizontal Position Errors and Availability Summarized.	111
6	Garage: Horizontal Speed Errors and Availability Summarized.	111
7	Parking Lot: Horizontal Position Errors and Availability Summarized.	124
8	Parking Lot: Horizontal Speed Errors and Availability Summarized.	124
9	Pedestrian Test: Availability Summarized of Position Solutions.	136
10	Pedestrian Test: Availability Summarized of Speed Solutions.	138
11	Vehicular Test: Availability Summarized of Position Solutions.	144
12	Vehicular Test: Availability Summarized of Speed Solutions.	145
13	Simulation: Horizontal Position Errors and Availability Summarized.	154

ABBREVIATIONS

AGPS	Assisted Global Positioning System
Alt-BOC	Alternative Binary Offset Carrier
AOA	Angle Of Arrival
AS	Anti-Spoofing
AT	Along-Track
BLUE	Best Linear Unbiased Estimate
BOC	Binary Offset Carrier
bps	bits per second
BPSK	Binary Phase Shift Keying
CDF	Cumulative Distribution Function
CDMA	Code Division Multiple Access
CL	Civil Long
CM	Civil Moderate
CS	Commercial Service
C/A	Coarse/Acquisition
DCS	Digital and Computer Systems
DGPS	Differential Global Positioning System
DLL	Delay Lock Loop

DoD	Department of Defense
DOP	Dilution Of Precision
DRMS	Distance Root Mean Squared
DTV	Digital Television
EC	European Commission
ECEF	Earth Centered Earth Fixed
EGNOS	European Geostationary Navigation Overlay System
ENU	East North Up
ESA	European Space Agency
EU	European Union
E112	Enhanced 112 emergency call requirements
E911	Enhanced 911 emergency call mandate
E-OTD	Enhanced Observed Time Difference
FAA	Federal Aviation Administration
FCC	Federal Communications Commission
FDE	Fault Detection and Exclusion
FDI	Fault Detection and Isolation
FLL	Frequency Lock Loop
GAGAN	GPS And GEO Augmented Navigation
Galileo	European Satellite Navigation System
GBAS	Ground-Based Augmentation System
GDOP	Geometric Dilution Of Precision
GEO	Geostationary

GIC	Global Navigation Satellite System Integrity Channel
GLONASS	The Russian Positioning System, Global'naya Navigatsionnaya Sputnikkovaya Sistema
GNSS	Global Navigation Satellite System
GPS	Global Positioning System
GTRF	Galileo Terrestrial Reference Frame
HAL	Horizontal Alarm Limit
HDOP	Horizontal Dilution Of Precision
HOW	Handover word
HPE	Horizontal Positioning Error
HPL	Horizontal Protection Level
HSGPS	High Sensitivity GPS
IAT	International Atomic Time
IEEE	The Institute of Electrical and Electronics Engineers
IF	Intermediate Frequency
IMU	Inertial Measurement Unit
INS	Inertial Navigation System
JCAB	Japan Civil Aviation Bureau
LAAS	Local Area Augmentation System
LBS	Location-Based Services
LF	Location Fingerprinting
LMS	Least Mean Square
LOS	Line Of Sight

LS	Least Squares
M	Military
MDB	Marginally/Minimum Detectable Blunder
MEDLL	Multipath Estimation Delay Lock Loop
MEMS	Micro Electro Mechanical System
MRSE	Mean Radial Spherical Error
MSAS	Multifunctional Transportation Satellite Based Satellite Augmentation System
NAVSTAR	Navigation System by Timing And Ranging
NCO	Numerically Controlled Oscillator
OS	Open Service
PAC	Pulse Aperture Correlation
PDOP	Position Dilution of Precision
PDR	Pedestrian Dead Reckoning
PLAN	Position, Location, And Navigation
PLL	Phase Lock Loop
PPS	Precise Positioning Service
ppm	parts per million
PRN	Pseudorandom Noise
PRS	Public Regulated Service
PSAP	Public Safety Answering Point
PVT	Position, Velocity, and Time
PZ-90	Earth Parameter System 1990

P(Y)	Precision(Encrypted)
QPSK	Quadrature Phase Shift Keying
R	Radial
RAIM	Receiver Autonomous Integrity Monitoring
RF	Radio Frequency
R-GEO	GEO-ranging
RHCP	Right Hand Circular Polarization
rms	root mean square
RNP	Required Navigation Performance
SA	Selective Availability
SBAS	Satellite-Based Augmentation System
SNR	Signal-to-Noise Ratio
SoL	Safety-of-Life service
SPS	Standard Positioning Service
SS	Spread Spectrum
SSE	Sum of Squared Error
SU	Soviet Union
SV	Space Vehicle
TCAR	Three-CARrier
TDOP	Time Dilution Of Precision
TEC	Total Electron Content
TLM	Telemetry word
TOA	Time Of Arrival

TPE	Total Positioning Error
TTFF	Time To First Fix
USERE	User Equivalent Range Error
UHF	Ultra High Frequency
URE	User Range Error
US	United States
USNO	United States Naval Observatory
UTC	Coordinated Universal Time reference
VCM	Variance Covariance Matrix
VDOP	Vertical Dilution Of Precision
VHF	Very High Frequency
VSAT	Very Small Aperture Terminal
XOR	eXclusive-OR
WAAS	Wide Area Augmentation System
WAD	Wide Area Differential
WGS	World Geodetic System
WLAN	Wireless Local Area Network
WLS	Weighted Least Squares
XT	Cross-Track

SYMBOLS

α	probability of false alarm
β	probability of missed detection
δ	non-centrality parameter
ρ	pseudorange
$\dot{\rho}$	pseudorange rate
ϕ	carrier phase
$\dot{\phi}$	measured Doppler
σ	standard deviation
$\hat{\sigma}_0^2$	a posteriori variance factor
Σ	variance covariance matrix of the observations
ζ	zenith angle
φ	latitude
λ	longitude
χ^2	Chi-square distribution
C/N_0	Carrier-to-Noise Ratio
$E1$	Galileo Signal Carrier Frequency at 1591 MHz
$E2$	Galileo Signal Carrier Frequency at 1559 MHz
$E5a$	Galileo Signal Carrier Frequency at 1164 MHz

$E5b$	Galileo Signal Carrier Frequency at 1215 MHz
$E6$	Galileo Signal Carrier Frequency at 1260-1300 MHz
$E(\cdot)$	Expectation function
ε	vector of errors
f	frequency
\mathbf{H}	linear connection matrix, i.e., the design matrix
H_0	null hypothesis of no integrity failure
H_a	alternative hypothesis of an integrity failure
$L1$	GPS Signal Carrier Frequency at 1575.42 MHz
$L2$	GPS Signal Carrier Frequency at 1227.60 MHz
$L5$	GPS Signal Carrier Frequency at 1176.45 MHz
n	number of observations
p	number of parameters to be estimated
r_i	redundancy number of observation i
\mathbf{R}	redundancy matrix
$\hat{\mathbf{v}}$	vector of least squares residuals
$V(\cdot)$	Variance covariance function
w_i	standardized residual of observation i
\mathbf{x}	vector of unknown parameters
\mathbf{y}	vector of observations

1. INTRODUCTION

This chapter gives an introduction to the thesis. First, motivation to the subject is given and the research objectives are stated. Secondly, contributions of the thesis are discussed and, finally, the thesis outline is given.

1.1 Motivation - Satellite-Based Personal Navigation and Reliability

Global Navigation Satellite Systems (GNSS), i.e., the United States (US) Global Positioning System (GPS), the Russian GLONASS system, and the future European satellite navigation system Galileo, are designed to provide position, velocity, and timing capabilities to users all over the world. Currently, the only fully operational system is the GPS operated by the US Department of Defense. Traditionally, satellite navigation has been utilized in applications in environments with relatively good signal line-of-sight reception conditions. However, there is a growing need to use satellite navigation for a variety of navigation problems. Navigation capability is also required in degraded signal environments such as in urban canyons and indoors. This is due to the emergency call positioning demands, i.e., the E911 mandate set by the Federal Communications Commission (FCC) in the US and the E112 directive set by the European Commission (EC) in Europe, and, e.g., location-based services (LBS) becoming increasingly popular in personal and vehicular telematics applications. The extended utilization of navigation promotes the need for special high sensitivity receiver processing techniques and certain assistance support through, e.g., wireless networks, to enable the acquisition and tracking of satellite signals in the attenuated and obstructed signal-environments of urban and indoor areas. Currently, high sensitivity GPS (HSGPS) receiver technology is used to acquire and track weak GPS signals in degraded signal environments in order to provide enhanced navigation availability for applications such as personal cellular telephone location. However, higher measurement noise due to lower signal strength and high signal reflection oc-

currence, i.e., multipath, prevents high sensitivity GPS from achieving the same level of performance regarding reliability and accuracy under obstructed signal environments than in outdoors. This promotes the need for reliability analysis and quality monitoring to assess, detect, and isolate failure situations, and exclude the erroneous measurements in the obstructed line-of-sight conditions with receiver autonomous integrity monitoring (RAIM).

In literature, publications directly about failure detection and exclusion for personal applications in degraded signal environments do not readily exist. Most of the RAIM research has been targeted to high-precision applications within reasonably good signal line-of-sight conditions requiring high levels of integrity, e.g., (Pervan et al., 1998; Hatch et al., 2003; Walter and Enge, 1995; Powe and Owen, 1997; Special ION Publication on RAIM, 1998). The focus within RAIM research has mainly been on aircraft applications but there has been some research done within marine navigation, e.g., (Ryan, 2002; MacGougan and Liu, 2002), as well as within integrated GPS/Galileo and GPS/GLONASS navigation, e.g., (Zink et al., 2000; Kinkulkin, 1997).

Since location accuracy and reliability are generally very poor under the degraded signal conditions, methods to improve these characteristics are essential. The multiple simultaneously occurring faults are more likely in urban areas than in, e.g., an airplane landing situation, where still, in general, the biggest concern is the failure of a satellite instead of a blunder in the measurement due to problems in the propagation path. The error detection function in degraded line-of-sight conditions is, moreover, much different from what it was originally designed to be in, e.g., the aviation community; detecting and isolating a signal from one failed satellite. In urban areas, there is a need to analyze, detect, and exclude multiple faults in the navigation system caused by, e.g., multipath propagation, cross-correlation effects, or echo-only signal reception, and thus ensure a desired level of performance. This motivates the need for autonomous reliability and quality checking procedures at user level, i.e., RAIM procedures aiming at fault detection and exclusion (FDE).

By effective fault detection and exclusion, navigation accuracy and reliability can be enhanced even in difficult signal environments in order to ensure reliable user position and velocity solutions. An important part of the successful detection and isolation function is proper variance modeling of the navigation measurements. In situations with sufficient availability, the accuracy of the user solution can also be predicted from RAIM detection parameters, the test statistic, which provides infor-

mation to the user about the current accuracy. Having an estimate of the reliability of the solution has great advantages; even knowing the uncertainty of a user position is an essential information, which allows the use of certain positioning applications relying on the latest reliable user position estimate and the certainty information. As additional information, the user can also be informed about the possible effect of an undetected failure in the navigation solution and the external reliability boundary that the system can marginally be protected against when fault detection and exclusion is applied. However, in personal applications, the essential failure detection and isolation capability is, overall, occasionally quite limited, e.g., due to the absence of sufficient redundancy to perform the statistical testing of RAIM and FDE, especially in case of standalone GPS. Height constraining, map-aiding, and additional measurement sources, such as self-contained sensors or cellular network signals increase the availability of a navigation solution as well as the reliability assessment.

Traditionally, an interest to the position solution integrity and reliability has been only within safety-critical navigation applications such as in aviation, especially in approach and landing situations. In addition, only position integrity and reliability has been of concern. Strict requirements for false alarm rates, missed detection probabilities, time-to-alarms, and overall protection limits of the system set by, e.g., the Federal Aviation Administration (FAA) in the US, dictate the integrity monitoring schemes introduced in the literature (Parkinson and Spilker, 1996; Kaplan (Ed.), 1996; Special ION Publication on RAIM, 1998). However, for personal positioning applications, there are no integrity requirements set, except for, e.g., the few accuracy requirements of the E911 mandate.

The requirements set for cellular handset navigation in emergency call situations, i.e., the E911 (Enhanced 911) mandate set in the US (E911, 2004) and the E112 (Enhanced 112) directive set in Europe (E112, 2002), seek to improve the effectiveness and reliability of mobile phone 911/112 service by providing emergency call dispatchers with additional information on calls. Phase II of the E911, as an example, requires wireless carriers to provide location information within 50 to 100 meters in most cases basically over a four-year roll-out schedule, which begun in the beginning of October 2001 and is to be completed by December 31, 2005. The EC E112 directive provides the legal framework to grant access to location information by emergency service operators. Initial objectives include a positioning accuracy of a mobile phone caller within 10 to 100 m depending on the environment with the position to be

available within 30 seconds of call initiation (CGALIES, 2002). However, despite the fact that no integrity requirements are set for most personal positioning applications, e.g., in route finding or recreational positioning, autonomous failure detection and isolation on the user level is essential when enhancing the overall performance. In addition, in less safety-critical personal positioning applications than mobile phone emergency call positioning, the availability is more likely a more important performance parameter than accuracy and reliability in obstructed signal conditions. Even an erroneous solution can be better than no solution at all, especially if there is information available on the uncertainty of the solution. The dilemma of availability versus accuracy is, however, highly application dependent.

1.2 Research Objectives

The erroneous navigation situations frequently encountered in personal navigation applications in degraded signal environments need to be detected and corrected with appropriate reliability monitoring techniques. Though adding complexity to the computation of the user navigation solution estimation, reliability and quality monitoring enhances navigation accuracy, or when not available or successful in identifying the outliers, at least provides accuracy and reliability predictions. The challenges in designing reliability testing schemes in the absence of, e.g., time-to-alarm and protection level requirements existing in aviation, lie in making sure that the assumptions made for the statistical tests about the error distributions are sufficiently valid. This includes taking into account the possibly occurring multiple blunders that are rare in good line-of-sight situations and their larger magnitudes. It is also a challenge to choose the proper false alarm rates needed to set the statistical test threshold. In addition, minimizing the computational burden of the FDE schemes is important.

The main objectives of this research underlie essentially in the error assessment and failure detection and exclusion functions for personal navigation applications in degraded signal environments. Overall, the user-level reliability testing procedures have to first try to certify the detection capability, face multiple erroneous signals, and then isolate the erroneous measurements sequentially. Sometimes, reliability monitoring is simply unavailable due to insufficient redundancy. However, overall, with attenuated signals, the detection and isolation function is extremely essential to ensure reliable user position and velocity estimates, and not just settling with increased

availability. It is necessary to demand reliable in addition to available, also in weak signal conditions.

1.3 Main Contributions

In this thesis, navigation observation errors are discussed with given real-life experiments in good, lightly, and heavily degraded signal conditions. The errors presented provide information about the performance levels obtainable in poor signal conditions. Variance models are introduced and they are based on the carrier-to-noise density ratio of the satellite signal. The variance models tie the weak and, therefore, erroneous observations better to the system model and improve the navigation results.

The core of the thesis is formed of the three fault detection and exclusion schemes developed for personal satellite navigation applications: observation Subset Testing scheme, Forward-Backward FDE, and Danish estimation method. The observation Subset Testing scheme consists of analysis of all the possible navigation measurement subsets in order to exclude the erroneous observations. The Forward-Backward FDE scheme involves recursive global and local reliability testing in order to detect and isolate errors. The Danish estimation method iteratively modifies the weights of the navigation observations by assessing measurement residuals in order to de-weight the effect of erroneous observations. The introduced FDE methods are novel approaches for navigation applications in degraded signal environments, they enhance the accuracy and reliability, and have no major differences but contain each some desirable features. The Subset Testing provides the highest availability of a reliable flagged solution but it is computationally the most expensive. The Forward-Backward FDE provides a good balance between the increased accuracy and the availability obtained, yet being computationally slightly expensive. The Danish Method is computationally light and provides the best obtained accuracy but it provides clearly the lowest availability of a reliable solution. The results suggest that proper observation weighting and all the FDE approaches completed by quality control improve the navigation results significantly, with the amount of improvement depending on the environment and the quality and quantity of the navigation observations.

The main contributions of this thesis can be summarized as follows

- Presenting and analyzing range and range rate error levels obtained with a high sensitivity receiver in indoor and urban experiments.
- Introducing navigation range and range rate observation variance models for degraded signal conditions to enhance solution estimation and reliability assessment.
- Bringing the statistical reliability theory and traditional navigation RAIM approaches closer together, and discussing position as well as velocity reliability monitoring.
- Presenting a navigation observation 'Subset Testing' scheme based on assessing least squares measurement residuals with chi-square statistics.
- Presenting a novel recursive 'Forward-Backward FDE' procedure including statistical testing based on least squares measurement residuals as well as taking into account the influentiality of the observations being assessed.
- Introducing a novel iteratively reweighted estimation scheme in navigation, the 'Danish Method', as an estimation technique including inherently the exclusion function of erroneous measurements by down-weighting.
- Presenting a navigation solution quality control scheme including assessing the consistency of the obtained solution, redundancy numbers of the observations as well as solution geometry.
- Comparing the external reliability, i.e., the theoretical boundary of the error that the system can marginally be protected against, and accuracy estimates of the obtained solutions with the true error levels.
- Presenting extensive results of the developed FDE methods with real-life experiments and a GPS/Galileo simulation broadening the general impressions what levels of accuracy and reliability can be obtained in poor signal conditions.

Applying the developed methods enhance significantly navigation accuracy and availability. In this thesis, only snapshot reliability monitoring schemes are considered but extensions to filtering approaches including dynamic information are possible.

1.4 Author's Contribution

The Subset Testing procedure was introduced by the author to be used as a fault detection and exclusion scheme in navigation applications in degraded signal environments. The Subset Testing and its performance have been reported earlier in [P5]. The Forward-Backward FDE method including the feature of checking the influentiality of the observation under assessment prior to the exclusion decision was constructed by the author. The author also reported similar, yet not identical FDE schemes in [P1] and [P3]. The novel Danish estimation method was also introduced by the author to be used with the specific test parameter presented in this thesis in the de-weighting of deteriorated navigation observables. However, the idea of iterative re-weighting was originally proposed in (Jørgensen et al., 1985), and later on extended to high-precision navigation in (Wieser, 2001). The idea of the Danish estimation is also discussed in [P1] and [P3]. The author presented a simple quality control procedure for degraded signal areas taking into account the consistency, redundancy, and the geometry aspects of the obtained navigation solution, which are known to affect the navigation performance. Quality control aspects of failure isolation and geometry assessment are discussed in [P7]. The author introduced exponential variance models for lightly and heavily degraded signal conditions and analyzed their applicability with real-life experiments. While showing the significant improvement gained with the different FDE and reliability enhancement procedures, the author also showed real-life high sensitivity GPS performance capability. HSGPS performance analysis has been presented in [P2], [P4], and [P6].

1.5 Thesis Outline

In Chapter 2, the basic navigation principles, i.e., signals, measurements, and receiver principles, are presented. In addition, the basics of high sensitivity receiver principles are discussed. Plans and current status of the European Galileo project are summarized together with a brief overview of the Russian GLONASS system and the land and satellite based augmentation systems. Navigation observables and signal error sources are discussed in Chapter 3, where in addition to a general error budget provided for satellite navigation systems, real-life measurement errors obtained from different navigation environments are presented to give an impression on the occa-

sional severity of the faults in actual applications.

The estimation of user position, velocity, and time solutions is discussed in Chapter 4 together with aspects on the geometry and accuracy estimation. In Chapter 5, reliability monitoring is discussed with introduction to different performance parameters, such as accuracy, availability, continuity, integrity, and reliability. In addition, the theory of reliability including internal and external reliability parameters and general hypothesis and statistical reliability testing, i.e., outlier detection based on residual analysis, is presented. Influentiality, also called separability, of observations subject to monitoring is briefly addressed.

Chapter 6 provides details about fault detection and exclusion: the different approaches of traditional GPS RAIM and their similarity to statistical reliability testing are discussed. The developed fault detection and exclusion methods are presented including Subset Testing, Forward-Backward FDE, and the Danish estimation method. The quality control procedure, which takes into account solution consistency and redundancy, observation redundancy numbers, and solution geometry, is also presented. New C/N_0 dependent variance models for the navigation observables are introduced for lightly and heavily degraded signal environments.

In Chapter 7, result of the quality control and reliability monitoring procedures on static and kinematic real-life high sensitivity GPS data and simulated GPS/Galileo data are assessed. The clear advantages of quality control and FDE are shown. Lastly, in Chapter 8, conclusions are given with final notes and remarks for future work.

2. GLOBAL NAVIGATION SATELLITE SYSTEMS

This chapter discusses global navigation satellite systems; basic operation and signal specifics. The discussion of this chapter on GNSS is based on the descriptions and discussions in, e.g., (Kaplan (Ed.), 1996; Leick, 2004; Strang and Borre, 1997; Misra and Enge, 2001; Parkinson and Spilker, 1996; Hofmann-Wellenhof et al., 2001; Poutanen, 1999; Lachapelle, 2003; ICD, 2000; SPS, 2001; FRP, 2001), and other references mentioned. The review of the GNSS principles in this section is not intended to be comprehensive, but more fundamental background, which is essential to be introduced before the discussion about navigation fault detection and exclusion. More specific and extensive explanations of the navigation system issues discussed can be found in the references. The chapter includes discussion about the GPS system, high sensitivity GPS, the future Galileo system, the Russian Glonass system, ground and space based augmentation systems, and, finally, briefly introducing a few GNSS assistance possibilities.

2.1 Overview of GPS

This section contains a brief coverage of the Global Positioning System.

2.1.1 System

The NAVSTAR (Navigation System by Timing And Ranging) GPS (Global Positioning System) is a line-of-sight, all weather, world-wide continuously available satellite-based radio-frequency (RF) positioning system providing 3-dimensional position, velocity, and time capability to an end-user with an appropriate receiver. GPS is implemented and operated by the United States Department of Defense (DoD) and it consists of space, control, and user segments. The space segment includes the

satellites, the control segment takes care of managing the satellite operations, and the user segment covers the civil and military GPS user equipment. The full operational constellation of GPS was declared in April 1995 with the baseline GPS system being specified for 24 satellites. However, the system currently employs more satellites than specified in the nominal constellation; by the writing of this thesis the GPS constellation consists of 29 Block II/IIA/IIR satellites (US Naval Observatory, 2004). The system utilizes the concept of one-way time of arrival (TOA) using satellite transmissions that are referenced to highly stable atomic standards onboard the satellites and synchronized with an internal GPS system time.

The GPS constellation includes 6 Earth-centered orbital planes, 60 degrees apart, nominally inclined 55 degrees to the equator. Each orbital plane contains thus 4-5 satellites. The altitude of a GPS satellite is 20183 km from the mean surface of the Earth, and the GPS satellites orbit the Earth in one-half of a sidereal day, i.e., in 11 hour 58 minute orbital periods. The navigation parameters of the GPS system are based in the ECEF (Earth Centered Earth Fixed) WGS-84 (World Geodetic System 84 datum) world-wide common grid reference system. The time base for the GPS system is maintained by the control segment and follows within specified limits the UTC(USNO), Coordinated Universal Time reference kept at the US Naval Observatory.

The system currently includes two navigation carrier signal frequencies for GPS satellite ranging code and navigation data transmissions: L1 (1575.42 MHz) and L2 (1227.60 MHz). At higher frequencies ranging error due to ionospheric refraction would decrease but space loss and atmospheric attenuation increase. The carrier frequencies are modulated by spread spectrum (SS) codes with a unique pseudo-random noise (PRN) sequence associated with each space vehicle (SV) and by the navigation data message. The satellite transmission are CDMA (Code Division Multiple Access) spread spectrum frequency and time synchronized signals and include two modulation codes for pseudorange: coarse/acquisition, C/A, and precision (encrypted), P(Y), codes. The civilian users of the standard positioning service (SPS) can only observe the public C/A-code on L1, and the users of the precise positioning service (PPS) available to the military and other authorized instances have access to also the encrypted P(Y)-codes on the L1 and L2 carriers. The prevention of the precision code to the civil segment has been accomplished with a technique called anti-spoofing (AS) resulting in the encrypted P(Y)-code. Selective Availability (SA)

was another technique used to limit the access of the GPS for SPS users until it was deactivated on 2 May 2000 with a US Presidential Decision. The SA purposefully degraded the signals available through satellite clock dithering, leading to erroneous timing marks on the ranging signals and imprecise values of the ephemeris parameters being broadcast to the user. These errors caused by the SA were larger than the errors inherent to the radionavigation system. Nowadays, with the SA turned off, the advantage of PPS over SPS is the increased robustness; higher resistance to jamming, the dual-frequency measurement available allowing compensation for the signal propagational effects of the ionosphere, faster codes leading to higher precision of range measurements, and lower error effects of multipath propagation.

The chipping rate of the civilian C/A-code is 1.023 MHz, whereas the chipping rate of the military P(Y)-code is ten times more, 10.23 MHz. The repeat time is 1 ms for the C/A-code and one week for the P(Y)-code. In order for the user receiver to track one SV in common view with several other SVs by the CDMA technique, the receiver must replicate the unique PRN sequence for the desired SV along with the replica carrier signal including also the Doppler effects caused by the relative motion of the satellite and the user, and finally make the necessary comparisons to solve the signal TOA. The navigation data provides the means for the user receiver to determine the location of the satellite at the time of the signal transmission. The navigation message, which contains information on the satellites, GPS time, clock behavior, and system status, is modulated on both the L1 and L2 carriers at a chipping rate of 50 bit per second (bps) with a bit duration of 20 ms.

To obtain the 3-dimensional user position utilizing the GPS system, the ranging measurements are needed to at least four satellites: the unknowns to be solved for are basically user latitude, longitude, height, all referenced to the WGS-84 frame, and the receiver clock offset from GPS system time. In addition, also the user velocity can be solved for in three dimensions from the range rate measurements.

2.1.2 Satellite Signal Structure

While traveling through the ionosphere, a linearly polarized radio frequency signal undergoes changes in its polarization. Thus, to avoid the changes in the polarization, known as Faraday rotation, the satellite signals are sent as right-hand circularly polarized electromagnetic waves (Ray, 2000). Each GPS signal consists of three com-

ponents: the carrier, the ranging code, and the navigation data. The carrier consists of the RF sinusoidal signal either with the frequency L1 or L2. The ranging codes, i.e., the PRN codes, are generated to have special properties to allow all satellites to transmit at the same frequency without interfering with each other. For example, each satellite transmits a different set of C/A-codes which belong to the Gold code family (Gold, 1967) and characteristically have low cross-correlation properties between the codes. Thus, it is possible to distinguish the signals received simultaneously from different satellites. Table 1 summarizes the GPS signal structure. Each code is com-

Table 1. GPS Signal Structures.

Signal	Ranging Signal	Code	Navigation Message
L1 1575.42 MHz	C/A P(Y)	300 m 1.023 MHz 30 m 10.23 MHz	Data Rate: 50 bps Chip Width: 20 ms
L2 1227.6 MHz	P(Y)	30 m 10.23 MHz	Duration: 12.5 min

bined with the navigation data by modulo-2 addition. The code and the navigation message is then modulated on the carrier using binary phase shift keying (BPSK) digital modulation. The modulated carrier signals that leave the GPS satellite are of the following form

$$s_{L_1}^j(t) = A_P P^j(t) \oplus N^j(t) \cos(2\pi f_1 t) + A_C C^j(t) \oplus N^j(t) \sin(2\pi f_1 t) \quad (1)$$

$$s_{L_2}^j(t) = B_P P^j(t) \oplus N^j(t) \cos(2\pi f_2 t) \quad (2)$$

where \oplus implies modulo-2 addition, i.e., the exclusive-or operation (XOR), j is the superscript identifying the PRN number of the satellite, A_P, A_C, B_P are the amplitudes of P(Y)-codes and C/A-code, $P^j(t)$ is the P(Y)-code, $C^j(t)$ is the C/A-code modulated on L1 in quadrature with P(Y)-code, $N^j(t)$ is the navigation data modulated onto L1 and L2, and f_1 and f_2 represent the L1 and L2 frequencies, respectively.

Impressing both the C/A and P(Y) on L1 is obtained by generating two carrier signals: an in-phase component and a quadrature component obtained by shifting it in phase by 90 degrees. GPS signals are spread spectrum making the GPS signals resistant to interference and decreasing the effect of a possible jammer at, e.g., the L1. The modulation of a carrier by a binary code spreads the signal energy over a wide frequency band: the C/A-code main lobe bandwidth is about 2 MHz and it is about

20 MHz for the P(Y)-code. The signal energy can be despread in a receiver when the code is known. Finally, the transmit time of the satellite signal can be estimated by correlating the received signal with its replica generated by the receiver.

The GPS signal structure is complex and will not be reviewed in more detail here. Instead, only a brief introduction was provided. For more details on the signal structure, refer to, e.g., (Parkinson and Spilker, 1996; Kaplan (Ed.), 1996; Misra and Enge, 2001).

A master control station uses data from a network of monitoring stations around the world to monitor the satellite transmissions, compute the broadcast ephemerides, calibrate the satellite clocks, and periodically update the navigation message. The navigation data contains, among others, orbital data for computing the satellite positions. The complete navigation message contains 25 frames, each consisting of 1500 bits. Each frame is subdivided into five 300-bit subframes, and each subframe consists of 10 words of 30 bits each. At the 50-bps chipping rate, it takes 6 seconds to transmit a subframe, 30 seconds to complete a frame, and 12.5 minutes for the whole navigation message to be completed. Each subframe begins with a telemetry word (TLM) and a handover word (HOW). The TLM contains a fixed synchronization pattern and the HOW is a truncation of the GPS time of week. Subframes 1-3 repeat the same information from frame to frame. Subframes 4-5 of the consecutive frames, on the other hand, consist of different pages of the navigation message. Subframe 1 contains the GPS week number, space vehicle accuracy and health status, satellite clock correction terms, clock reference time, the differential group delay information, and the issue of date clock term. Subframes 2 and 3 contain ephemeris parameters for the transmitting satellite, and subframes 4 and 5 contain special messages, ionospheric correction terms, coefficients to convert GPS system time to Coordinated Universal Time (UTC), and almanac data. The navigation message also contains information of the user range error (URE), which is a projection of ephemeris curve fit errors onto the user range and includes effects of satellite timing errors.

2.1.3 Receiver Operation

In terms of code measurements, the precision code theoretically provides better overall performance. Unfortunately, the P(Y)-code is currently encrypted to limit its use to the military community, and, therefore, due to the civilian personal positioning

orientation of this work, the focus in this thesis is merely on the L1 carrier and the civilian C/A-code.

To acquire a signal, the receiver generates a replica of the known C/A-code, and attempts to align it with the incoming code. In the receiver, a sharp correlation peak is obtained when the code replica is aligned with the code received from the signal. The time shift required to align the receiver-generated code replica and the incoming signal is the apparent transmit time. The code tracking is accomplished in a feedback control loop, called a delay lock loop (DLL), which continuously adjusts the replica code to keep it aligned with the code in the incoming signal. After the alignment is complete, the PRN code is removed from the signal leaving the carrier modulated by the navigation message. Then, another feedback control loop is employed, a phase lock loop (PLL), where essentially the receiver generates a sinusoidal signal to match the frequency and phase of the incoming signal and, in addition, extracts the navigation message. The Doppler shift of the satellite-to-user signal is also measured in the PLL. In addition, a frequency lock loop (FLL) can be utilized to estimate the frequency error of the signal. It is possible to use a combined FLL/PLL initially, and then switch to PLL, or, alternatively, the FLL can be used continually to aid the PLL (Kaplan (Ed.), 1996).

GPS provides code phase measurements from the code tracking procedure and carrier phase measurements from the carrier tracking process. The code phase measurements from different satellites have a common bias due to the receiver clock bias, and are therefore called pseudoranges. The carrier phase gives a precise measurement of change in the pseudorange over a time interval, and an estimate of its rate, i.e., the Doppler frequency. The GPS measurements in the receiver consist of replica code phase, and replica carrier Doppler phase if the GPS receiver is in phase lock with the satellite carrier signal or replica carrier Doppler frequency if the receiver is in frequency lock with the satellite carrier signal. The replica code phase can be converted into satellite transmit time, which is used to compute the pseudorange measurement. The replica carrier Doppler phase or frequency can be converted into delta pseudorange. The replica carrier Doppler phase measurement can also be converted into an integrated carrier Doppler phase measurement used for ultra-precise static and kinematic surveying. Thus, the obtained GPS signal measurements include, in general, pseudorange, carrier phase, and Doppler. The pseudoranges are derived from the PRN codes and are therefore classified according to code and frequency as L1-C/A,

Receivers may nowadays have up to 24 channels each of which designed to process data from a single satellite either on L1 or L2 frequency. The operations on a single channel in the signal processing part include Doppler removal, correlation, where the signal is mixed with the user generated local copy of the C/A-code, integration, i.e., accumulation, acquisition, and, finally, the carrier and code tracking.

Acquisition is the first step in processing the sampled GPS IF data (Lachapelle, 2003). The three key parameters to be determined in the acquisition is the C/A-codes, their respective C/A-code phases, and carrier frequency with individual Doppler shifts. With no initial aiding information, the search space in acquisition consists of all possible C/A-codes, 1023 C/A-code chips shifts (time), and any associated Doppler shifts (frequency). Thus, the acquisition is a 2-dimensional search over frequency and time. The changing code offset is then tracked with a DLL and the Doppler frequency with a PLL. In the DLL, the received signal is correlated with the local C/A code using usually three different offsets: the early, prompt, and late correlators. A discriminator in the DLL determines the current offset from the actual code offset. The PLL matches the incoming carrier phase with the local inphase carrier. A carrier phase discriminator provides then an estimate of the phase error.

The third part of the receiver, the navigation processor, consists of computing the position, velocity, and time (PVT) using the raw pseudorange measurements, Doppler, and the navigation bits. The navigation processor can include reliability monitoring functions in addition to the PVT estimation processes.

2.1.4 *GPS Modernization*

With the SA still active, the SPS was defined to provide the user a predictable horizontal positioning accuracy of 100 meters, given in 95-percentage (FRP, 1999). The specification was conservative and the actual SPS performance while SA was active was considerably better (Misra and Enge, 2001). No official post-SA specifications are currently readily available, but it has been estimated that with SA set to zero the total standalone horizontal accuracy of SPS, in 95-percentile, would be from 22.5 m (Sandhoo and Shaw, 2000) to 19.1 m (McDonald and Hegarty, 2000), to as good as 10 m (Misra and Enge, 2001). The dominant error source of the SPS in good line-of-sight conditions with SA discontinued is the mismodeling of the ionosphere (Parkinson and Spilker, 1996).

GPS is, however, a vulnerable system to radio frequency interference because the signals are extremely weak and the spread spectrum processing gain against interference is quite modest. Currently, GPS is undergoing major modernization to meet the current and future military and civil navigational demands with the objective of improving the resistance to interference and accuracy of the position, navigation, and timing services for both military and civil users. GPS modernization is made possible by the advances in satellite and receiver technology. Additional signals will be transmitted to the users with the effect from future satellite generation launches improving the overall performance of the GPS. In addition, the modernization allows a better distinction between the military and civilian uses of GPS.

An essential element of GPS modernization involves sharing, or dual use, of the current L-band spectrum by multiple signals that provide enhanced radionavigation service for civilian and military users (Betz, 1999). Additional objectives of the modernization process include improved anti-jamming capability and shortened time-to-first-fix (TTFF) due to the upcoming C/A-code on L2, L2C, and providing the civilian community an extra safety-of-life signal, L5 centered at 1176.45 MHz. In addition, the new L2C signal will provide the civilian community a more robust signal capable of improving resistance to interference and allowing for longer integration times in the receiver. Thereby, the tracking noise will be reduced and accuracy increased as well as the positioning capability inside buildings improved. Overall, making the SPS more accurate and robust is planned to be accomplished by the C/A-coded signal on L2 and a stronger, wide-band signal on L5. At the same time, new military codes, M-codes, will be added to L1 and L2 but will spectrally be separated from the civil codes by being centered 6-9 MHz above and below the L1 and L2 centers. In addition, future GPS satellites will be designed to be capable of broadcasting regionally the M-codes at a 20 dB higher power. Plans of upgrading the control segment have also been made by, e.g., increasing the number of monitor stations for real-time data collection and processing used for ephemeris and clock parameter prediction.

Fig. 2 illustrates the modernized GPS signal evolution from the current signal architecture to the future military and civil signal services. The evolution starts with the current signal architecture, i.e., the C/A-code only on L1 and the encrypted P(Y)-code on both the L1 and L2 frequencies. It evolves to add the capabilities of the C/A-code on L2, and then the M-code and the L5 signal (Fontana and Latterman, 2000; Misra and Enge, 2001). The planned progression of the modernization in terms of

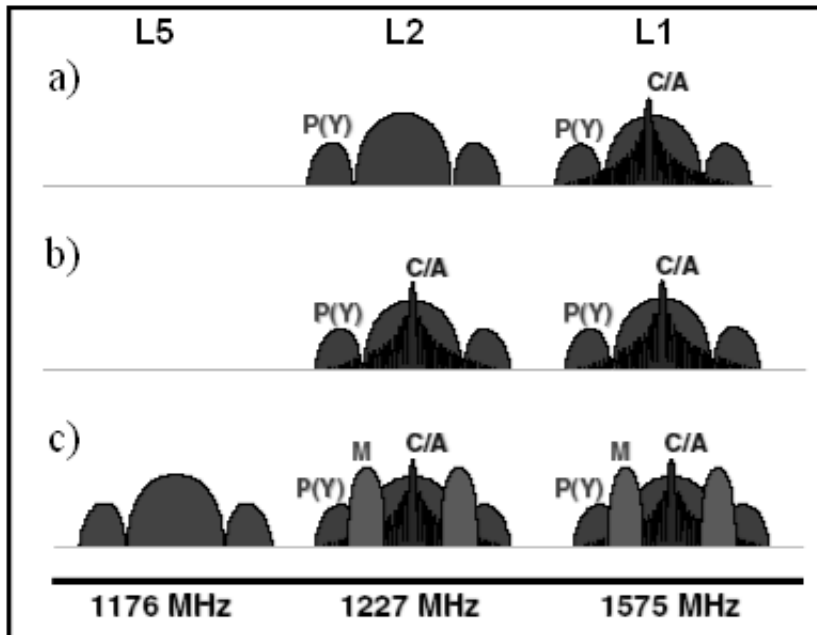


Fig. 2. a) Present Signal, b) New Civil Signal, and c) Signal for Civil Safety-of-Life Applications and New Military Signals.

the different generations of satellites is shown in Table 2 (Fontana et al., 2001; Leick, 2004). The deployment of the fully modernized GPS system is planned to begin in year 2005. In reality, the deployment of the modernized satellites has been somewhat delayed. Nowadays, it is estimated that eight Block IIR satellites will be modernized to radiate the new military M-coded signal on both the L1 and L2 channels as well as the more robust civil signal, L2C, on the L2 channel (JPO, 2005). The first modernized Block IIR, designated as the IIR-M, is now planned for launch in 2005. The first Block IIF satellite, the next generation of the GPS SVs that will provide all the capabilities of the previous blocks with some additional benefits as well is now scheduled for launch in 2006 (JPO, 2005). Improvements include an extended design life of 12 years, faster processors with more memory, and the new civil signal on the third frequency, L5.

The L2C civil signal will consist of a 10230-length CM-code (civil moderate length) that carries data and a 767250-length CL-code (civil long). Both of the codes will have a chipping rate of 511.5 kHz as opposed to the chipping rate of 1.023 MHz on

the C/A-code on L1. Thus, the L2CM-code will last 20 ms and the L2CL will last 1.5 s. The CM will carry data and the CL is a pilot signal. The pilot signal has been designed for high sensitivity applications requiring long integration periods (Mattos, 2004). In addition, the very long codes help to combat against the cross-correlation problem when trying to separate the wanted signal from the unwanted ones. However, while the tracking sensitivity will be enhanced having the pilot signal, the extremely long codes will make it impractical to use for acquisition. Thus, in practice, it will become necessary to acquire the L1 code first, or, simply, just compromise between reasonable acquisition times when the signal is strong, and high sensitivities when the signal is weak, albeit then at slow acquisition times.

The future GPS L5, will have a code length of 10230 chips, a chipping rate of 10.23 MHz, and be built in layers, so that when having a strong signal, the acquisition can be performed on a single layer with switching to the full length code only when required (Mattos, 2004). Each code will be a modulo-2 sum of two subsequences, whose lengths will be 8190 and 8191 chips that recycle to generate the 10230 codes. The Block IIR-M and IIF satellites will transmit a new military M-code signal on L1 and L2 that uses binary-valued modulations by a technique called binary offset carrier (BOC) (Leick, 2004). The difference between the BOC and the conventional rectangular spreading code modulation is seen in the power spectral densities, as shown in general terms in Fig. 2. The offset carrier modulation (Betz, 1999; Lucia and Anderson, 1998) provides a simple and effective way of moving signal energy away from band center, offering a high degree of spectral separation from conventional phase shift keyed signals, whose energy is concentrated near band center. The resulting split spectrum signal effectively enables frequency sharing, while providing

Table 2. *Expected Generations of Satellites in GPS Modernization.*

Signal	Block IIR, 1978-2003	Block IIR-M, 2003-	Block IIF, 2005-
L1 C/A	X	X	X
L1 P(Y)	X	X	X
L1M		X	X
L2C		X	X
L2 P(Y)	X	X	X
L2M		X	X
L5C			X

attributes that include simple implementation, good spectral efficiency, high accuracy, and enhanced multipath resolution (Betz, 1999). The new military M-code will use BOC(10,5), which results in a subcarrier frequency of 10.23 MHz and a spreading code rate of 5.115 MHz. The densities for BOC(10,5) are maximum at the nulls of the P(Y)-codes, which is an essential aspect to obtain increased spectral separation of different code modulations.

A full constellation, often defined as consisting of a minimum of 18 satellites, with a C/A-code on both L1 and L2 is expected around 2010 if the satellite launches progress as planned. The horizontal position error performance in 95-percentile is estimated to be as good as 5 m with the two civil signals present from around year 2010 onwards (Misra and Enge, 2001), and (Luba et al., 2004) estimates that the SPS 95% horizontal accuracy with the dual civil frequency will be as good as 3.7 m. A full constellation with the new civil code on L5 is unlikely before year 2015. With the three civil signals available, a rough estimate for the 95-percentage horizontal position error is a stunning 1 m (Misra and Enge, 2001). These error estimates, however, assume so called 'normal' signal circumstances with average error conditions and proper signal reception.

2.1.5 *High Sensitivity GPS*

In degraded signal conditions, weak signals such as attenuated line-of-sight signals, diffracted signals, multipath signals, or echo-only signals inherently include large associated noise and other errors. The expansion of GPS due to, e.g., location-based services, to areas with poor signal conditions requires, however, high sensitivity receiver processing (Peterson et al., 1997; Moeglein and Krasner, 1998; Garin et al., 1999; Chansarkar and Garin, 2000; MacGougan et al., 2002; MacGougan, 2003). Therefore, the thereby obtained weak and erroneous signals are required to be used, if the objective is to obtain a position solution with respect to no solution at all. In addition, the cellular positioning mandates, i.e., the E911 and the E112, drive high sensitivity and also assisted GPS (AGPS) development (Lachapelle, 2003). With high sensitivity processing inherently including a higher positioning availability, which is even further increased if aiding information is provided to the system through a network, i.e., assisted GPS, capabilities to a much wider range of applications are therefore opened.

HSGPS operation principles

The GPS signal faces losses during its propagation from the satellite to the Earth. The line-of-sight GPS signals received by users are -160 dBW in strength as presented in Table 3 showing the total GPS signal power budget (Lachapelle, 2003). The dimen-

Table 3. *GPS Signal Power Budget.*

SV Antenna Power	13.4 dBW
SV Antenna Gain	13.4 dBW
User Antenna Gain	3.0 dBW
Free-Space Loss	-184.4 dBW
Atmospheric Attention Loss	-2.0 dBW
Depolarization Loss	-3.4 dBW
User received power	-160.0 dBW

sion dBW denotes the ratio of power relative to 1 Watt. The -160.0 dBW corresponds to -130 dBm, which denotes power with respect to 1 mW. The free-space loss, i.e., the geometrical spreading effect, accounts for the largest loss in the GPS signal power budget. The GPS signals are not to exceed the internationally agreed upon power values set to avoid interference with other users and systems.

The noise power within the main lobes of L1 C/A code signal before the correlation process is well below the noise level. The signal is managed to be acquired and tracked by correlation and integration. In conventional GPS, the signal can be acquired and tracked because integrating the despread signal reduces the noise bandwidth. In poor signal conditions, the power of the satellite signal is even further decreased: metals and concrete result in up to a 20 dB loss or more, plywood sheets may lead to a 3 dB loss, drywall into a loss of about 1 dB, trees typically into a loss of 5 to 8 dB and up to 20 dB or even more, depending on the tree size and density of foliage. Thus, the amount of signal attenuation depends on the material, its density, and how much material the signal passes through (MacGougan, 2003). High sensitivity GPS (HSGPS) is known as a technology utilizing longer integration of signals to make signal peaks visible out of noise even for very low-power GPS signals (Peterson et al., 1997). To obtain and track the attenuated signals, which can be attenuated up to a signal strength of about -155 dBm, very long signal integration times are needed to increase the signal-to-noise ratio above the noise floor. High sensitivity GPS receiver

manufacturers are mostly aiming to operate at attenuations of up to 27 to 33 dB with respect to the typical received power.

Coherent integration in the receiver consists of simple summation. The navigation message, however, limits the coherent integration time. During integration, i.e., correlation, the autocorrelation peak grows faster than the noise enabling the acquisition and tracking of the signal. Non-coherent integration, on the other hand, consists of accumulation of the square root of the sum of the squared output of the coherent integration causing a squaring loss due to the squaring of also the noise. In general, to acquire the weak GPS signals, coherent integration and non-coherent accumulation are performed to effectively increase the total signal dwell time. The coherent integration period is limited to 20 ms due to the length of the navigation bits and, in addition, residual frequency errors during the coherent integration period. Residual frequency errors are caused by satellite motion, receiver clock instability and user motion induced Doppler effects. Navigation bit prediction, when knowing the GPS time well enough, can, however, extend the coherent signal integration time. The total accumulation time of the signal in high sensitivity processing can be expressed as N times M ms, where N is the coherent integration time in ms, and M is the amount of non-coherent accumulation in ms. The total dwell-time of HSGPS receivers can be up to hundreds of milliseconds while for conventional GPS it is less than the 20 ms coherent integration interval maximum.

There are a number of factors affecting HSGPS performance that have to be taken into consideration in the design process of the receivers. Firstly, thermal noise should be minimized to maintain the tracking and avoid carrier tracking error. The ability to predict a bit transition is important in order to obtain a long coherent interval. Furthermore, the residual frequency error can be reduced by using a more stable oscillator. In general, high sensitivity methods can be implemented in either aided (AGPS) or unaided modes. In aided mode, high sensitivity receivers rely on assistance data including time, approximate position, satellite ephemerides, and possibly code differential GPS corrections (Syrjärinne, 2001; Agarwal et al., 2002). Assisted GPS works by giving the receiver a hint of which frequency bins to search (van Diggelen, 2002). This speeds up the acquisition time, or, alternatively, allows the receiver to dwell longer in each frequency/code bin resulting in higher sensitivity. To obtain the extra processing gain required for indoor operation, the receiver must also have the capability to search all possible code bins in parallel. Thus, massive parallel corre-

lation is necessary to facilitate the complex task of searching for the weaker GPS signals while using long coherent integration periods and further non-coherent accumulation (van Diggelen and Abraham, 2001; van Diggelen, 2002, 2001; Eissfeller et al., 2004). In unaided mode, the high sensitivity receiver lacks the ability of the aided receiver to acquire weak signals if it has no a-priori knowledge. However, if the receiver is initialized with the same assistance data, by acquiring and tracking four or more GPS satellites with strong signals, it has the same functional capability as an assisted GPS receiver so long as it can maintain timing, approximate position, and satellite ephemerides [P2].

The increased tracking capability of HSGPS is highly beneficial in terms of solution availability and increased redundancy for reliability of navigation. However, simultaneously, severe interference effects in the poor signal conditions of indoor and urban environments lead to large measurement errors when the receiver fails to accurately estimate the time of arrival of the line-of-sight signal. The measurement errors are generally caused by measurement noise, distortion of the line-of-sight correlation peak due to non-line-of-sight combination, and complete blockages of line-of-sight signal leading to acquisition of long-delay multipath signals, cross-correlation peaks or echo-only signals. The robustness of the tracking loop in the presence of weak signals can be, however, somewhat enhanced by implementing, e.g., a tracking scheme capable of monitoring the quality of the autocorrelation function (Fantino et al., 2004). However, the severe observation errors cannot be avoided, and reliability and integrity analysis and monitoring in terms of proper fault detection and exclusion (FDE) becomes increasingly important in HSGPS for degraded environment positioning [P2, P6]. In addition, the higher time-to-first fix (TTFF) of the navigation solution due to the longer integration times causes a significant problem with HSGPS for some applications.

2.2 Overview of Future Galileo

The permanent European reference in time and space, Galileo, is intended to be launched by the European Union (EU) and the European Space Agency (ESA) within the next couple of years. Commercially Galileo is expected to be operational by the year 2008. The Galileo system is intended specifically for civil purposes as opposed to the GPS aimed first of all to US military requirements.

2.2.1 System

The planned Galileo system consists of 30 satellites divided between three circular orbits inclined at 56 degrees at an altitude of 23616 km to cover the Earth's whole surface. Ten satellites will be spread evenly around each plane, with each taking about 14 hours to orbit the Earth. Each plane will also have one active spare satellite, which is able to cover for any failed satellite in that plane.

The satellites orbiting the Earth will be supported and monitored by a worldwide network of ground stations. Two Galileo control centers in Europe will control the constellation as well as the synchronization of the satellite atomic clocks, integrity signal processing, and data handling of all internal and external elements. Then, a global communications network will interconnect all the ground stations and facilities using terrestrial and very small aperture terminal (VSAT) satellite links. Data transfer to and from the satellites will be performed through a global network of Galileo uplink stations, each with a 'telemetry, telecommunications and tracking' station and a mission uplink station. Galileo sensor stations around the world will then monitor the quality of the satellite navigation signal. Information from these stations will be sent out by the Galileo communications network to the two ground control centers. In addition, regional components will independently provide integrity information of Galileo services. Authorized uplink channels provided by Galileo will be used to disseminate regional integrity data. It is planned that the system will guarantee that a user will always be able to receive integrity data through at least two satellites with a minimum elevation angle of 25 degrees in order to provide extra accuracy or integrity around, e.g., airports, harbors, railheads and in urban areas to possibly extend navigation services also to indoor users.

The Galileo Terrestrial Reference Frame (GTRF) is almost coinciding with the WGS-84 coordinate system used by the GPS. Galileo will use the International Atomic Time (IAT) in the timing, as opposed to GPS using Universally Coordinated Time. The Galileo system will transmit ten navigation signals in right hand circular polarization (RHCP): six will serve open and safety-of-life services, two are aimed at commercial services, and two are intended to public regulated services. These signals will be broadcast at the following frequency bands: E5a-E5b, 1164-1215 MHz; E6, 1260-1300 MHz; and E2-L1-E1, 1559-1591 MHz. The E2-L1-E1 bandwidth is already used by the GPS, so this joint frequency transmittance will be done on a

non-interference basis in order to avoid affecting current GPS services while offering users still simultaneous access to GPS and Galileo at minimal increases in cost and complexity of the user equipment. All the Galileo satellites will make use of CDMA compatible with the GPS approach.

2.2.2 Services

The Galileo infrastructure is being implemented in three phases. The development and in-orbit validation phase is planned to take place between the years 2000 and 2005 and it will consist of the consolidation of the mission requirements, the development of 2-4 satellites and ground-based components, and the validation of the system in orbit. The deployment phase is planned to take place between the years 2006 and 2007 and it will consist of the construction and launch of the remaining 26-28 satellites and the installation of the complete ground segment. The third phase is the commercial operations phase and it is expected to be operational from 2008 onwards.

The various service requirements that Galileo is designed to satisfy can be divided into five different service groups (Onidi, 2002; Dutton et al., 2002; Hein et al., 2002; Galileo Brochure, 2003), and they are presented below.

The Galileo open service (OS) is designed for mass-market applications and it will provide signals for timing and positioning free of charge. OS will be available to any user equipped with a receiver capable of navigating with Galileo signals. It is, anyhow, expected that most applications in future will use a combination of Galileo and GPS signals, which will improve performance in severe environments, such as in urban areas. OS will provide integrity information computed by the system but the quality of the signals can still only be estimated by integrity monitoring algorithms at the user level. OS will not guarantee any service or liability issues.

The safety-of-life (SoL) service will be used for most transportation applications that are somehow safety-critical. The SoL service will provide the same accuracy in position and timing as the OS with the main difference being the high integrity level obtained by means of integrity data messages within the OS signals for safety-critical applications, where guaranteed accuracy is essential. The SoL service will be certified and its performances will be obtained through a dual-frequency receiver (e.g., frequency bands L1 and E5a).

The commercial service (CS) is aimed at market applications requiring higher performance than offered by the OS. It will provide added-value services on payment of a fee by adding two signals to the open access signal. This pair of additional signals is protected at receiver level through commercial encryption using access-protection keys, which will be managed by the service providers and a future Galileo operating company. The value-added services that the commercial service will enable are, e.g., high data-rate broadcasting, service guarantees, precise timing services, the provision of ionosphere delay models, and local differential correction signals for extreme-precision position determination.

The fourth service that Galileo will provide is the public regulated service (PRS) that is expected to be used by groups such as the police and customs. Civil institutions will control access to the encrypted public regulated service, which is required to be operational due to the robustness of its signal at all times and in all circumstances, notably during periods of crisis, when some other services may be intentionally jammed.

The fifth service the Galileo system will provide, the search and rescue service, will allow important improvements in the existing humanitarian search and rescue services. These will include near real-time reception of distress messages from anywhere on the Earth, when the current average waiting time is an hour. In addition, improvements will include precise location of emergency alerts, multiple satellite tracking to overcome terrain blockage in severe conditions, and increased availability of the space segment when 30 medium earth orbit Galileo satellites will be present in addition to the four low earth orbit and the three geostationary satellites.

2.2.3 *Signal Structure*

The Galileo navigation signals will consist of ranging codes and data messages. The ranging codes will be generated by highly stable, autonomous atomic clocks aboard each satellite. The data messages will be uplinked to the satellites from the ground stations, stored onboard, and transmitted continuously using a packet data structure. The satellite data messages are expected to include not only satellite clock, orbit ephemeris, identity and status flags, and constellation almanac information, but also an accuracy signal giving a prediction of the satellite clock and ephemeris accuracy over time. With this accuracy signal, users can weight their measurements of each satellite to improve the overall navigation accuracy.

The Galileo satellites will be designed to transmit up to four L-band carriers. A range of data message rates at 50-1000 symbols per second is being considered. Low rates cause minimum disturbance to the navigation signal, while high rates maximize the potential for value-added services such as weather alerts, accident warnings, traffic information, and map updates. In all, data broadcasting capacity in the Galileo satellites must be maximized without compromising the navigation accuracy.

Galileo will provide services on signals mainly on four frequencies labeled E5a, E5b, E6 and L1. Galileo OS signals will be transmitted on E5a, E5b and L1. Each OS signal consists of two navigation code signals, transmitted in quadrature. One of the OS code signals is an unmodulated pilot, which can be used for signal acquisition in poor reception conditions, and the other is modulated with a navigation data message. The SoL service will use the OS signals with the addition of integrity data added to the navigation messages on E5b and L1. The CS will use the OS signals possibly with supplementary messages as well as the special-purpose E6 signal, which will comprise a pilot and a data channel using secret codes that will be accessible by subscription. The PRS will use spectrally separated signals with secure and secret codes on the E6 and L1 frequencies.

The E5a and E5b signals will be generated together using alternative binary offset component modulation (Alt-BOC) in order to use a single transmitter in the satellite for both signals. The E5a signal is designed for low carrier-to-noise ratio, C/N_0 , applications with a very low-rate data signal not sufficient for Safety-of-Life applications. The E5b signal will have a higher data rate, which will accommodate open service, safety-of-life, and possibly also commercial service data. The E6 signal will probably carry BOC(10,5) modulation for the PRS together with quadrature phase shift keying (QPSK) components for the commercial service. The latter can be encrypted to allow a fee to be charged for the very accurate three-carrier (TCAR) positioning service. The OS Galileo L1 signal is planned to have a code length of 8184 with a 2.046 MHz chipping rate and be BOC(1,1) modulated to ensure the necessary compatibility with GPS L1. The L1 signal will carry two BOC-components, the data channel B and pilot channel C, for open, CS and SoL services. A BOC(15, 2.5) signal, again spectrally separate, will be provided for the public regulated service (Mattos, 2004; Dinwiddy et al., 2004; Hein et al., 2004).

The Galileo partners, the European Space Agency (ESA) and the European Commission (EC), have agreed that Galileo will offer guaranteed performance to its users

(Dinwiddy et al., 2004). The performance, which should be obtained by a standard receiver working in a normal environment when using only L1 in Galileo OS, has been estimated to be 15 m in horizontal position error accuracy, expressed in 95-percentage, (Dinwiddy et al., 2004), and when using both E5a and L1 or E5b and L1, 4 m. A standard receiver is generally specified with typical antenna gain, noise figure, clock stability, and other characteristics, while the environment is specified with commonly experienced levels of tropospheric, ionospheric and multipath distortions, and of user visibility, user dynamics and external interference. A typical horizontal positioning accuracy for combined Galileo OS and GPS C/A is estimated in (Rodriguez et al., 2004) to be as good as 2.15 m.

2.3 Overview of GLONASS

The Russian GLONASS (Global'naya Navigatsionnaya Sputnikkovaya Sistema) satellite system originates from as far back as 1982, when the first satellite of this system was launched. Nominally, the satellites of the GLONASS system are in three orbital planes separated by 120 degrees, and equally spaced within each plane with a nominal inclination of 64.8 degrees. The nominal orbits are circular with each radius being about 25500 km resulting in an orbital period of approximately 11 hours and 15 minutes. Each GLONASS satellite transmits at its own frequencies currently according to

$$f_{L1,2} = (178 + \frac{K}{16}) * Z \quad (3)$$

where K is an integer value between -7 and +12, $Z=9$ for L1, and $Z=7$ for L2 (Kaplan (Ed.), 1996). The frequencies are expressed in MHz. L1 is around the central frequency 1602 MHz and L2 around 1246 MHz.

There are C/A-codes on L1 and C/A and P-codes on L2, as in GPS, however, with naturally different code structures from the GPS codes. The GLONASS satellite clocks are steered according to UTC(SU), Coordinated Universal Time, Soviet Union, and the GLONASS broadcast navigation message contains satellite positions and velocities in the PZ-90 geocentric reference system, the Earth Parameter System 1990. GLONASS navigation message as a part of the navigation radiosignal includes the broadcast ephemerides, the time scale shifts of the satellites relative to the GLONASS System Time and UTC(SU), time marks, and GLONASS almanac. Currently, the

state of the GLONASS system has deteriorated due to lack of finances, and at the writing of this thesis, there are thirteen operational GLONASS satellites. Thus, GLONASS observations have primarily been used to supplement and strengthen GPS solutions. However, the GLONASS program is also undergoing modernization to improve the ground support segment, the augmentation of the system with differential services, and, most importantly of all, the space segment with more GLONASS satellites. In future, with more GLONASS satellites available, the Galileo system becoming operational, and the modernization of GPS, the user of global navigation satellite systems can expect an outstanding radionavigation performance of in terms of availability and accuracy.

Fig. 3 describes the frequency allocation of the three GNSS: the GPS, the Galileo, and the GLONASS.

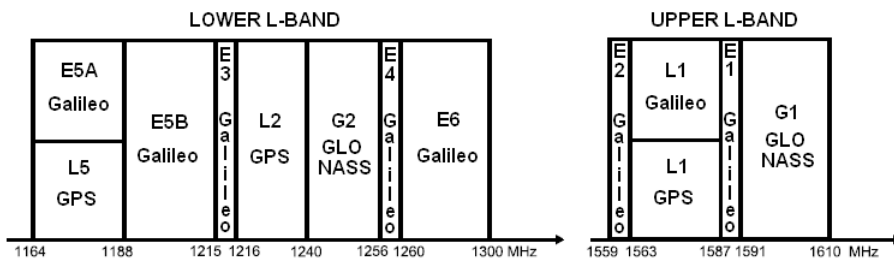


Fig. 3. Allocation of GPS, Galileo, and GLONASS Frequency Bands.

2.4 Satellite Augmentation Systems

Standalone satellite navigation is not adequate for all navigation and positioning applications. Many civil applications, e.g., related to harbors and restricted waterways in marine navigation and to guidance and approach situations in aviation navigation, require greater accuracy than provided by standalone navigation systems. Navigation solution estimates can be improved by mitigating measurement errors by using differential corrections to remove common errors from two or more receivers viewing the same satellites. Measurement errors are both spatially and temporally correlated, and, thus, a reference receiver with a known location can determine the biases in its measurements due to, e.g., atmospheric delays and receiver noise, and provide them as differential corrections to user receivers in the same area. The users incorporate

the corrections to improve the accuracy of their position solutions. With GPS, this is denoted as differential GPS, DGPS, e.g., (Kaplan (Ed.), 1996; Misra and Enge, 2001; Parkinson and Spilker, 1996). The accuracy of differential navigation depends most of all on the closeness of the user to a reference receiver and also on the delay in the corrections transmitted over a radio link. However, the accuracy with DGPS can in optimal cases be even in the sub-meter level.

Differential services, both commercial and federally provided, are nowadays widely available (Misra and Enge, 2001). GNSS augmentation systems, such as local ground-based augmentation systems (GBAS) or regional satellite-based augmentation systems (SBAS) provide correction data to remove or reduce some of the error components of a GNSS ranging signal.

2.4.1 Local Area Ground-Based Augmentation Systems

In local area ground-based augmentation systems, each reference station determines the pseudorange measurement errors at its location and passes the information to the users (Kaplan (Ed.), 1996). Local area augmentation usually serves users with differential corrections via a radio link within close proximity, since it is limited by spatial decorrelation of the errors. The US Coastguard provides differential corrections to users for free on marine radiobeacon frequencies. A number of countries have implemented systems compliant with the US Maritime DGPS standards to enhance safety on waterways (Misra and Enge, 2001). In addition, the US Federal Aviation Administration (FAA) is implementing an augmentation system called local area augmentation system (LAAS) (Enge, 1999) to be deployed at airports to guide aircrafts during approach and landing operations under poor visibility. The LAAS reference stations will be set up on airports and their carrier-smoothed code measurements will be transmitted to aircraft resulting in a position estimate relative to the reference receiver (Misra and Enge, 2001).

2.4.2 Wide Area Satellite-Based Augmentation Systems

In wide area satellite-based augmentation systems, a network of monitoring stations determines and continually updates the time-varying and spatially varying components of the total error over an entire region of coverage and makes the correction

values available to users within the coverage region (Kaplan (Ed.), 1996). A set of reference stations is deployed in a region of interest and measurements from each are processed centrally to form the differential corrections. The corrections are broadcast separately from geostationary satellites for different error sources, i.e., satellite clock, ephemeris, and ionosphere, so that each user can apply the differential correction vectors appropriately depending on the user's location. In addition, the ranging signals from the geostationary satellites provide an additional signal increasing the navigation redundancy.

US FAA developed wide area augmentation system (WAAS) (Enge et al., 1996; Skone et al., 2004) for GPS is a solution for the requirements of safety in civil aviation. Dual-frequency (L1-L2) measurements from about 25 WAAS reference stations distributed over the US are processed at a master station to estimate differential corrections and error bounds. The corrections are separated into three components: a fast changing component due to the clock error and two slow-growing components due to ephemeris error and ionospheric propagation delays for a set of points corresponding to a latitude and longitude grid (Misra and Enge, 2001). The differential corrections are coded in a navigation message of GPS/SPS-like signals transmitted at L1 from geostationary satellites. A WAAS-equipped receiver needs to be able to receive the additional ranging signal and to demodulate the navigation message for the differential corrections.

Currently, a WAAS-like GPS augmentation system is also being deployed in Europe. The system is called the European geostationary navigation overlay system (EGNOS) (Soley et al., 2004; Gauthier et al., 2003; Kirjner et al., 2003). The EGNOS system provides a GEO-ranging (R-GEO) service that will consist of transmission of GPS-like signals from 3 GEO satellites to augment the number of navigation satellites available to the users, a GNSS integrity channel (GIC) service that include broadcasting GPS/GLONASS integrity information up to the level required for civil aviation precision approaches, and a wide area differential (WAD) service comprising the broadcasting of differential corrections to increase the accuracy of the GPS/GLONASS navigation service (Gauthier et al., 2003). The Japanese are also developing their own satellite-based wide-area GPS augmentation system called the multifunctional transportation satellite based satellite augmentation system (MSAS). MSAS is developed and operated by the Japan Civil Aviation Bureau (JCAB) that is compatible with the United States WAAS and the European EGNOS systems (Tomita

et al., 2003). In addition, India is developing a wide-area differential GPS service. The Indian space-based augmentation system is known as GAGAN (GPS And GEO Augmented Navigation). The Indian SBAS, when operationalized, is expected to fill the gap between the European EGNOS and the Japanese MSAS to provide seamless navigation to civilian aircrafts (Sisodia et al., 2003).

2.5 *Assisting Personal Satellite Navigation*

GNSS is unable to provide navigation capability continuously indoors in a standalone mode, especially if thick layers of building material hinder the signal reception and if assistance data aiding for the signal acquisition and tracking processes is not available. Additional sensor systems, such as self-contained sensors of micro electro mechanical systems (MEMS), can provide navigation capability in the case of a gap in GNSS availability. In addition, e.g., fingerprinting with wireless local-area networks (WLAN), or, alternatively, triangulation or location by cell identification of cellular positioning techniques can also be used in parallel and in assisting GNSS performance. Using hybrid solutions or assisting the GNSS navigation extends the positioning capability of satellite navigation systems from environments with line-of-sight to satellite signals to areas where blockages hinder proper satellite navigation. Using hybrid systems with multiple sensor types compensates for the shortcomings of a single technology, and seamless navigation from outdoors to indoors is the ultimate goal.

2.5.1 *Cellular Networks*

Assisted GPS (Syrjärinne, 2001; Garin et al., 1999), AGPS, includes inherently a channel for providing the necessary assistance information in order to extend high sensitivity operation even to very harsh signal environments. Assisted GPS provides the necessary assistance data via a wireless link, and shortens thereby the TTFF and may protect the navigation system from the acquisition of long-delay multipath peaks and cross-correlation by providing approximate location and time.

There are also multiple independent cellular network positioning techniques, e.g., time-of-arrival (TOA), angle-of-arrival (AOA), enhanced observed time difference

(E-OTD) positioning, or location fingerprinting (LF) (Syrjärinne, 2001), just to mention a few. These cellular positioning techniques provide user location information within the cellular network coverage, however, with orders of magnitudes of lower accuracy that GNSS offers when available. In addition, a fusion of measurements from a cellular network positioning method and GNSS might enable positioning in the cases in which neither of the methods has a sufficient amount of observations to position calculation (Syrjärinne, 2001).

As a brief mentioning, there are some new, evolving techniques related to using digital television (DTV) signals in obtaining user location information, and as an example of this kind of a technique, augmenting GPS with television signals is discussed in (Rabinowitz and Spilker, 2004).

2.5.2 *Self-Contained Inertial Sensors*

Miniature inertial navigation system (INS) sensors, such as micro electro mechanical system (MEMS) gyroscopes and accelerometers, can be utilized in providing a navigation solution to the user when satellite signals are completely blocked. Alternatively, if there are satellite signals available, sensor and satellite navigation system data can be integrated in order to obtain enhanced positioning performance, e.g., (Mezentsev, 2005).

The inertial measurement unit (IMU) sensor systems provide information on the user orientation and dynamics. To aid the GNSS navigation in, e.g., a pedestrian application, the self-contained sensors can be processed in pedestrian mechanization mode by exploiting an acceleration pattern to detect and count foot steps. In such mechanizations, the position error depends on the heading error and the step length estimation error. Once a GNSS solution is unavailable, such systems, thus, mostly navigate in a pure inertial or pedestrian dead reckoning (PDR), e.g., [P4], mode, where the error drift in time is substantial. However, INS and PDR require initial values and also information for the system calibration from an absolute positioning system, i.e., the GNSS, and, thus, the output errors are related to GNSS errors.

In this thesis, reliability monitoring aspects of only satellite navigation systems are considered in cases where degraded satellite navigation measurements have been obtained and a navigation fix with the available measurements is necessary. However,

when having access to multiple types of measurements, the reliability monitoring capability can, in principle, be extended to the hybrid systems.

3. NAVIGATION OBSERVABLES AND ERROR SOURCES

This section discusses navigation observables and their error sources.

3.1 Observables

First, navigation observables, i.e., code, phase, and Doppler measurements are presented.

3.1.1 Code Pseudorange Measurement

The apparent transit time of the satellite signal from a satellite to the user receiver can be measured as the amount of shift required to align the C/A-code replica generated at the receiver with the signal received from the satellite (Misra and Enge, 2001). The received signal is identified and aligned with the receiver clock generated signal using the autocorrelation properties of the PRN codes. Multiplying the transit time with the speed of light results in the measured satellite-to-user range. Timing errors between the receiver clock and the satellite clock from system time cause the measured range, however, to differ from the geometric distance corresponding to the instants of transmission and reception of the satellite signal. Therefore, the measured range is called the pseudorange. In addition to the clocks causing the pseudorange to differ from the geometric range, the pseudorange measurement contains various other error components. The measured code pseudorange from satellite i , ρ^i , can be denoted in unit of meters as

$$\rho^i = r^i + c(dT - dt^i) + d\rho^i + d_{iono}^i + d_{tropo}^i + \epsilon_p^i \quad (4)$$

where

r^i is the geometric range between satellite i and receiver antenna [m]

c	is the speed on light [m/s]
dT	is the receiver clock error with respect to GPS time [s]
dt^i	is the satellite clock error with respect to GPS time [s]
$d\rho^i$	is the ephemeris error [m]
d_{iono}^i, d_{tropo}^i	are the ionospheric and tropospheric delays, respectively [m]
ϵ_p^i	consists of noise, unmodelled errors, and multipath error [m].

The receiver noise in the code pseudorange measurement is from 5 cm to 300 cm for the C/A-code (Lachapelle, 2003). In theory, if the line-of-sight signal is present, the code multipath error can reach magnitudes of half a code chip in length at the maximum (Ray, 2003; Lachapelle, 2003; Parkinson and Spilker, 1996), with the half a chip representing a distance of around 150 m for the C/A-code.

3.1.2 Carrier Phase Measurement

The most accurate satellite-to-user distances can be obtained from a carrier phase observation which contains the difference in phase of the incoming satellite carrier signal and the receiver generated carrier signal with the same frequency. The carrier phase measurement is an indirect and an ambiguous measurement of the signal transit time (Misra and Enge, 2001). The initial observation consists only of the fractional part of the carrier phase difference. When tracking is continued, the fractional part plus the integer number of cycles since the signal left the satellite is recorded, moreover, with the initial integer number of whole cycles, denoted as the integer ambiguity, as an unknown that has to be solved for. Similar to the code measurement, the measured carrier phase observation from satellite i , ϕ^i , contains many error components as expressed in unit of meters in the following

$$\phi^i = r^i + c(dT - dt^i) + d\rho^i + \lambda N - d_{iono}^i + d_{tropo}^i + \epsilon_\phi^i \quad (5)$$

where

r^i	is the geometric range between satellite i and receiver antenna [m]
c	is the speed on light [m/s]

dT	is the receiver clock error with respect to GPS time [s]
dt^i	is the satellite clock error with respect to GPS time [s]
$d\rho^i$	is the ephemeris error [m]
λ	is the carrier wavelength [m]
N	is the integer ambiguity
d_{iono}^i, d_{tropo}^i	are the ionospheric and tropospheric delays, respectively [m]
ε_{ϕ}^i	consists of noise, unmodelled errors, and multipath error [m].

The ionospheric delay error has a negative sign in the carrier phase expression due to that the ionosphere causes a carrier phase advance. The receiver noise in the carrier phase measurement can reach up to approximately 5 mm. Multipath effects in the phase measurement stay approximately within a magnitude of 0.25λ (Lachapelle, 2003; Ray, 2003), where λ is the wavelength of the carrier, i.e., with L1, approximately $\lambda=19$ cm.

Due to the ambiguous starting value of the carrier phase observation, in standalone navigation mode, there is no way of knowing the whole number of carrier cycles between the satellite and the user antenna and using the carrier phase for absolute estimation of user position. In relative navigation, however, the obstacle of the unknown number of whole carrier cycles can be overcome by integer ambiguity resolution techniques, resulting in navigation solutions of high-accuracy.

3.1.3 Doppler Measurement

The relative motion of a satellite and the user results in changes in the observed frequency of the satellite signal (Misra and Enge, 2001). Doppler is a measurement of the instantaneous phase rate of a tracked satellites signal. The Doppler shift, or equivalently the range rate, caused by satellite and user motion can be considered as a projection of the relative velocity vector onto the line of sight vector. The velocity of the user with respect to the satellites can be determined with the Doppler measurement. The equation for the measured Doppler for satellite i , $\dot{\phi}^i$, in units of m/s is expressed as

$$\dot{\phi}^i = \dot{r}^i + c(d\dot{T} - \dot{d}t^i) + d\dot{\rho}^i - \dot{d}_{iono}^i + \dot{d}_{tropo}^i + \varepsilon_{\dot{\phi}}^i \quad (6)$$

where

\dot{r}^i is the geometric range rate between satellite i and receiver antenna [m/s]

c is the speed on light [m/s]

$d\dot{T}$ is the receiver clock error drift with respect to GPS time [seconds/second]

$d\dot{t}^i$ is the satellite clock error drift with respect to GPS time [seconds/second]

$d\dot{\rho}^i$ is the ephemeris error drift [m/s]

d_{iono}^i, d_{tropo}^i are the ionospheric and tropospheric delay drifts, respectively [m/s]

ε_{ϕ}^i consists of noise and rate of change of multipath delay [m/s].

Since the carrier is tracked continuously, the integer ambiguity term is dropped out from the Doppler equation of change in carrier phase measurement over a time interval. The noise in the Doppler measurement, ε_{ϕ}^i , can reach up to 5 mm/s (Lachapelle, 2003). Due to the frequency offset, i.e., the receiver clock bias rate, the rate of change of the carrier phase measurement, the measured Doppler, can actually be denoted as a pseudorange rate $\dot{\rho}$, which is made up of the actual range rate and the receiver clock frequency bias (Misra and Enge, 2001), and it is the basis of determining the velocity of the user. The pseudorange rate measurement discussed widely in this thesis is, thus, the measured Doppler observation in m/s.

3.2 Error Sources

Errors in navigation ranging signals can be grouped into three categories: satellite-based errors, signal propagation errors, and receiver-based errors. Satellite-based errors include satellite clock and ephemeris errors. Signal propagation errors include errors associated with the atmospheric propagation delay due to the ionosphere and the troposphere and multipath propagation delay and interference. Receiver-based errors include receiver noise affecting the precision of a measurement and smaller errors, such as, e.g., inter-channel biases and antenna errors. The ability to obtain accurate and reliable position, velocity, and time from satellite navigation signals depends upon the predictability, controllability, and detectability of the measurement

errors. Thus, knowing the major sources of possible errors is essential in the pursuit of obtaining user position solutions with desired performance levels. In any given error, important characteristics include the magnitude and the temporal and spatial variability of the measurement fault.

In the following, the different error sources of pseudorange measurements are discussed specifically, and they are directly transferable to the errors in pseudorange rate observations, i.e., the measured Doppler.

3.2.1 Satellite-Based Range Errors

Satellite-based range errors consist of the errors in the orbital and satellite clock parameters broadcast in the navigation message of which the GPS control segment is responsible of. The prediction error of the satellite ephemeris and clock parameters grows with the age of data, i.e., the time since the last parameter upload. Thus, the more frequent the data uploads by the control segment to the satellites and the more accurate the models used to estimate and predict the ephemeris and clock parameters, the less significant are the satellite-based range errors.

Ephemeris Errors

The ephemeris error $d\rho^i(t)$ results when the transmitted broadcast ephemeris in the navigation message does not correspond to the true satellite location. The satellite ephemeris parameters broadcast to the user via the navigation message are purely estimates made by the control segment based on previous measurements of satellite motion and knowledge about the Earth's gravity field, and they contain thus a residual error.

There are three ephemeris error components along orthogonal directions defined relative to the satellite orbit: along-track (AT), cross-track (XT), and radial (R) error components. The radial component of the error directly affects the range measurement. The magnitude of the ephemeris prediction error is, however, realized when the total error vector is projected onto a user line-of-sight unit vector. The ephemeris error components are shown in Fig. 4. With typical data uploads once a day by the control segment, a current estimate of the root-mean-square (rms) range error due to the ephemeris parameters is about 1.5 m (Misra and Enge, 2001). In an estimated

SPS C/A-code pseudorange error budget in (Kaplan (Ed.), 1996), the one- σ error of the ephemeris prediction is estimated as 4.2 m.

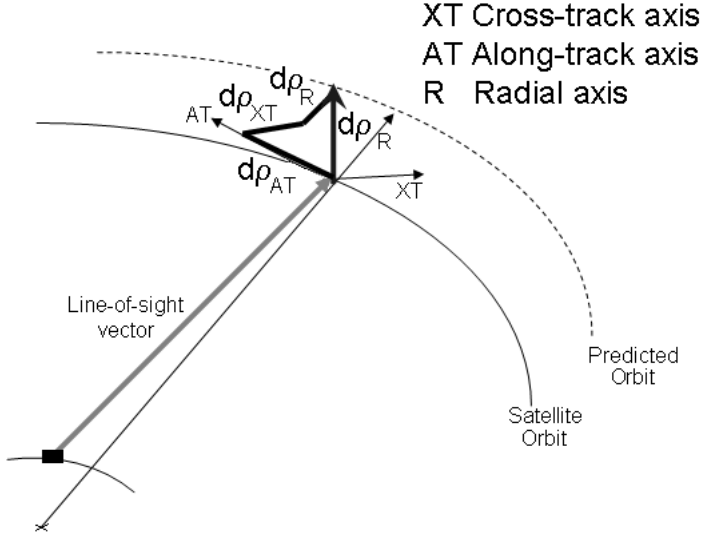


Fig. 4. Ephemeris Error Components.

Satellite Clock Errors

The satellites contain highly stable atomic clocks that control all timing operations including broadcast signal generation. However, overall, the satellite clock error may deviate up to approximately 1 ms from GPS system time (Kaplan (Ed.), 1996). The satellite clock error is similar to that of the orbital error. Satellite clock behavior is predicted by the master control station from previous measurements of the satellite clock error, and the clock error model parameters are transmitted to the satellite for rebroadcast to the users in the navigation message. The broadcast error model assumes quadratic error growth as presented in the satellite clock error model equation for satellite i in Eq. 7.

$$dt^i = a_{f0}^i + a_{f1}^i(t - t_{oc}) + a_{f2}^i(t - t_{oc})^2 + \Delta t_r \quad (7)$$

where

a_{f0}^i is the clock bias [m]

a_{f1}^i is the clock drift [s/s]

a_{f2}^i is the frequency drift [s/s²]

t_{oc} is the reference time of clock data [s]

t is the current time epoch [s]

Δt_r is the correction due to relativistic effects [s].

To take into account both special and general relativity, the satellite clock frequency is adjusted from the default 10.23 MHz to 10.22999999545 MHz prior to launch (Kaplan (Ed.), 1996). The relativistic correction Δt_r is necessary to be included in the polynomial clock correction model in order to take into account that the satellite orbit's slight eccentricity causes the satellite to travel through different levels of gravitational potential and a change in the velocity of the satellite and, thus, a change in the clock. When the satellite is at perigee, i.e., closest to the Earth, the satellite velocity is higher and the gravitational potential is lower, both causing the satellite clock to run slower. When the satellite is at apogee, i.e., at a greatest distance from the Earth, the satellite velocity is lower and the gravitational potential is higher, both causing the satellite clock to run faster. In addition, with the typical once-per-day control segment uploads, the current estimate of the rms range error due to the clock error parameters is about 1.5 m (Misra and Enge, 2001). In the SPS error budget (Kaplan (Ed.), 1996) it has been estimated that the ranging error due to the satellite clock errors are in the order of 3 m (the one- σ value).

3.2.2 Signal Propagation Errors

GPS signals are affected by the medium through which they travel from the satellites to the receiver antenna. At a height of about 1000 km from the surface of the Earth, the signals enter the ionosphere. At a height of about 40 km, the signals encounter the electronically neutral gaseous troposphere. In the vicinity of the receiver antenna, multipath propagation effects introduce interfering signals degrading the code and also carrier measurements.

Ionosphere Errors

The ionosphere is a dispersive medium which extends from about 50 to about 1000 km above the Earth and is characterized by free electron and ions. Ultraviolet rays from the sun ionize a portion of gas molecules in the ionosphere and release free electrons which affect electromagnetic wave propagation (Kaplan (Ed.), 1996). The signal delay due to the ionosphere is directly proportional to the integrated electron density along the signal path, i.e., the total electron content (TEC), and inversely proportional to the squared frequency of the signal (Strang and Borre, 1997). TEC is defined as the number of electrons in a tube of 1 m^2 cross section extending from the receiver to the satellite (Misra and Enge, 2001). Therefore, since the ionosphere is a dispersive medium, i.e., the refractive index of the ionosphere is dependent on the frequency of the RF signal, two-frequency (L1-L2) GPS users can take advantage of this property of the ionosphere to measure and correct for the first order ionospheric range and range rate effects directly (Klobuchar, 1996). The ionospheric delay I for zenith in measurements of pseudorange (ρ) and carrier phase (ϕ), which are dependent of the frequency of the radio wave f and the TEC, are equal in magnitude but opposite in sign as presented in the following

$$I_{\rho} = -I_{\phi} = \frac{40.3 \cdot \text{TEC}}{f^2} \quad (8)$$

The code phase measurements are delayed with the same amount that the carrier phase measurements are advanced.

The general major effects the ionosphere can have on the GPS signals include delay of the signal modulation, i.e., absolute range error, carrier phase advance, i.e. relative range error, Doppler shift, i.e., range rate error, refraction or bending of the radio wave, distortion of pulse waveforms, and signal amplitude and phase scintillation (Klobuchar, 1996).

The density of the free electrons in the ionosphere varies strongly with the time of day and the latitude. During the day, there can be up to five times more delay due to the ionosphere as during the night. In addition, the time of the year has an effect on the effect on the ionosphere. Solar flares and the resulting magnetic storms can, especially in polar areas, create quickly varying electron densities (Misra and Enge, 2001). In addition, changes in solar activity in the solar cycles that reach a maximum every 11 years directly influence the ionosphere and, thus, the GPS performance. At

solar activity maximums, the ionospheric delay can be up to four times more as in minimum periods. In all, for a signal arriving vertically with respect to a user, the ranging delay due to the ionosphere can be from about 3 m at night to about 15 m at daytime. At low satellite viewing angles up to 10 degrees, the delay can range from 9 m at night to as high as 45 m during the day (Kaplan (Ed.), 1996).

Models of the ionosphere should be employed to correct for the ionospheric delay. For example, an ionospheric delay compensation model by Klobuchar removes, on the average, about 50 percent of the ionospheric delay at midlatitudes by assuming that the vertical ionospheric delay can be approximated by utilizing the satellite broadcast ionospheric delay coefficients in a model including half a cosine function of the local time during daytime and a constant level during nighttime (Kaplan (Ed.), 1996; Misra and Enge, 2001). The ionospheric delay can be determined from broadcast parameter values and the user's latitude, longitude, satellite elevation, azimuth angles, and local time. The ionospheric delay of the Klobuchar model can be expressed as a function of zenith angle ζ as follows (Misra and Enge, 2001)

$$d_{iono}(\zeta) = d_{iono, z} \cdot OF_{iono}(\zeta) \quad (9)$$

where $d_{iono, z}$ is a zenith delay, and $OF_{iono}(\zeta)$ is an obliquity factor for zenith angle ζ .

A zenith ionospheric delay estimate at local time t can, according to Klobuchar, be expressed as

$$\frac{\hat{d}_{iono, z}}{c} = \begin{cases} A_1 + A_2 \cos \frac{2\pi(t-A_3)}{A_4} & \text{if } |t - A_3| < A_4/4 \\ A_1 & \text{otherwise} \end{cases}$$

where A_1 is a nighttime value of the zenith delay fixed at 5×10^9 , A_2 is an amplitude of the cosine function for daytime values, A_3 is the phase corresponding to the peak of the cosine function fixed at 14 h local time, and A_4 is the period of the cosine function. This model for the zenith ionospheric delay is also called the broadcast model. The values of A_2 and A_4 are specified in the navigation message broadcast by the satellites and updated daily.

The path length of a signal traveling through the ionosphere depends on the elevation angle of the satellite, and is accounted for in the form of the obliquity factor (Misra and Enge, 2001). The obliquity factor can be expressed as

$$OF_{iono}(\zeta) = \left[1 - \left(\frac{R_E \sin \zeta}{R_E + h_I} \right) \right]^{-1/2} \quad (10)$$

where R_E is the average radius of the Earth and h_I is the mean ionospheric height. The value of $OF_{iono}(\zeta)$ varies from one at the zenith direction ($\zeta=0$) to about three for a satellite elevation angle of 5 degrees (Misra and Enge, 2001).

There are also other models for ionospheric compensation, for example wide area models, global grid-based ionospheric models, a 3-D model based on ground-based tomography, or a voxel approach that represents and estimates the ionosphere and its electron density (Lachapelle, 2003). The major effects of the ionosphere on a single-frequency GPS user can be mitigated greatly when applying differential corrections; at least when the relative geographic area of the differential region used is small such as in harbors or in aircraft landing areas. However, when the differential approach is attempted over a wide area, the differential ionospheric time delay across a large region can become again a significant limitation to the overall positioning accuracy (Klobuchar, 1996).

In the SPS error budget (Kaplan (Ed.), 1996), it is estimated that the one- σ value due to the residual ionospheric delay is in the order of 5 m.

Troposphere Errors

The lower part of the Earth's atmosphere, the troposphere, consists of dry gases, i.e., the dry component, and water vapor, i.e., the wet component, causing the GPS signals to be refracted. Water vapor generally exists only below altitudes of 12 km above sea level and most of the water vapor is below 4 km. The dry component of the troposphere, mainly N_2 and O_2 gases, extends to a height of about 40 km. The dry gases, however, can be found in gradually thinning layers at altitudes of hundreds of meters (Misra and Enge, 2001). At the GPS frequencies, oxygen O_2 is the dominant source of attenuation.

The troposphere is a non-dispersive medium, i.e., it affects the signals at L1 and L2 similarly. Thus, in the troposphere, a refractive index n , which represents a factor by which a signal is slowed down relative to vacuum, does not depend on the frequency (Misra and Enge, 2001). The refractive index is dependent on the local temperature, pressure, and relative humidity (Kaplan (Ed.), 1996). Refractivity N can be defined by the refractive index as $N = (n - 1) \times 10^6$, and it can be divided into wet and dry components as follows

$$N = N_{dry} + N_{wet} \tag{11}$$

The refractivity can be interpreted as a parts per million (ppm) error. The speed of the GPS signals is lower in the troposphere than in free space, and the typical range error due to the tropospheric delay is from about 2.5 m to 25 m depending on the satellite elevation angle and thus signal path length. The troposphere produces also attenuation on the signals, generally, however, remaining under 0.5 dB (Parkinson and Spilker, 1996). About 90 percent of the tropospheric delay is due to the dry component and it is easily predictable based on the user latitude, season, and altitude. The wet atmosphere consisting of water vapor is much harder to be estimated since it varies with local weather and can change rapidly. Models of the troposphere attempt to estimate the dry and wet refractivities along the satellite signals paths in order to predict the total tropospheric delay (Misra and Enge, 2001).

It is impractical to measure the precise temperatures and pressures along the propagation path of the signal with weather instruments, and, thus, models of standard atmosphere for the day of the year and the user's latitude and altitude are usually used to predict the required meteorological information. Tropospheric models trying to account for the height dependence of the tropospheric effects include, to mention the two most common ones, the empirically derived Hopfield two quartic model (Spilker, 1996) that assumes the refractivity varies with altitude and includes two different quartics for the dry and wet atmospheric profiles, and the Saastamoinen total delay model (Saastamoinen, 1972; Spilker, 1996), which uses gas laws and assumptions regarding changes in pressure, temperature, and humidity with altitude. More tropospheric delay models and mapping functions, i.e., obliquity factors, can be found in (Spilker, 1996). In general, for most users and circumstances, a simple model is effectively accurate to about one meter (Spilker, 1996). In (Kaplan (Ed.), 1996), the one- σ value for the residual tropospheric delay is estimated as 1.5 m.

Orbital error, satellite clock error, and atmospheric delays are spatially correlated and can significantly be mitigated by differencing the measurements with a receiver at a known location, i.e., differential GPS (DGPS). In addition, the analytic error modeling based on the parameters included in the broadcast navigation message need to be utilized in order to reduce the errors.

Signal Multipath Errors

In multipath propagation, the measurement error is caused by reflected signals from the Earth and nearby objects, such as buildings and vehicles, entering the front end of a GPS receiver, and masking the real correlation peak by distorting the peak due to the presence of indirect signals (Parkinson and Spilker, 1996). In typical multipath, the antenna receives the line-of-sight (LOS) signal and one or more of its often weaker reflections. A simple picture describing the modes of degradation with attenuated signals and signals from multiple paths entering the receiver in poor signal-environments is shown in Fig. 5. Multipath can be divided into specular and diffuse multipath. In

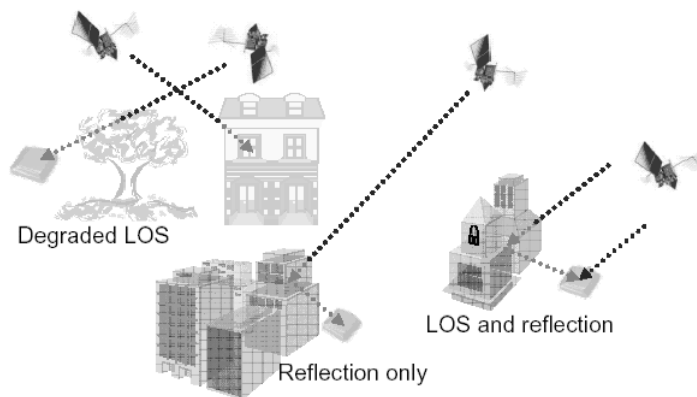


Fig. 5. Modes of Degradation in Urban Environments: Attenuation and Multipath Propagation.

specular multipath, parallel incident rays remain parallel after reflection, and in diffuse multipath, the incident wave is reflected in many directions. Specular multipath occurs on smooth surfaces, when the rays remain parallel, and diffuse multipath occurs due to rough surfaces, e.g., on an ocean surface, and results in scattered rays and loss of field strength in the direction of the antenna (Lachapelle, 2003). Multipath decorrelates spatially very rapidly and, thus, multipath cannot be reduced through differential processing. However, multipath is correlated from day-to-day for a given location, due to the periodic nature of the satellite orbits, if the reflection geometry is constant over time.

The interfering multipath signals actually change the phase being measured (Misra and Enge, 2001). Multipath generally causes a systematic error in the measurements

and can cause the measured range to be too large or too small with respect to the true range depending on the phase of the reflected signal or signals. Pseudorange

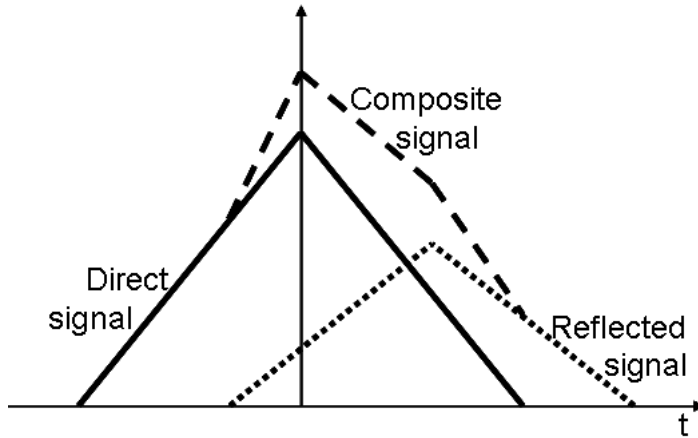


Fig. 6. Pseudorange Multipath Formulation.

multipath can be described as in Fig. 6, where the correlation function is presented in a fundamental level for the direct line-of-sight signal, the reflected signal, and the composite signal, which the receiver observes, i.e., the sum of the received signals. The reflected signal has a lower amplitude due to imperfect reflection. The range measurement error due to multipath depends on the strength of the reflected signal and the delay between the direct and reflected signals (Misra and Enge, 2001). Multipath affect both code and carrier measurements but the magnitude of the error is greater on the code measurement. In theory, pseudorange multipath error can reach magnitudes of about 0.5 of a code chip, i.e, 150 m in C/A case, depending on the receiver correlation technology. For narrow correlator receivers, the effect of multipath is lower.

Multipath error is dependent on the reflecting geometry. Overall, multipath can be mitigated by proper antenna site selection, receiver design, and error detection techniques. The antenna site should be selected in a way that there is a minimum amount of obstructions surrounding the antenna location. In addition, an antenna can be selected, which minimizes multipath, e.g., a groundplane or a choking antenna. In receiver design, multipath can also be taken into account in the hardware technology mostly for code multipath mitigation by using narrow correlators (van Dierendonck et al., 1992), strobe correlators, pulse aperture correlators (PAC), or multipath es-

timation delay lock loop (MEDLL) technology (Ray, 2000; Lachapelle, 2003). In the effort of mitigating multipath induced measurement errors, error detection and quality control algorithms such as RAIM and fault detection and isolation/exclusion (FDE/FDI) are also essential. GPS multipath error is greatly varying depending on the reflecting geometry surrounding the receiver antenna, and it can reach from under a meter with a carefully picked antenna type and location to over a hundred meters in worst cases in urban areas near large, high-rise buildings. Thus, since multipath is so difficult to model, it is a severe problem to the position accuracy. In (Kaplan (Ed.), 1996), a rough estimate of 2.5 m is estimated as the one- σ error due to multipath.

Multipath is indeed the largest error source in degraded signal environments, which are of most concern in this thesis. Due to the continuously changing satellite geometry and the motion of the user, the satellite signal reflections from the user surrounding obstructions are unpredictable, and the effects of multipath are very hard to foresee. A special case of multipath, especially when poor signal conditions are considered, is echo-only signal tracking, which is also shown in Fig. 6. The direct line-of-sight signal is faded to a non-acquirable power level but a few strong signal reflections still reach the antenna (Mezentsev, 2005). The range error caused by this type of phenomenon is theoretically unlimited.

3.2.3 Receiver-Based Range Errors

Receiver-based errors include antenna errors, the receiver clock error to be estimated in the solution computation, inter-channel biases, receiver noise, and timing and tracking errors.

Receiver inherent noise affects the resolution of the GPS code and carrier signals randomly. Receiver noise is a broad term including RF radiation sensed by the antenna in the band of interest unrelated to the signal, and noise introduced by the antenna, amplifiers, cables, and the receiver. Interference from other GPS signals and GPS-like broadcasts from system augmentations and signal quantization noise can also be counted as receiver noise (Misra and Enge, 2001).

In the delay-lock-loop of a GPS receiver, the dominant sources of pseudorange error are thermal noise jitter and the effects of dynamic stress error. The secondary sources of error include code hardware and software resolution and oscillator stability (Kaplan (Ed.), 1996). The C/A code receiver noise is generally one order of magnitude

higher compared to that of the P(Y) code due to the chip width of the C/A code being ten times that of the P(Y) code chip width (Ray, 2000; Kaplan (Ed.), 1996). In a typical modern receiver, the one- σ error of the receiver induced noise and resolution is estimated to be on the order of 1.5 m for the C/A-code (Kaplan (Ed.), 1996).

3.3 Signal Strength and Interference

Carrier-to-noise density, C/N_0 , is a measure of signal strength and it represents the current signal power conditions independently of receiver implementation, i.e., of the processing bandwidth. The C/N_0 is the most fundamental parameter describing the navigation signal quality. The units of C/N_0 are in dBHz. Typically, for a very strong GPS signal, the C/N_0 is larger than 40 dBHz. When the C/N_0 value goes beyond approximately 28 dBHz, the signal is weak, likely erroneous, and the receiver is also likely to lose lock on this signal (Lachapelle, 2003).

Signal-to-noise ratio, SNR, on the other hand, is a measure of signal strength relative to a processing bandwidth, and, thus, it is a measure of how well a given receiver will perform. The units of SNR are in dB, i.e., it is a dimensionless ratio.

The satellite navigation frequency bands are protected by international and Federal Communication Commission (FCC) frequency assignments. However, there is a chance of unintentional interference and even intentional interference on the satellite navigation signals (Parkinson and Spilker, 1996). Any radionavigation system can be disrupted by interference of sufficiently high power. Extra-terrestrial interference caused by fluctuations in the total electron content in the ionosphere diffract the radiofrequency signals into a pattern of amplitude and phase variations that move across the surface of the Earth in an effect known as scintillation. Terrestrial interference caused by out-of-band emissions of other signal sources, such as mobile and fixed very high frequency (VHF) and ultra high frequency (UHF) transmitters, broadcast television, and ultra-wideband radar and communications may produce harmonics in the L-band. GNSS signals are also vulnerable to disruptions in continuous functionality caused by unintentional human misunderstandings.

The intentional emission of radiofrequency energy of sufficient power and characteristics to prevent receivers in a target area from tracking GPS signals is called jamming (Lachapelle, 2003). Jamming can be accomplished by continuous wave, wideband,

narrowband, or GPS-type signals exceeding typically the GPS signal power by 40 dB to jam an already locked GPS receiver. Spoofing is an intentional interference mechanism aiming at shifting the position solution to be solved for by injecting misleading information to the system. A spoofing signal can be swept across the GPS signal time delay portion, where the receiver correlator gates are centered, and then be captured and pulled away from the true range. The spoofer must know the relative position of the target receiver and be able to predict the next code pulse to shorten the measured range (Lachapelle, 2003). The anti-spoofing encryption on the GPS P(Y)-code makes it difficult to be spoofed due to the spoofer being unaware of which code chip comes next in P(Y) but, however, the C/A-code is susceptible to spoofing. Techniques to improve jam resistance of GPS receivers may be classified into precorrelation methods that are waveform specific and include, e.g., adaptive spatial, temporal and spectral processing (Lachapelle, 2003), and postcorrelation methods including, e.g., the implementation of additional sensors. In addition, RAIM and FDE methods are also able to mitigate the effects of unintentional and intentional interference effects by detecting the inconsistency.

The planned GPS modernization efforts, i.e., the higher signal power, a C/A-code on the L2 frequency band, and a more robust civil code on L5, will reduce the susceptibility of civil GPS applications to interference (Lachapelle, 2003).

3.4 User Error Budgets

Based on the discussed pseudorange error constituents, a user error budget can be gathered to aid the understanding of standalone GPS accuracy. Since the error sources are reasonably independent, the square root of the sum of the squares of errors can be expressed as the user equivalent range error (UERE) in meters as follows

$$\sigma_{UERE} = \sqrt{\sigma_{eph}^2 + \sigma_{sc}^2 + \sigma_{iono}^2 + \sigma_{tropo}^2 + \sigma_{MP}^2 + \sigma_{noise}^2} \quad (12)$$

where σ_{eph}^2 is the error due to the ephemeris data, σ_{sc}^2 is the error due to the satellite clock, σ_{iono}^2 is the residual error due to the ionosphere, σ_{tropo}^2 is the residual error due to the troposphere, σ_{MP}^2 is the error due to multipath, and σ_{noise}^2 is the error due to receiver induced noise.

The probability level of UERE is about 68%. With the estimates for the standard deviations of the pseudorange error constituents in (Kaplan (Ed.), 1996), the approx-

imate total one- σ value for the UERE can be set as $\sigma_{UERE} \approx 8$ m. In real-life, the pseudorange error can rarely be represented with one unified estimate, since the error depends on the path length that the satellite signal passes through the atmosphere, i.e., the elevation angle, and often also on the power of the received signal, i.e., the carrier-to-noise ratio. A unified estimate for the range rate error, similar to the UERE, is not readily available to be formed, since the error constituents are in literature usually given only for the range observations. Overall, however, the position error is a function of both pseudorange errors and user-to-satellite geometry and, in the same manner, the velocity error is a function of both pseudorange rate errors and the solution geometry. Multiplying the UERE value with a dilution of precision (DOP) parameter, a value describing the user/satellite geometry, and estimated standard deviation of the position error can be obtained. The user/satellite geometry is discussed in later chapters of the thesis more thoroughly.

3.5 Real-Life Estimated Pseudorange and Pseudorange Rate Errors

This section presents real-life observed pseudorange and pseudorange rate errors obtained by post-processing when knowing the reference position and velocity in good, lightly degraded, and heavily degraded signal conditions. The pseudorange and pseudorange rate residuals were obtained by fixing the user position and velocity coordinates to known values and removing them from position and velocity computation leaving only the clock errors to be estimated. The residuals from this process can thus be regarded as unbiased estimates of the pseudorange and pseudorange rate errors, including atmospheric errors as well as multipath and receiver noise.

3.5.1 Good Signal Conditions

Pseudorange and pseudorange rate errors from good line-of-sight conditions are first presented with data obtained from a rooftop antenna presented in Fig. 7 with a SiRF XTrac-LP high sensitivity GPS (HSGPS) receiver for 23 minutes at afternoon hours. The reference position for the experiment was very accurate due to the location of the antenna being at a surveyed reference station.

The following Figures 8, 9, and 10 demonstrate that the errors are generally small in the good signal conditions, with a standard deviation of 4 m for the pseudorange



Fig. 7. Outdoor Roof: Multistorey Building.

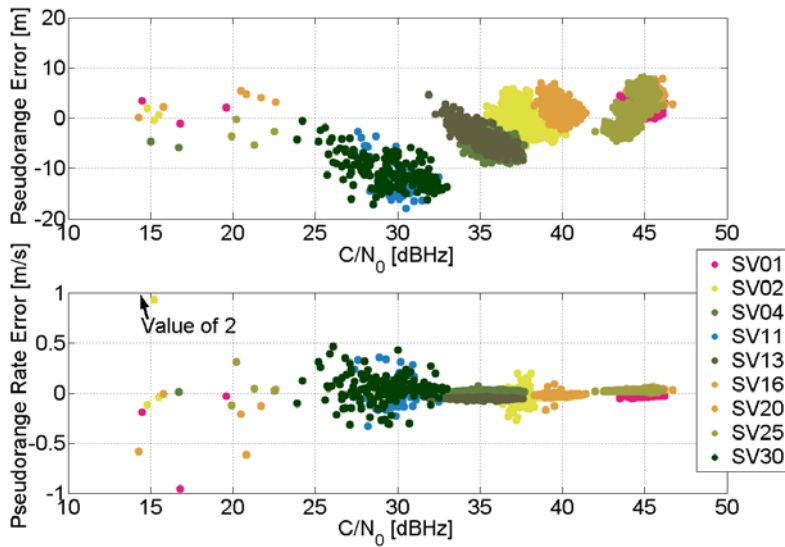


Fig. 8. Outdoor Roof: Pseudorange and Pseudorange Rate Errors vs. Carrier-to-Noise Ratios.

errors and 0.05 m/s for the pseudorange rate errors in this short experiment. First, errors are presented for each available satellite in the test as a function of their carrier-to-noise ratios, C/N_0 . Then, histograms of the errors as well as empirical cumulative

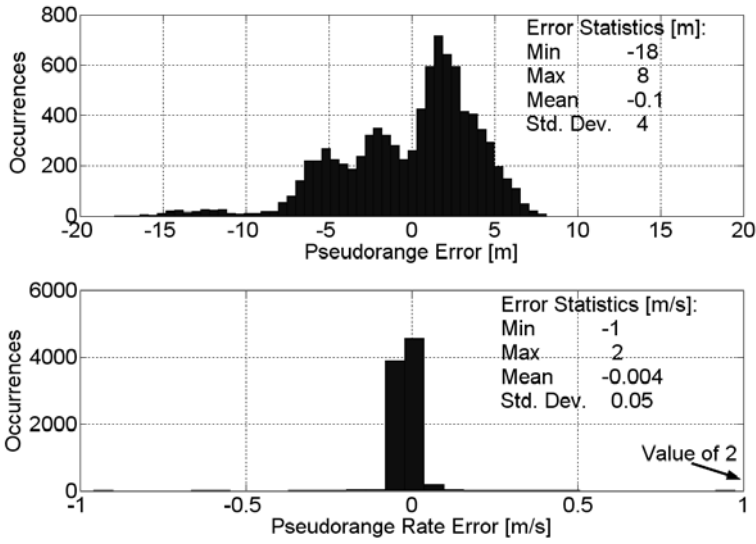


Fig. 9. Outdoor Roof: Histograms of Pseudorange and Pseudorange Rate Errors.

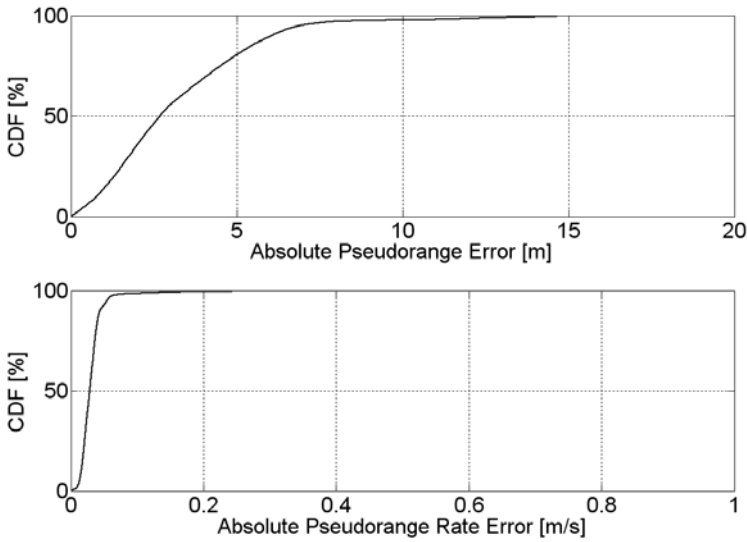


Fig. 10. Outdoor Roof: Empirical Cumulative Distribution Functions of Absolute Pseudorange and Pseudorange Rate Errors.

distribution functions of the absolute values of the errors describe the distribution of the errors in the pseudoranges and pseudorange rate observations, respectively. Error statistics for the pseudorange and pseudorange rate measurements are shown along with the histograms in Fig. 9.

3.5.2 Lightly Degraded Signal Conditions

Pseudorange and pseudorange rate errors from an indoor-experiment are shown, where HSGPS data were collected inside a wooden, residential garage for 12 hours using a SiRF XTrac-LP HSGPS receiver. The garage in question is shown in Fig. 11. The reference position for the test was obtained by surveying, and the reference is accurate within centimeters. The reference velocity for the static test is naturally zero.



Fig. 11. Indoor: Residential Garage.

Figures 12, 13, and 14 present the pseudorange and pseudorange rate errors for each satellite as functions of C/N_0 , as histograms, and as empirical cumulative distribution functions of the absolute error values, respectively. In addition, in Fig. 13, error statistics for the observations are provided.

In the wooden garage, the maximum errors caused mainly by multipath and cross-correlation effects are severe but overall the error level is moderate with the standard deviation for the pseudorange measurements being around 10 m and around 0.5 m/s for the pseudorange rate measurements.

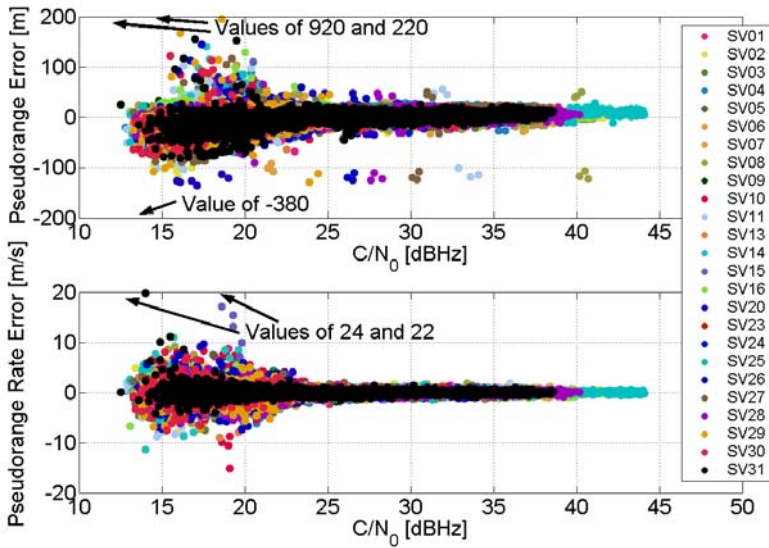


Fig. 12. Indoor: Pseudorange and Pseudorange Rate Errors vs. Carrier-to-Noise Ratios.

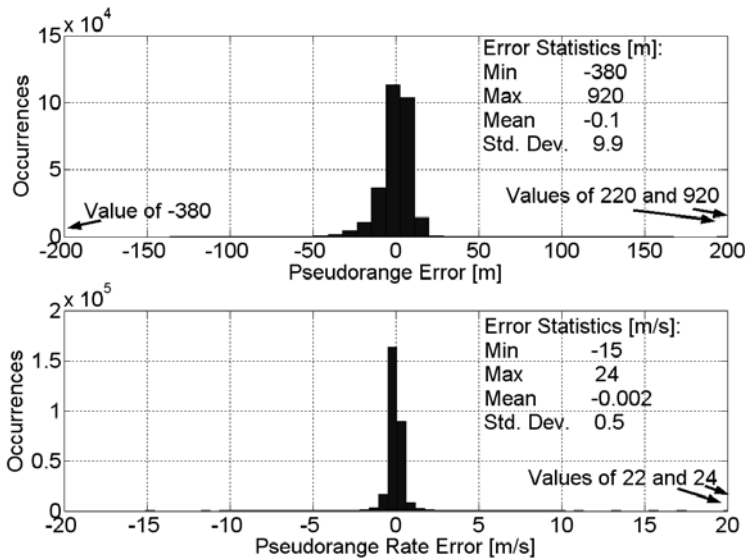


Fig. 13. Indoor: Histograms of Pseudorange and Pseudorange Rate Errors.

3.5.3 Heavily Degraded Signal Conditions

Pseudorange and pseudorange rate errors are presented from a 35-minute HSGPS test in a parking lot in a deep urban canyon shown in Fig. 15. The reference point

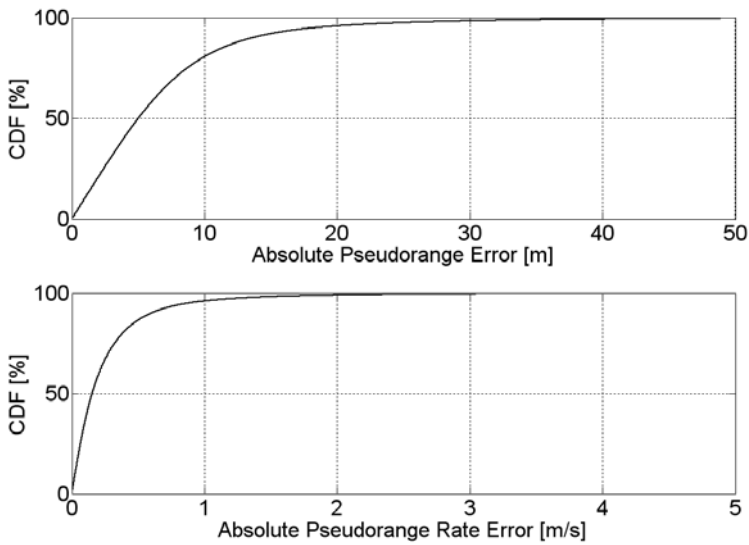


Fig. 14. Indoor: Empirical Cumulative Distribution Functions of Pseudorange and Pseudorange Rate Errors.

for the experiment accurate to a couple of meters was obtained by averaging reliable solutions and map matching. Naturally, the reference velocity was 0 m/s.



Fig. 15. Urban Canyon: Parking Lot.

Figures 16, 17, and 18 demonstrate the heavily deteriorated measurements obtained

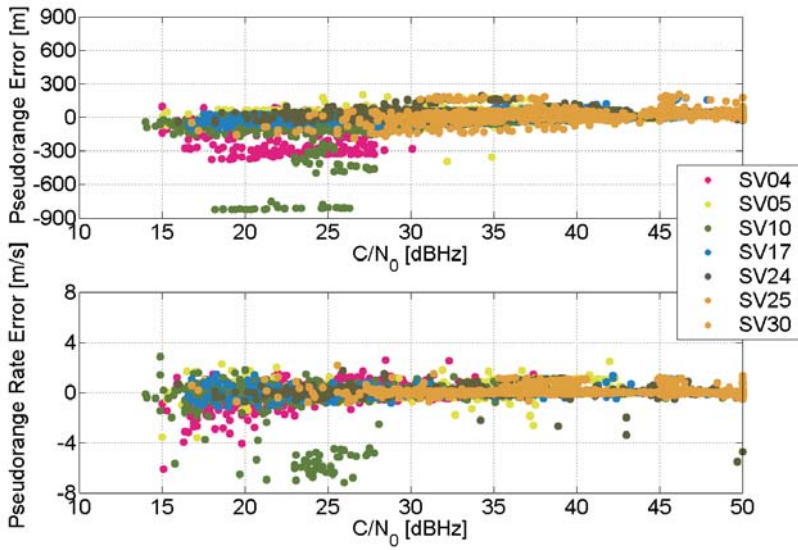


Fig. 16. Urban Canyon: Pseudorange and Pseudorange Rate Errors vs. Carrier-to-Noise Ratios.

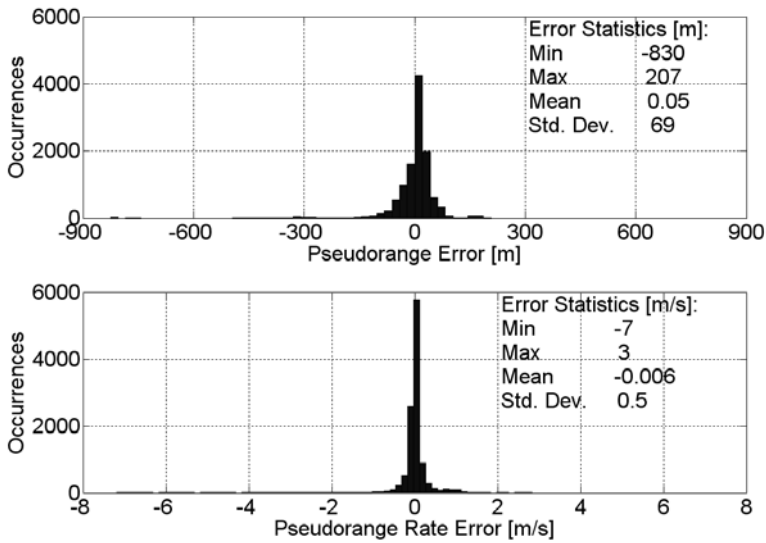


Fig. 17. Urban Canyon: Histograms of Pseudorange and Pseudorange Rate Errors.

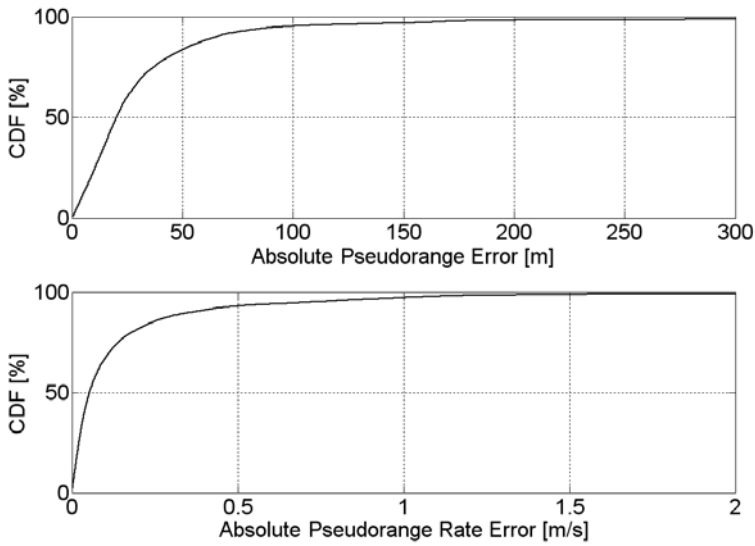


Fig. 18. *Urban Canyon: Empirical Cumulative Distribution Functions of Pseudorange and Pseudorange Rate Errors.*

in the parking lot in the urban area by presenting pseudorange and pseudorange rate errors as functions of C/N_0 , as histograms of the errors, and as cumulative distribution functions of the absolute errors. The signals in the short urban test are highly attenuated and contaminated by multipath and echo-only signals, with a standard deviation of the pseudorange error reaching 69 m and pseudorange rate error reaching 0.5 m/s, as presented in Fig. 17. The pseudorange errors are generally proportionally more deteriorated in this urban canyon experiment than the pseudorange rate measurements.

4. GNSS NAVIGATION SOLUTION ESTIMATION

This section discusses the estimation processes of user position, velocity, and time.

4.1 User Position, Velocity, and Time Solution

Positioning with GNSS is based on computing the user position from biased measurements of the satellite-to-user ranges, pseudoranges. Pseudoranges are here denoted with the symbol ρ . The user velocities are estimated from biased measurements of the satellite-to-user range rates, pseudorange rates. Pseudorange rates are denoted with the symbol $\dot{\rho}$.

First, position estimation is considered.

In order to determine user position in three dimensions and the offset of the receiver clock from system time, pseudorange measurements need to be made to at least four satellites. A single pseudorange is represented by

$$\rho_j = \|\mathbf{r}_j - \mathbf{r}\| + ct + \varepsilon_{\rho_j} \quad (13)$$

where j ranges from 1 to n and reference the satellites. The parameter n represents the number of satellites available. Vector \mathbf{r}_j is the satellite position vector at signal transmit time, \mathbf{r} is the receiver position vector at signal receive time, t is the bias in the receiver clock from system time in seconds, c is the speed of light, and ε_{ρ_j} is the composite of errors produced by, e.g., atmospheric delays, satellite ephemeris mis-modeling, and receiver noise. The pseudorange errors were discussed in the previous chapter.

To extract the user state to be estimated, $\mathbf{x} = [x, y, z, -ct]^T = [\mathbf{r}^T, -ct]^T$, where x , y , and z refer to the user position coordinates in Earth Centered Earth Fixed (ECEF) WGS-84 coordinate frame, the measurement equation (13) must be linearized about

a nominal value. Usually, this nominal value is a current best estimate (Parkinson and Spilker, 1996). With a nominal estimate of the state, $\mathbf{x}_0 = [\mathbf{r}_0^T, -ct_0]^T$, and estimates of bias contributions caused by ionospheric and tropospheric delays, relativistic effects, and satellite clock errors, $\epsilon_{\rho_j, 0}$, a prediction of the pseudorange measurement j can be obtained as follows

$$\rho_{j, 0} = \|\mathbf{r}_j - \mathbf{r}_0\| + ct_0 + \epsilon_{\rho_j, 0} \quad (14)$$

A reduced pseudorange measurement vector, $\Delta\rho$, is obtained as

$$\Delta\rho = \rho_0 - \rho \quad (15)$$

where ρ_0 and ρ are vectors of the predicted pseudoranges from Eq. 14 and the actually measured pseudoranges, respectively. If the linearization point is sufficiently close to the true values of position and receiver clock error, the reduced pseudorange measurements can be modeled as linearly related to the error in the state estimate, $\Delta\mathbf{x} = [\Delta\mathbf{r}^T, -c\Delta t]^T$ (Kaplan (Ed.), 1996; Parkinson and Spilker, 1996). By performing a Taylor expansion about the current state estimate, a linearized pseudorange equation is obtained as

$$\Delta\rho = \mathbf{H}\Delta\mathbf{x} + \Delta\epsilon_\rho \quad (16)$$

where \mathbf{H} denotes a linear connection matrix consisting of direction cosines of line of sight unit vectors pointing from the approximate user position to the available satellites. The vector $\Delta\epsilon_\rho$ contains residual pseudorange errors after the known biases have been removed, and it is assumed to be normally distributed according to $\Delta\epsilon_\rho \sim \mathbf{N}(0, \Sigma)$, where Σ is a diagonal covariance matrix of the observations. The linear connection matrix \mathbf{H} can be expressed as

$$\mathbf{H} = \begin{bmatrix} a_{x1} & a_{y1} & a_{z1} & 1 \\ a_{x2} & a_{y2} & a_{z2} & 1 \\ \vdots & \vdots & \vdots & \vdots \\ a_{xn} & a_{yn} & a_{zn} & 1 \end{bmatrix} \quad (17)$$

where

$$a_{xj} = \frac{x_j - x_0}{\|\mathbf{r}_j - \mathbf{r}\|} \quad (18)$$

$$a_{yj} = \frac{y_j - y_0}{\|\mathbf{r}_j - \mathbf{r}\|} \quad (19)$$

$$a_{zj} = \frac{z_j - z_0}{\|\mathbf{r}_j - \mathbf{r}\|} \quad (20)$$

and x_j , y_j , and z_j refer to the coordinates of satellite j and x_0 , y_0 , and z_0 refer to the coordinates of the approximate user position \mathbf{x}_0 .

The linearized model in Eq. (16) is the fundamental pseudorange measurement equation in navigation (Parkinson and Spilker, 1996). The unknown array $\Delta\mathbf{x}$, defined as

$$\Delta\mathbf{x} = [\Delta x, \Delta y, \Delta z, -c\Delta t]^T \quad (21)$$

is the vector offset of the user's true position and time bias, \mathbf{x} , from the values at the linearization point, \mathbf{x}_0 . Once the unknowns $\Delta\mathbf{x}$ are obtained, the user coordinates and the receiver clock offset are obtained as follows

$$\mathbf{x} = \mathbf{x}_0 + \Delta\mathbf{x} \quad (22)$$

Since $\Delta\rho$ is contaminated by unknown random errors as discussed in Chapter 3, equation (16) should be treated as a stochastic equation and the unknown to be estimated for, $\Delta\mathbf{x}$, should be determined using parameter estimation techniques such as least squares estimation. The estimation of parameters in linear models means essentially the estimation of the expected values of the observations (Koch, 1999).

As in the first step of position computation the system of equations must be linearized, then in the second step the solution has to be calculated with the help of an iterative procedure. If the displacement from the linearization point to be solved for exceeds an acceptable value, the process is reiterated with ρ_0 being replaced by a new estimate of pseudorange from equation (14) based on the calculated point coordinates x , y , and z (Kaplan (Ed.), 1996). The iterations are stopped when the displacement is within close proximity to the current linearization point.

For user velocity computation, a similar estimation process as for the user position can be conducted. The pseudorange rate observation can be expressed as

$$\dot{\rho}_j = (\mathbf{v}_j - \mathbf{v}) \cdot \frac{\mathbf{r}_j - \mathbf{r}}{\|\mathbf{r}_j - \mathbf{r}\|} + ct + \varepsilon_{\dot{\rho}_j} \quad (23)$$

where t is the receiver clock drift in seconds/s, the vector \mathbf{v}_j is the satellite velocity vector at signal transmit time, \mathbf{v} is the receiver velocity vector at signal receive time, and $\varepsilon_{\dot{\rho}_j}$ is the error in the observation in m/s. Again, the observation can be predicted based on the current estimates, and, thus, the predicted pseudorange rate observation can be written as

$$\dot{\rho}_{j,0} = (\mathbf{v}_j - \mathbf{v}_0) \cdot \frac{\mathbf{r}_j - \mathbf{r}_0}{\|\mathbf{r}_j - \mathbf{r}_0\|} + ct_0 + \varepsilon_{\dot{\rho}_{j,0}} \quad (24)$$

The vector of the reduced pseudorange rate measurements is obtained as

$$\Delta\dot{\rho} = \dot{\rho}_0 - \dot{\rho} \quad (25)$$

The linearized Doppler measurement equation is then obtained as follows (Kaplan (Ed.), 1996; Parkinson and Spilker, 1996; Misra and Enge, 2001)

$$\Delta\dot{\rho} = \mathbf{H}\dot{\mathbf{x}} + \Delta\varepsilon_{\dot{\rho}} \quad (26)$$

with the unknown user velocity estimate vector being $\dot{\mathbf{x}} = [\dot{x}, \dot{y}, \dot{z}, -ct]^T$.

4.2 Least Squares Navigation Solution

In order to reduce the influence of errors in the observations, a greater number of measurements than the number of unknown parameters in the model can be used (Björck, 1996). Thus, when using measurements from more than four satellites, the resulting problem is to solve an overdetermined linear system of equations.

To address the problem more generally than just for the user position and velocity estimation, let's assume that the n -dimensional vector $\mathbf{y} \in \mathbf{R}^n$ of observations is related to the p -dimensional unknown parameter vector $\mathbf{x} \in \mathbf{R}^p$ by a linear relation of the following form

$$\mathbf{y} = \mathbf{H}\mathbf{x} + \varepsilon \quad (27)$$

where the $n \times p$ -dimensional matrix $\mathbf{H} \in \mathbf{R}^{n \times p}$ is a known linear connection matrix and ε is a vector of random errors normally distributed as $\mathbf{N}(0, \Sigma)$. In addition, in the linearized model, it is assumed that

$$E(\mathbf{y}) = \mathbf{H}\mathbf{x} \quad (28)$$

$$V(\mathbf{y}) = \Sigma \quad (29)$$

where $E(\cdot)$ is the expectation function and $V(\cdot)$ is the variance covariance function (Draper and Smith, 1981). The general linear model presented in Eq. 27 follows a Gauss-Markoff model (Koch, 1999).

A least squares solution (LS) minimizes the sum of the squared residuals (Björck, 1996; Kay, 1993; Koch, 1999), i.e.,

$$\min_{\mathbf{x}} \|\mathbf{H}\mathbf{x} - \mathbf{y}\|^2 \quad (30)$$

When applied to the navigation problem, the minimization problem can be expressed as

$$\min_{\Delta \mathbf{x}} \|\mathbf{H}\Delta \mathbf{x} - \Delta \rho\|^2 \quad (31)$$

for the position estimation case, and as

$$\min_{\dot{\mathbf{x}}} \|\mathbf{H}\dot{\mathbf{x}} - \Delta \dot{\rho}\|^2 \quad (32)$$

for the velocity estimation case. The $\|\cdot\|$ denotes the Euclidean vector norm.

A weighted least squares (WLS) estimate is equal to a best linear unbiased estimate (BLUE) (Koch, 1999) if the inverse of the variance covariance matrix (VCM) of the observations, Σ^{-1} , is used as weight matrix. The BLUE is the most convenient estimate for practical implementations because it yields the lowest estimation error among all linear estimators (Kay, 1993). Weighted least squares tries to arrive at a best solution by minimizing the sum of the weighted discrepancies among observations (Kuang, 1996). With the assumption that $\mathbf{H}^T \Sigma^{-1} \mathbf{H}$ is non-singular, which is the case if Σ is non-singular and there are at least as many independent observations as unknowns, the BLUE of the unknown user parameters \mathbf{x} is (Draper and Smith, 1981; Neter et al., 1996; Huber, 1981)

$$\hat{\mathbf{x}} = (\mathbf{H}^T \Sigma^{-1} \mathbf{H})^{-1} \mathbf{H}^T \Sigma^{-1} \mathbf{y} \quad (33)$$

Similarly, the weighted least squares solution of the incremental user position $\Delta \mathbf{x}$ is

$$\Delta \hat{\mathbf{x}} = (\mathbf{H}^T \Sigma_{\rho}^{-1} \mathbf{H})^{-1} \mathbf{H}^T \Sigma_{\rho}^{-1} \Delta \rho \quad (34)$$

and the BLUE of the user velocity $\dot{\mathbf{x}}$ is

$$\hat{\dot{\mathbf{x}}} = (\mathbf{H}^T \Sigma_{\dot{\rho}}^{-1} \mathbf{H})^{-1} \mathbf{H}^T \Sigma_{\dot{\rho}}^{-1} \Delta \dot{\rho} \quad (35)$$

The weight matrix, i.e., the inverse of the covariance matrix of the observations, can be obtained from general assumptions or models, and by assessing the observations. Signal elevation or strength dependent variance models can be used, and they will be discussed more in the following chapters.

When in velocity estimation the resulting BLUE estimate of Eq. 35 is the user velocity estimate, in position computation, on the other hand, the estimate of the unknown user position coordinates, $\hat{\mathbf{x}}$, is obtained by adding the incremental component $\Delta \hat{\mathbf{x}}$ of Eq. 34 to the linearization point as follows

$$\hat{\mathbf{x}} = \mathbf{x}_0 + \Delta \hat{\mathbf{x}} \quad (36)$$

The optimality of the previous BLUE requires that the linearization error is negligible, and to ensure this, the estimation is repeated with the previous estimate as new approximation until convergence is obtained.

The advantage in using parameter estimation and actually treating the observations as random values rather than computing a unique solution from just as many observations as necessary is to have access to the redundancy, which is the basis of both improved precision and quality control. Assuming a correct measurement model, observational residuals defined as the difference between the estimated values of the observations and their corresponding measured values (Kuang, 1996) indicate the extent to which the measurements agree with each other. Outliers, i.e., gross errors, pose a serious threat to least squares analysis (Barnett and Lewis, 1978; Miyashita, 1982). Residuals are, therefore, useful for monitoring the quality of the estimated parameters. Least squares estimation by itself has a breakdown point of 0%, which reflects the extreme sensitivity of the least squares method to outliers (Rousseeuw and Leroy, 1987). The breakdown point can be defined as the smallest fraction of contamination that can cause the estimator to take values arbitrarily far from the regression coefficients (Rousseeuw and Leroy, 1987).

Often, additional information on the user position is available, e.g., the height. The additional information will result in an increased measurement redundancy for the solution computation as well as the quality checking availability. This information can be incorporated strictly as a condition; however, to account for the uncertainty of this additional information it is often better to treat it as an additional measurement. This is also easily accomplished, since after a simple coordinate transformation to the local level frame, no modification to the above model is required except for adding a row to the design matrix \mathbf{H} and $\Delta\rho$ and a row and column to Σ_p . If the variance of this additional observation is low w.r.t. that of the pseudorange measurements as is the case when the height is known, the observation acts like a constraint and leaves only horizontal and time components as unknowns to be estimated. This approach is denoted as height constraining, and it is incorporated in the computation of the results in the section presenting the testing and analysis.

4.3 Kalman Filtering in Navigation

The least squares approach takes into account only the current measurements when estimating the unknown user position or velocity. Kalman filtering (Gelb, 1974; Brown and Hwang, 1997), however, combines information of the statistical nature of system errors with information of system dynamics, as represented by a state space model, to arrive at an estimate of the state of the navigation system (Kaplan (Ed.), 1996). A Kalman filter is a recursive algorithm that uses a series of prediction and measurement update steps to obtain an estimate of the state vector. The advantage of the Kalman filter is the ability to take past measurements and aid the current epoch by propagating past measurement to the present. However, if the dynamic model is incorrect, the solution will be suboptimal even with good measurements (Ryan, 2002).

Kalman filtering is often the most preferred choice for navigation applications. However, due to the low accuracy level, the absence of additional sensors apart from the GPS receiver, and the poor knowledge about the user dynamics, the usual advantages of a Kalman filter do not apply in the severely degraded signal conditions of concern in this thesis. The dynamic model needed for filtering may not be known in personal satellite-navigation applications. However, all the strategies for reliability monitoring and quality control can easily be applied to Kalman filtering as well (Kuusniemi et al., 2004). The weight models can be used without modifications, and the global and local reliability tests to be discussed can be performed using the innovations in the testing as described in (Teunissen, 1998). If the predicted state is also erroneous, the FDE can be performed as described in this thesis later on but applied on the estimated filtering residuals of an extended least squares model (Wieser et al., 2004; Hewitson and Wang, 2004), which results from adding the predicted states as direct observations to the measurement model.

4.4 Robust Estimation Techniques in Navigation

In addition to least squares estimation or the Kalman filtering approach, different estimators that are robust against errors can be chosen for the navigation solution computation. Not much effort will here be invested into the different robust techniques and only a few remarks on the existence of such estimators will briefly be

discussed.

An outlier in a set of data can be defined as an observation, which appears to be inconsistent with the remainder of that set of data (Barnett and Lewis, 1978; Beckman and Cook, 1983). The observations might be falsified by outliers, which change the distribution of the observations. An estimator is to be said robust if its distribution is insensitive to small changes in the distribution of the population (Koch, 1999) or deviations from the assumptions (Huber, 1981; Hampel et al., 1986), i.e., if it, to some extent, tolerates outliers.

A least median of squares (LMS) method (Rousseeuw and Leroy, 1987) is an estimator that is very robust with respect to outliers and is capable of surviving outliers in the data set if they are less than 50%. However, the LMS cannot be easily migrated from a single parameter case with independent, identically distributed observations to a heterogeneous multiparameter case. Certain M-estimators, that are generalizations of maximum likelihood estimation, are fairly robust against outliers, and were originally introduced by Huber (Huber, 1981). However, the M-estimators cannot be established if the distribution of the observations is unknown. In addition, there exist certain empirical robust estimation procedures with no generally valid statistical explanation, such as, e.g., an iteratively re-weighted least squares estimator, e.g., (Rousseeuw and Leroy, 1987; Jørgensen et al., 1985), which is simple, computationally efficient, and has been found to perform well in practical implementations. Its application into navigation in degraded signal environments will be presented in the later chapters of this thesis.

4.5 Geometrical Aspects

The quality of the user position estimate depends not only on the quality of the range measurements but also on the user/satellite observation geometry. The dilution of precision (DOP) concept provides a simple quality measure of the user/satellite geometry (Kaplan (Ed.), 1996; Misra and Enge, 2001; Strang and Borre, 1997; Hofmann-Wellenhof et al., 2001). DOP is a measure of the geometrical strength of the satellite configuration (Wells et al., 1987). Bad geometry may amplify random errors and biases and, therefore, produce large position errors.

The concept of dilution of precision is the idea that the position error that results from

measurement errors depends on the user/satellite relative geometry, as formulated in (Kaplan (Ed.), 1996). In a simplified example in Fig. 19, a user receiver obtains measures for the distances between the receiver and a pair of satellites, S_1 and S_2 , at known locations. If the range measurements were perfect, the user receiver would obtain its location exactly at the intersection of two circles centered at S_1 and S_2 with the measured ranges as their radii (Misra and Enge, 2001). However, due to range measurements being imperfect, uncertainty is obtained in the user location with the amount of uncertainty depending besides the range measurement errors on the user/satellite geometry. While in the two cases a) and b) in Fig. 19 the quality of the range measurements is the same, clearly the quality of the position estimates is better in case a) due to the area of uncertainty, the shaded area, is consequently smaller. Overall, case a) has better geometry, and, thus, smaller dilution of precision.

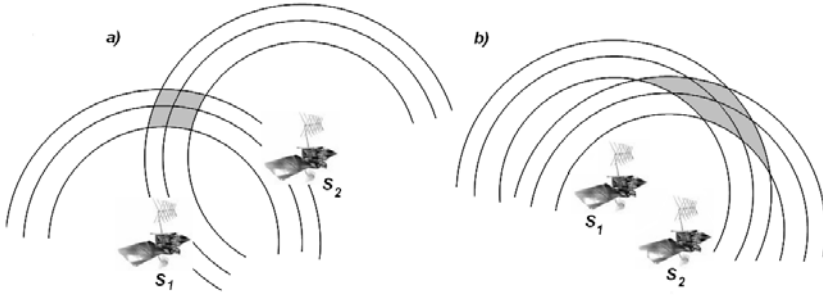


Fig. 19. Relative Geometry and Dilution of Precision.

The formal derivation of the DOP concept is provided in, e.g., (Kaplan (Ed.), 1996; Parkinson and Spilker, 1996). Basically, the DOP parameters can be computed from the elements of a cofactor matrix $\mathbf{Q} = (\mathbf{H}^T \mathbf{H})^{-1}$ expressed as

$$\mathbf{Q} = \begin{bmatrix} q_{xx} & q_{xy} & q_{xz} & q_{xt} \\ q_{yx} & q_{yy} & q_{yz} & q_{yt} \\ q_{zx} & q_{xy} & q_{zz} & q_{zt} \\ q_{tx} & q_{ty} & q_{tz} & q_{tt} \end{bmatrix} \quad (37)$$

The matrix \mathbf{H} is the design matrix, i.e., the linear connection matrix defined in Eq. 17. The commonly used DOP parameters include GDOP (Geometric DOP), PDOP (Position DOP), and TDOP (Time DOP), and they are defined as

$$GDOP = \sqrt{q_{xx} + q_{yy} + q_{zz} + q_{tt}} \quad (38)$$

$$PDOP = \sqrt{q_{xx} + q_{yy} + q_{zz}} \quad (39)$$

$$TDOP = \sqrt{q_{tt}} \quad (40)$$

The position deviation vector from the linearization point, the vector $\Delta \mathbf{x}$, was defined in the ECEF coordinate frame but with an orthonormal matrix \mathbf{R}_L it can be represented in a topocentric local east north up (ENU) coordinate frame (Misra and Enge, 2001) as

$$\Delta \mathbf{x}_L = \mathbf{R}_L \Delta \mathbf{x} \quad (41)$$

where $\Delta \mathbf{x}_L = [\Delta x_E, \Delta y_N, \Delta z_U]^T$ and \mathbf{R}_L is expressed by

$$\mathbf{R}_L = \begin{bmatrix} -\sin(\lambda) & \cos(\lambda) & 0 & 0 \\ -\sin(\varphi)\cos(\lambda) & -\sin(\varphi)\sin(\lambda) & \cos(\varphi) & 0 \\ \cos(\varphi)\cos(\lambda) & \cos(\varphi)\sin(\lambda) & \sin(\varphi) & 0 \end{bmatrix} = \begin{bmatrix} \mathbf{R}_{L_{1,2}} \\ \mathbf{R}_{L_3} \end{bmatrix} \quad (42)$$

where the parameters φ and λ represent the latitude and longitude of the geodetic coordinates of the user, respectively. Transforming the cofactor matrix \mathbf{Q} from the equatorial system to the topocentric local coordinate system by using the transformation matrix \mathbf{R}_L while ignoring the time parameter can be expressed as (Hofmann-Wellenhof et al., 2001)

$$\mathbf{Q}_L = \mathbf{R}_L \mathbf{Q} \mathbf{R}_L^T = \begin{bmatrix} q_{xLxL} & q_{xLyL} & q_{xLzL} \\ q_{yLxL} & q_{yLyL} & q_{yLzL} \\ q_{zLxL} & q_{zLyL} & q_{zLzL} \end{bmatrix} \quad (43)$$

The elements of the transformed cofactor matrix yield to HDOP (Horizontal DOP) and VDOP (Vertical DOP), and they are expressed as

$$HDOP = \sqrt{q_{xLxL} + q_{yLyL}} \quad (44)$$

$$VDOP = \sqrt{q_{zLzL}} \quad (45)$$

4.6 Accuracy Estimation

When the general linear model of Eq. 27 is assumed and redundant observations have been obtained, least squares residuals in a navigation situation can be formed as

$$\hat{\mathbf{v}} = \mathbf{H}\hat{\mathbf{x}} - \mathbf{y} \quad (46)$$

The a posteriori variance factor of the estimation process can be expressed as

$$\hat{\sigma}_0^2 = \frac{\hat{\mathbf{v}}^T \boldsymbol{\Sigma}^{-1} \hat{\mathbf{v}}}{n - p} \quad (47)$$

The covariance matrix of the estimated unknowns gives a measure of the accuracy of the estimated parameters and their correlation

$$\boldsymbol{\Sigma}_{\hat{\mathbf{x}}} = (\mathbf{H}^T \boldsymbol{\Sigma}^{-1} \mathbf{H})^{-1} \quad (48)$$

Estimates of the accuracy and reliability of the user parameters, both for position and velocity, can be obtained when multiplying the a posteriori variance factor, $\hat{\sigma}_0^2$, with the covariance matrix of the estimated user parameters, $\boldsymbol{\Sigma}_{\hat{\mathbf{x}}}$, resulting in mean radial spherical error (MRSE) and distance root mean squared (DRMS) estimates (Leick, 2004). In the local level frame, an estimated covariance matrix of the estimated unknowns can thus be expressed as

$$\hat{\boldsymbol{\Sigma}}_{\hat{\mathbf{x}},L} = \hat{\sigma}_0^2 \mathbf{R}_L \boldsymbol{\Sigma}_{\hat{\mathbf{x}}} \mathbf{R}_L^T = \hat{\sigma}_0^2 \mathbf{R}_L (\mathbf{H}^T \boldsymbol{\Sigma}^{-1} \mathbf{H})^{-1} \mathbf{R}_L^T = \begin{bmatrix} \hat{\sigma}_N^2 & \hat{\sigma}_{NE} & \hat{\sigma}_{NU} \\ \hat{\sigma}_{NE} & \hat{\sigma}_E^2 & \hat{\sigma}_{EU} \\ \hat{\sigma}_{NU} & \hat{\sigma}_{EU} & \hat{\sigma}_U^2 \end{bmatrix} \quad (49)$$

which leads to the three-dimensional MRSE and two-dimensional DRMS accuracy estimates

$$M = \sqrt{\hat{\sigma}_N^2 + \hat{\sigma}_E^2 + \hat{\sigma}_U^2} \quad (50)$$

$$D = \sqrt{\hat{\sigma}_N^2 + \hat{\sigma}_E^2} \quad (51)$$

The estimates M and D can be used to assess the trustworthiness and accuracy of the estimated solution. The M estimate contains about 61% probability (Leick, 2004; van Diggelen, 1998) while the measure D contains about 63% of probability (Hofmann-Wellenhof et al., 2001; van Diggelen, 1998).

5. RELIABILITY THEORY

The advantage in using parameter estimation and actually treating the observations as random values rather than computing a unique solution from just as many observations as necessary is to have access to the redundancy, which is the key to improved precision and quality control. The relation between satellite measurements and unknown navigation parameters is comprised in the functional model, while the uncertainty is described in the stochastic model. Gross errors like outliers, i.e., blunders, are not captured in the functional relation, and since gross errors are different from ordinary noise modeled by the stochastics, the stochastic model can not either account for the blunders. The occurring blunders will bias the navigation solution and, thus, it is important to detect the anomalies in the observations and exclude them. The detection of model errors is based on statistical hypothesis testing to which the presence of redundant measurements is crucial (Tiberius, 1998). Assuming a correct measurement model, observational residuals defined as the difference between the estimated values of the observations and their corresponding measured values (Kuang, 1996) indicate the extent to which the measurements agree with each other. Residuals are, therefore, useful for monitoring the quality of the estimated parameters. Without sufficient redundancy, no consistency checks can be performed, quality control becomes infeasible, and there is no way of testing whether the data can be considered to be statistically consistent with the assumed model (Teunissen, 1990).

The performance of a navigation situation can be defined with parameters such as accuracy, availability, integrity, continuity, and reliability. Accuracy is the ability of the system to maintain the position within a total system error and availability is the percentage of time that the services of a navigation system are usable. Integrity is often defined as the ability of the navigation system to provide timely warnings to the user when the system should not be used for navigation and continuity as the capability of a system to provide navigation accuracy and integrity throughout an intended operation (Ober, 2003). Reliability refers to the ability to detect blunders

and to estimate the effects that undetected blunders may cause on a solution (Leick, 2004) and it is defined more carefully in this chapter.

When redundant observations have been made and the general linearized model is assumed, least squares residuals of the observations \mathbf{y} can be obtained as

$$\hat{\mathbf{v}} = \mathbf{H}\hat{\mathbf{x}} - \mathbf{y} = -\mathbf{R}\mathbf{y} \quad (52)$$

where \mathbf{R} is a projector from the reduced observations to the LS residuals. For the redundancy matrix, the following equation can be derived

$$\mathbf{R} = \mathbf{C}_{\hat{\mathbf{v}}}\Sigma^{-1} \quad (53)$$

where the matrix $\mathbf{C}_{\hat{\mathbf{v}}}$ denotes the covariance matrix of the residuals and is computed as follows

$$\mathbf{C}_{\hat{\mathbf{v}}} = \Sigma - \mathbf{H}(\mathbf{H}^T\Sigma^{-1}\mathbf{H})^{-1}\mathbf{H}^T \quad (54)$$

The trace of the matrix \mathbf{R} is the overall redundancy, i.e., the degree of freedom, e.g., (Schaffrin, 1997), and, therefore, \mathbf{R} is referred to as the redundancy matrix. With uncorrelated observations, this matrix plays a key role in quality control. The i th diagonal element of matrix \mathbf{R} , r_i , corresponds to the contribution of the i th observation to the overall redundancy but it is also the scale factor with which a bias of an observation will be reflected by its residual. It can be proven (Kuang, 1996; Leick, 2004) that each r_i is always between 0 and 1 and they sum up the total redundancy of the system. The r_i can be seen as the contribution of the observation \mathbf{y}_i to the total redundancy of the system (Kuang, 1996). A balanced adjustment problem would have all the diagonal elements of the redundancy matrix approximately equal. When r_i is close to zero, the i th observation contributes very little to the redundancy, which also implies that it is hardly controlled by the other observations. Thus, very small redundancy numbers are not desirable, and a zero redundancy number implies an uncontrolled observation, e.g., (Leick, 2004).

The effect, $\nabla_i\hat{\mathbf{v}}_i$, of an error $\nabla\mathbf{y}_i$ in observation \mathbf{y}_i onto its corresponding residual is determined by the i th diagonal element of \mathbf{R} as

$$\nabla_i\hat{\mathbf{v}}_i = -r_i\nabla\mathbf{y}_i \quad (55)$$

Since r_i is always between 0 and 1, possibly only a small part of an error shows up in the residuals and the rest of it will be absorbed in the determination of the

unknown parameters. An error in a observation that has a large redundancy number will affect more the corresponding residual and is easier to be detected. The effect of a gross error $\nabla \mathbf{y}_i$ in observation \mathbf{y}_i onto the other residuals $\hat{\mathbf{v}}_j$ ($j \neq i, j = 1 : n$), $\nabla_i \hat{\mathbf{v}}_j$, is determined by the off-diagonal elements of the redundancy matrix \mathbf{R} as

$$\nabla_i \hat{\mathbf{v}}_j = -r_{ji} \nabla \mathbf{y}_i, \quad j \neq i, \quad j = 1 : n \quad (56)$$

Thus, due to the correlation of the residuals, a gross error in an observation might have spread over all the residuals. If a blunder is large enough to cause many reliability test failures, resulting in many alternatives, it is essential to ensure that any two alternatives are separable (Hewitson, 2003). Therefore, in order to pinpoint the erroneous observation \mathbf{y}_i through examination of its corresponding residual $\hat{\mathbf{v}}_i$, the following equation (Kuang, 1996) must be assessed

$$r_i > |r_{ji}| \quad (j \neq i, \quad j = 1 : n) \quad (57)$$

If Eq. 57 does not hold, localization of the gross error is difficult.

The residual vector, $\hat{\mathbf{v}}$, can be used to test the internal consistency among the observations (Kuang, 1996). The vector can also be used to check the validity of the assumptions underlying the used functional and stochastic models and further to detect and identify a potential model error (Teunissen, 1998). In this thesis, reliability is considered to consist of reliability testing, i.e., detecting and identifying a measurement error as in RAIM, and statistical reliability, i.e., assessing theoretical reliability conditions.

5.1 Reliability Testing

Conceptually, statistical reliability tests serve to determine whether or not anything has gone wrong with the basic postulates assumed. A null hypothesis (H_0) denoting a fault-free situation is a reference level from which any deviation of the different alternative hypothesis (H_a) has to be detected by statistical testing. Due to the finiteness of the available sample in statistical testing, no definite statistical decision can be made (Kuang, 1996). There are always two types of potential errors involved in a statistical test identified as type I and type II errors. Type I error is defined as the error of rejecting the null hypothesis H_0 when H_0 is actually true. The probability of committing a type I error is called the significance level, denoted as α , and the probability

of making a correct decision is called the confidence level $(1 - \alpha)$. A type II error is defined as the error of accepting H_0 when it is actually false, and the probability of committing this type of error is denoted by β . The probability of rejecting H_0 when it is indeed false is called the power of the test $(1 - \beta)$. Table 4 summarizes the statistical testing of the null hypothesis against the alternative hypothesis (Kuang, 1996). It

Table 4. Statistical Testing of a Null Hypothesis against an Alternative Hypothesis.

Situation	Decision	Accept H_0	Reject H_0
H_0 is true		Correct decision Confidence level $1 - \alpha$	Type I error Significance level α
H_0 is false		Type II error Probability β	Correct decision Power of the test $1 - \beta$

is assumed that under H_0 and H_a the probability density functions of a chosen statistic take the same form but have different mean and variance values as shown in Fig. 20. In Fig. 20, the power of the test also defines the smallest difference δ that can be detected if the test has been executed at a significance level α (Kuang, 1996). If the

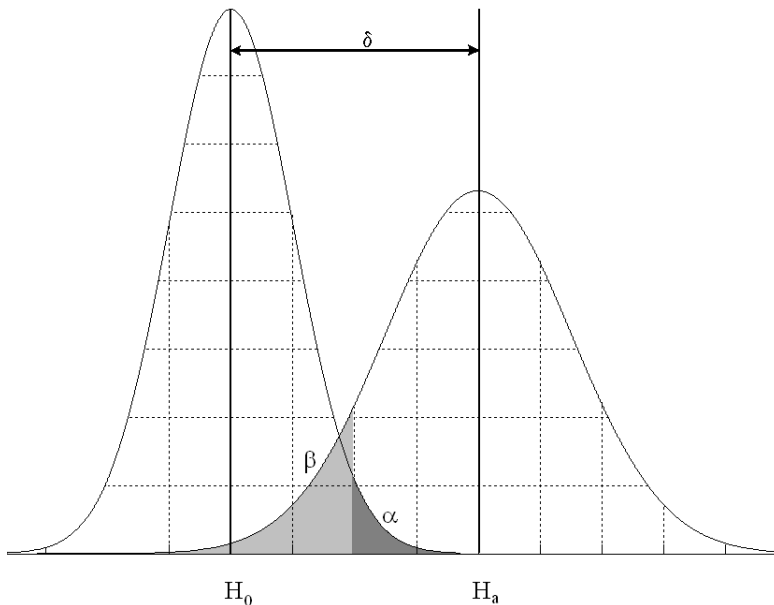


Fig. 20. Type I Error α and Type II Error β in an One-Tailed Test.

probability of both types I and II of error is wished to be decreased, δ , the internal reliability, will be increased, i.e., the detectable difference between H_0 and H_a , will be larger.

To detect a measurement error, the least squares residuals can be statistically tested. In a 'global test', the null-hypothesis H_0 states that the adjustment model is correct and the distributional assumptions meet the reality, as opposed to the alternative H_a which states that the adjustment model is not correct (Leick, 2004; Baarda, 1968; Kuang, 1996; Ryan, 2002). If the global test fails, a 'local test' with more specific alternative hypotheses needs to be performed for failure isolation.

The outlier detection and isolation is based on statistical testing of the estimated observational residuals. The estimated residuals are, in principle, indicative of the behavior of both the observation and the mathematical model. However, it is very difficult to separate the two since mathematically either a bad geometrical model and model assumptions or bad observations will affect the residuals in the same way. In the error detection and isolation process, the errors in the linearized model are assumed Gaussian zero-mean in the unbiased error-free case.

5.1.1 Global Test

The global test for detecting an inconsistent adjustment model is based on the quadratic form $\hat{\mathbf{v}}^T \Sigma^{-1} \hat{\mathbf{v}}$, which follows a central chi-square distribution with $n - p$ degrees of freedom if the observation errors are normally distributed as $\mathbf{N}(0, \Sigma)$ (Kuang, 1996; Leick, 2004). The parameter p denotes the number of parameters to be estimated and n the number of available observations. If the test statistic exceeds a threshold $\chi^2_{1-\alpha, n-p}$ where α represents the false alarm rate, i.e., the significance level of the global test, the null hypothesis H_0 is rejected in favor of H_a . Fig. 21 presents the central and non-central χ^2 density functions for eight degrees of freedom, $n - p = 8$, that represent the null-hypothesis, H_0 , and the alternative hypothesis, H_a , of the global consistency test. In Fig. 21, parameter β represents the probability of a missed detection and δ the non-centrality parameter of the biased χ^2 distribution. The hypothesis testing in the global test is conducted as

$$H_0 : (\text{No Integrity Failure}), \quad \hat{\mathbf{v}}^T \Sigma^{-1} \hat{\mathbf{v}} \leq \chi^2_{1-\alpha, n-p} \quad (58)$$

$$H_a : (\text{Integrity Failure}), \quad \hat{\mathbf{v}}^T \Sigma^{-1} \hat{\mathbf{v}} > \chi^2_{1-\alpha, n-p} \quad (59)$$

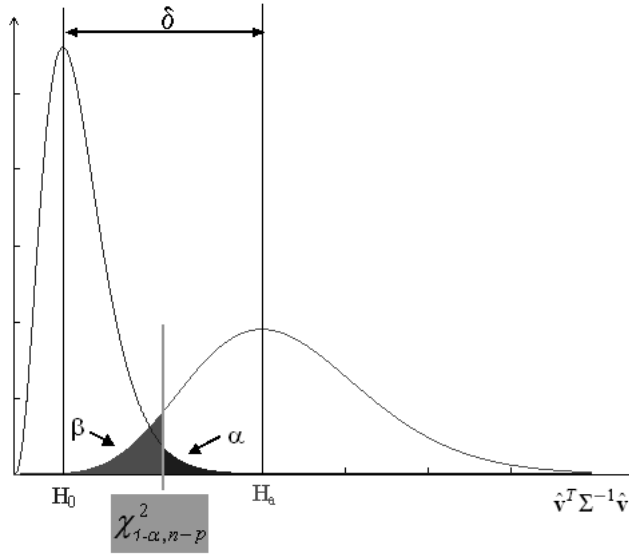


Fig. 21. Central and Non-Central χ^2 Density Functions in Global Testing, $n - p = 8$.

If the null hypothesis H_0 must be rejected and H_a accepted, an inconsistency in the assessed observations is assumed, and the existing errors should be identified and mitigated.

5.1.2 Local Test

The most likely reason for the rejection of H_0 in the global test is the presence of outlying observations. Strict testing is easy under the assumption that there is only one outlier in the current time instance, which is the usual assumption in, e.g., traditional RAIM. The attempt to identify such an individual measurement error may be performed if the redundancy is at least two. The residuals, $\hat{\mathbf{v}}$, can be standardized as

$$w_i = \left| \frac{\hat{\mathbf{v}}_i}{\sqrt{(\mathbf{C}_{\hat{\mathbf{v}}})_{ii}}} \right|, \quad i = 1 : n \quad (60)$$

where n denotes the number of observations and the matrix $\mathbf{C}_{\hat{\mathbf{v}}}$ denotes the covariance matrix of the residuals and is shown in Eq. 54. The standardized residuals can be used for outlier detection with uncorrelated, normally distributed observations in a sense that if the i th observation is not an outlier, w_i is normally distributed as $w_i \sim \mathbf{N}(0, 1)$. Each standardized residual w_i is compared to a α_0 -quantile of the standard normal

distribution, $\mathbf{n}_{1-\frac{\alpha_0}{2}}$, with the predetermined false alarm rate, the significance level α_0 . The null-hypothesis $H_{0,i}$, which denotes that the i th observation is not an outlier, is rejected if the w_i exceeds the threshold $\mathbf{n}_{1-\frac{\alpha_0}{2}}$. The underlying assumptions of the local test include that the model and the assumption that the measurement error vector follows $\varepsilon \sim \mathbf{N}(0, \Sigma)$ are correct except for the single constant bias of the i th observation. The standardized residuals are then normally distributed (Teunissen, 1998; Leick, 2004) with zero expectation when $H_{0,i}$ is correct, and with a non-zero expectation otherwise. The local testing is based on the comparison

$$H_{0,i}: (i \text{ not an outlier}), w_i \leq \mathbf{n}_{1-\frac{\alpha_0}{2}} \quad (61)$$

$$H_{a,i}: (i \text{ an outlier}), w_i > \mathbf{n}_{1-\frac{\alpha_0}{2}} \quad (62)$$

Thus, the $H_{0,i}$ is rejected, i.e., $H_{a,i}$ is recognized, if the critical value is surpassed. Fig. 22 presents the unbiased and biased density functions of the normal distribution

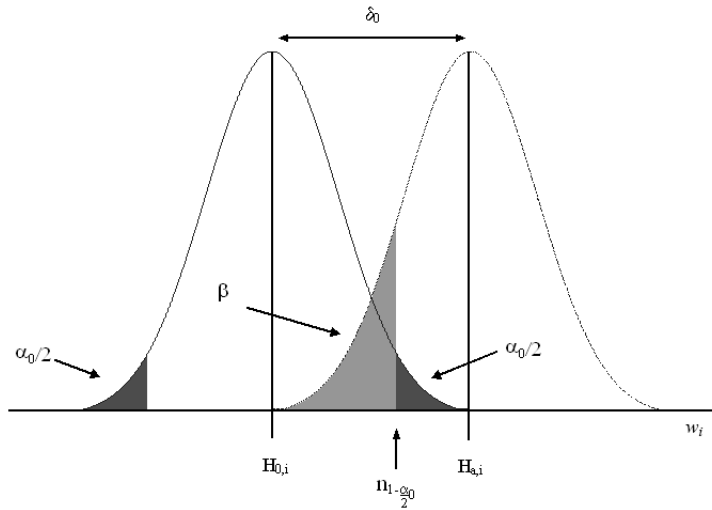


Fig. 22. Density Functions of the Unbiased and Biased Normal Distributions in the Local Test.

that represent the null-hypothesis, $H_{0,i}$, and the alternative hypothesis, $H_{a,i}$, of the local outlier test of observation i . The required probability α_0 is split equally to be contained in the right-hand side tail and the left-hand side tail, respectively.

Only if H_0 of the global test is rejected, the local test is carried out for fault identification and only the observation with the largest value of w_i is tested and possibly

rejected. An outlier in one observation generally causes several w_i to be increased. The measurement with the largest standardized residual exceeding the threshold is regarded as an outlier and that measurement is excluded from the solution computation (Teunissen, 1998), i.e., the k th observation is suspected to be erroneous when

$$H_{a,k} : w_k \geq w_i \forall i, \wedge w_k > \mathbf{n}_{1-\frac{\alpha_0}{2}} \quad (63)$$

The global and local consistency tests are a part of a statistical reliability testing/outlier detection procedure introduced originally by Baarda in 1968 (Baarda, 1968) for the detection and identification of outliers in geodetic networks, and known as data snooping. If H_0 in the global test is rejected, the local test is carried out for fault identification. The parameters α , α_0 , β are interrelated (Baarda, 1968; Caspary, 1988) and only two of them can be chosen arbitrarily. The risk level α of the global test must be related to the corresponding parameter in the local test, α_0 , together with the probability of missed detection β , which is the same for both tests. An erroneous measurement that causes the global test to fail should be indicated by the corresponding local test with the same probability. The α , α_0 , and β values are linked by the following equations

$$\delta = \delta_0^2 = (\mathbf{n}_{1-\frac{\alpha_0}{2}} + \mathbf{n}_{1-\beta})^2 \quad (64)$$

$$\chi_{\beta, n-p, \delta}^2 = \chi_{1-\alpha, n-p}^2 \quad (65)$$

where δ is the non-centrality parameter of a non-central chi-square distribution related to the global hypothesis testing and δ_0 is the expected value of the biased normal distribution related to the local test.

The assumption of a single outlier is a severe restriction, especially if degraded signal conditions are considered. However, it was found that data snooping can also cope with multiple blunders if it is performed iteratively (Hawkins, 1980; Petovello, 2003). After exclusion of an observation, the parameter estimation, statistical tests, and possibly the rejection of an observation can be repeated for that epoch until no more outliers are identified.

5.2 Statistical Reliability

This section discusses the statistical reliability boundaries in a positioning situation.

Choosing values of α_0 and β determine a bias or a so-called non-centrality parameter of $H_{a,i}$, and it is denoted by δ_0 , the internal reliability (Leick, 2004; Ryan, 2002). Internal reliability quantifies the blunder δ_0 that can be detected on each measurement through statistical reliability testing. The smallest such blunder that can be detected is called the marginally, or alternatively minimum, detectable blunder (MDB). External reliability, on the other hand, is quantified by the size of the error in the navigation solution that is caused by an undetected error of the same size as the respective MDB (Leick, 2004; Kuang, 1996; Baarda, 1968; Ryan, 2002; Petovello, 2003). These measures are described in the following.

5.2.1 Internal Reliability

A minimum detectable blunder, MDB, i.e., a parameter of internal reliability, is a measure of the capability to detect a blunder with the probability $(1-\beta)$ with $(1-\alpha_0)$ percent of confidence with the underlying assumptions including the presence of only a single blunder at a time and uncorrelated measurements. For the given probability levels α_0 and β , the MDB for observation i , denoted as m_i , is expressed as

$$m_i = \frac{\delta_0(\Sigma)_{ii}}{\sqrt{(\mathbf{C}_{\hat{\mathbf{v}}})_{ii}}} \quad (66)$$

where δ_0 is the non-centrality parameter defined in Eq. 64. The MDB represents the theoretical limit of an observation error that can marginally be detected and isolated but often, in reality, it is likely that the occurring faults are smaller than the MDB values.

5.2.2 External Reliability

The MDB itself is not of much interest but the effect, which an undetected outlier could have on the result, is important. The external reliability acts as a measure of this effect. External reliability, denoted as \mathbf{e}_i , describes the effect a marginally detectable blunder in the i th measurement has on the state estimate, and is computed as

$$\mathbf{e}_i = -(\mathbf{H}^T \Sigma^{-1} \mathbf{H})^{-1} \mathbf{H}^T \Sigma^{-1} \mathbf{m}_i \quad (67)$$

where the vector \mathbf{m}_i is a column vector containing all zeros except for the minimum detectable blunder of the i th observation, m_i , in the i th position. The external reliability

bility represents the error of the estimated parameters that may be caused by an individual bias of the size of the MDB. The system can be marginally protected against this error with given probabilities α_0 and β . For this reason, the external reliability can also be called the protection level. If only certain elements of the protection level vector are of interest, they can be investigated individually (Petovello, 2003). The rotation matrix \mathbf{R}_L rotates the WGS-84 x, y, and z coordinates into a local level system, i.e., into an east north up (ENU) coordinate system. $\mathbf{R}_L = \begin{bmatrix} \mathbf{R}_{L1,2} \\ \mathbf{R}_{L3} \end{bmatrix}$ was expressed in Eq. 42. A three-dimensional total positioning error (TPE) due to the *i*th MDB, Δp_i , can be defined as

$$\Delta p_i = \sqrt{\mathbf{e}_i^T \mathbf{R}_L^T \mathbf{R}_L \mathbf{e}_i} = \sqrt{\mathbf{e}_{i1}^2 + \mathbf{e}_{i2}^2 + \mathbf{e}_{i3}^2} \quad (68)$$

Moreover, a horizontal positioning error (HPE) due to the *i*th MDB, Δq_i , can be defined as

$$\Delta q_i = \sqrt{\mathbf{e}_i^T \mathbf{R}_{L1,2}^T \mathbf{R}_{L1,2} \mathbf{e}_i} \quad (69)$$

where $\mathbf{R}_{L1,2}$ is the submatrix of the rotation matrix \mathbf{R}_L in Eq. 42, and it extracts the horizontal components from the parameter vector and converts them to local components, east and north. The matrix $\mathbf{R}_{L1,2}$ thus assist in extracting the radial two-dimensional position error computed from the position error in the x, y, and z in WGS-84 ECEF coordinates that corresponds to the effect of the MDB of the *i*th observation in the *i*th observation.

6. FAULT DETECTION AND EXCLUSION

The estimation problem of a user navigation solution involves linearization, and the least squares adjustment has to be accomplished iteratively. A large gross error in the observations may damage the linearization process and cause the iteration procedure to diverge leading to no solution (Kuang, 1996). Therefore, pre-adjustment data screening is essential. It can be performed, e.g., by comparing predicted measurements based on the previous epoch and forward prediction and the obtained measurements. A simple threshold of a large magnitude can be implemented in a pre-adjustment monitor to make sure all the huge outliers, e.g., in the order of kilometers for the pseudorange case, are excluded before going to user navigation solution estimation and the following fault detection and exclusion.

Fault detection and exclusion (FDE) is an essential part of navigation integrity monitoring and reliability assurance. The reliability monitoring can be performed on all types of navigation system observables, but in this discussion, it is assumed that pseudorange and pseudorange rates are monitored in parallel in order to assure reliable position and velocity solutions of a user in poor line-of-sight conditions. The assumption of the measurement errors being normally distributed is unfortunately not necessarily true in degraded signal environments. When there is only a single blunder, methods for outlier identification work quite well. However, it is more difficult to diagnose outliers when there are several of them and assessment for such multiple blunders often give rise to extensive computations (Rousseeuw and Leroy, 1987).

There are different approaches to provide an independent assurance of the integrity of the system. In this thesis, the attention is focused on approaches, which are referred to as a snapshot schemes due to that they are based upon assessing single epoch solutions with only current redundant measurements being used in the self-consistency check. In general, system integrity monitoring, i.e., RAIM can be improved when available dynamic information is fused together with GNSS range measurements in

a Kalman filter (Hewitson and Wang, 2004; Ryan and Lachapelle, 1999). The state and observation model assumptions must be correct in order to the Kalman filtering to provide optimal estimations of the navigation parameters. Unmodelled errors can occur as well as deviations from the assumed models, i.e., outliers among measurements and the predicted state vector (Wieser et al., 2004). Therefore, reliability monitoring is essential even in filtering. If formulation of all the possible failure scenarios existing is feasible, failure detection, identification, and model adaptation (DIA) can be performed (Wieser et al., 2004; Teunissen, 1998) in order to complete the reliability testing of the filter solution.

Due to the low accuracy level and the usually poor knowledge about the user dynamics, the usual advantages of a Kalman filter do not clearly apply in the severely degraded signal conditions of concern in this thesis. Fault detection and exclusion procedures developed and assessed in this thesis for personal navigation applications test for inconsistency and the individual outliers on the epoch level and, thus, the concentration is mainly on single-epoch RAIM and FDE in the following discussions. The snapshot approaches to be discussed are, however, applicable, extendable, and transformable into a filtering environment,

Before introducing the different FDE approaches developed for personal applications in degraded signal environments, traditional RAIM methods are first brought up.

6.1 Traditional RAIM for Safety Critical Applications

Traditionally receiver autonomous integrity monitoring (RAIM) has been used in aviation application for specific phases of flight. Integrity monitoring in these safety-critical applications is highly essential to ensure a certain degree of integrity for the navigation function. Navigation system integrity refers to the ability of the system to provide timely warnings to users when the system should not be used for navigation. The basic GPS system provide integrity information to the users via the navigation message but this is not timely enough for some applications (Farrell and Graas, 1998). Receiver autonomous integrity monitoring, referred to simply as RAIM, is an additional means of providing integrity and to detect when a satellite failure has occurred (Parkinson and Spilker, 1996). RAIM allows errors to be detected by the GPS receiver itself without expensive ground equipment (Brown, 1987). One redundant measurement is necessary for detecting a faulty measurement source. If additional

redundant measurements are available, it is possible to isolate the faulty measurement source or exclude it from the navigation solution (Sturza, 1988). Overall, RAIM is a technique that uses an overdetermined solution to perform a consistency check, and the RAIM methods must detect if the horizontal error goes beyond a certain threshold within a specified level of confidence (Kaplan (Ed.), 1996).

Many RAIM schemes have been proposed in literature (Parkinson and Spilker, 1996) and they all are based on some kind of self-consistency check among the available measurements. The schemes proposed in literature can be described as snapshot approaches because they use a single set of GPS measurements collected simultaneously. Three RAIM methods for safety-critical applications have received special attention: a least-squares-residuals method, a parity method, and a range comparison method. The primary emphasis on these methods is on failure detection only and to protect against excessive horizontal position error (Parkinson and Spilker, 1996; Parkinson and Axelrad, 1988; Brown, 1992). In addition, a maximum residual algorithm by R. J. Kelly (Kelly, 1998) based on a likelihood ratio test has received special attention in its isolation capability for safety critical applications. The three most discussed and applied traditional RAIM algorithms in the GPS literature are proven to be equivalent, and in addition, with the same confidence levels, they are shown to be mathematically equivalent to the maximum residual algorithm as well.

6.1.1 Screening Out Poor Geometries

Before applying a RAIM method in the safety-critical applications it has to be assured that the level the system can theoretically be protected against does not exceed the level of performance required for the specific application. This consists of generating an upper bound in the navigation solution space called the horizontal protection level (HPL), which equals the external reliability boundary discussed in the reliability section, and comparing this HPL to a horizontal alarm limit (HAL) predetermined by the system requirements. Screening out bad geometries is crucial in safety-critical navigation applications in order to stay within the requirements. However, in personal navigation applications, due to the lack of requirements, there is no need to screen out a solution based on the theoretical external reliability boundary, which states the error level the system can, in theory, be marginally protected against.

6.1.2 Least-Squares-Residuals RAIM Method

In the least-squares-residuals method, a measure of consistency is the range residual vector $\hat{\mathbf{v}}$ presented earlier, which is the difference between the empirical measurements in \mathbf{y} and the predicted measurements based on least squares solution (Kaplan (Ed.), 1996). The sum of the squares of the residuals plays the role of the basic observable in the least-squares-residuals RAIM method and it is called the *SSE* and presented in the following (Brown, 1992)

$$SSE = \hat{\mathbf{v}}^T \hat{\mathbf{v}} \quad (70)$$

The *SSE* is a nonnegative scalar quantity, which makes for a simple decision rule. Namely the semi-infinite real line has to be partitioned into two parts, one for 'no failure' and the other for 'failure'. The dividing point is called the threshold (Parkinson and Spilker, 1996). If all elements of the error vector $\boldsymbol{\varepsilon}$ have the same independent zero-mean Gaussian distribution, the statistical distribution of *SSE* is completely independent of the satellite geometry for any n . Therefore it is easy to implement a constant alarm-rate algorithm, where the thresholds, that yield to the desired alarm rate for the various anticipated values of n , are precalculated (Parkinson and Spilker, 1996). For the zero-mean Gaussian assumption made for all the elements of $\boldsymbol{\varepsilon}$, *SSE* has a chi-square distribution with $(n - 4)$ degrees of freedom (Brown, 1992), if it assumed that there are 4 unknowns. On the other hand, if the elements of $\boldsymbol{\varepsilon}$ are biased, the *SSE* has a noncentral chi-square distribution with also $(n - 4)$ degrees of freedom (Chin et al., 1992). To determine the threshold for the number of satellites in view using the *SSE* value in the test statistic, chi-square statistics is applied with a constant alarm rate (Kaplan (Ed.), 1996; Parkinson and Spilker, 1996).

The least-squares-residuals RAIM method is mathematically equivalent to the global test of Chapter 5.1.1 applicable for failure detection.

6.1.3 Parity RAIM Method

In the parity RAIM scheme, a linear transformation is performed on the measurement vector as follows

$$\mathbf{p} = \mathbf{P}\mathbf{y} \quad (71)$$

The $(n - p) \times 1$ vector \mathbf{p} is called the parity vector (Parkinson and Spilker, 1996) and it is the result of operating on the measurement vector \mathbf{y} with a special $(n - p) \times (n)$

matrix \mathbf{P} , whose rows are mutually orthogonal, unity in magnitude, and also mutually orthogonal to the columns of the design matrix \mathbf{H} . The matrix \mathbf{P} can be obtained for example with QR-factorization on the linear connection matrix \mathbf{H} (Kaplan (Ed.), 1996).

Under the assumption that the elements of the error vector $\boldsymbol{\varepsilon}$ are independent similar zero-mean Gaussian random variables, the following statements can be made

$$E(\mathbf{p}) = 0 \quad (72)$$

$$E(\mathbf{p}\mathbf{p}^T) = \sigma^2\mathbf{I} \quad (73)$$

where $E(\cdot)$ denotes the expectation function, \mathbf{I} the identity matrix, and σ^2 is the variance associated with any particular element of $\boldsymbol{\varepsilon}$. Conceptually, in the parity method, the vector \mathbf{p} is used as a test statistic. However, because of the special properties of the parity vector, the individual elements of \mathbf{p} are decoupled and have the same variance. For simple detection, all information needed about \mathbf{p} is obtained merely at looking at its magnitude or its magnitude squared (Parkinson and Spilker, 1996). Thus, in the parity method, the test statistic for detection reduces to a scalar, just as in the least-squares-residuals method. It is also shown in (Sturza, 1988) that the sums of the squares of the elements of \mathbf{p} and SSE are identical as presented in the following (Parkinson and Spilker, 1996)

$$\mathbf{p}^T \mathbf{p} = \hat{\mathbf{v}}^T \hat{\mathbf{v}} = SSE \quad (74)$$

Therefore, although the dimensionality of \mathbf{p} and $\hat{\mathbf{v}}$ are different, their magnitudes are the same. Thus, if the test statistic $\mathbf{p}^T \mathbf{p}$ is the only interesting quantity, the trouble of finding the orthogonal transformation \mathbf{P} that leads to \mathbf{p} is not necessary, and only the SSE , directly from the measurement-residual space, can be used. So, in detection application, which is the most common integrity function in safety critical applications, the least-squares-residuals and parity methods lead to identical observables. Then, in case of a failure detection with these methods in the safety-critical applications, the user is usually encouraged to switch to other navigational means than the satellite navigation system.

6.1.4 Range Comparison RAIM Method

Let us imagine having more than four satellites in view. A solution can be obtained that satisfies the first four measurement equations. The resulting solution can then

be used to predict the remaining measurements, and the predicted values can then be compared with the actual measured values. If the differences are small, there is a near-consistency in the measurements, and the detection algorithm declares 'no failure'. On the other hand, if some of the residuals are large, the algorithm declares 'failure'. This is the essence of the range comparison method (Lee, 1998; Parkinson and Spilker, 1996).

6.1.5 *Maximum Residual RAIM Algorithm*

An integrity monitoring scheme called the maximum residual algorithm presented by R.J. Kelly in (Kelly, 1998) includes the detection and isolation of a measurement under the assumption of only one satellite channel failure based on a likelihood ratio test. It obtains its performance standards from airspace required navigation performance (RNP). The maximum residual algorithm is basically similar to the local test described above in the reliability testing section for outlier isolation. More details on Kelly's maximum residual algorithm for can be found in (Kelly, 1998).

The four above mentioned and discussed RAIM algorithms published in GPS literature in the context of aviation are mathematically equivalent to each other. The statistics community uses the same algorithms for data outlier detection and identification. Therefore, the statistical reliability testing procedures presented earlier are similar to these traditional RAIM algorithms. The naming conventions are, however, different in statistics community and, e.g., the aviation integrity monitoring literature. For error exclusion, the aviation community has also applied observation subset tests as, e.g., using the failure detection test statistic in the decision making for the best subset, or, e.g., using a maximum separation of solutions -method discussed in (Parkinson and Spilker, 1996; Brown, 1998). However, the assumption of a single satellite failure has been strongly dominant in the error exclusion methods in, e.g., the aviation community. Nowadays, with the future Galileo in the horizon, also multiple failures have been considered in a few of the aviation community integrity algorithms, e.g., (Lee, 2004; Macabiau et al., 2005) and (Misra and Bednarz, 2004), which presents a robust integrity monitor for GPS and Galileo that selects satellite subsets with good geometries.

6.2 Developed FDE for Personal Satellite Navigation Applications

In personal satellite navigation applications in degraded signal-environments, no integrity requirements limit the fault detection algorithms. However, failure occurrence is higher and there is a high probability of encountering multiple simultaneous observation errors, blunders, due to the high level of multipath interference and attenuation. In the same time, there is a lack of redundancy in many cases, which restricts the availability of fault detection and exclusion. Nevertheless, performing proper failure monitoring and isolation is essential in order to improve the reliability and accuracy in the environments with deteriorated line-of-sight signal reception. In the following, different methods are proposed to be used for the failure detection and exclusion function and the reliability enhancement in degraded signal environments.

6.2.1 Observation Subset Testing

Usually, a large error can be localized by assessing the least squares residuals by statistical testing. However, the least squares procedure may smooth out multiple gross errors across an entire data set, and also a specific large error might be smoothed out throughout its neighboring observations. In this case, localization of the gross errors based on statistical rejection of residuals available from least squares adjustment is very difficult. Therefore, performing several least squares adjustments by taking out or re-inputting one or more of those observations at a time in order to locate the right observations containing the gross error may be necessary (Kuang, 1996).

Observation subset testing with the test statistic of the global test as the decision parameter may be conducted to find a subset from which the supposed blunders are excluded. This is done by searching for a subset that most clearly passes the global test, i.e., which satisfies its selfconsistency test with the smallest test statistic. In subset testing, the test statistics for the global consistency test are computed for all the possible subsets that include $p + 1$ to $n - 1$ measurements, i.e., from which $n - (p + 1)$ to 1 observation has been excluded. Parameter n denotes the number of available measurements and the parameter p represents the number of unknown parameters to be solved for. The subset that has the smallest acceptable test statistic, i.e., the smallest test statistic below the threshold, and, in addition, the largest number of measurements, is chosen to provide the best position solution, as shown in Fig. 23. However,

the subset testing procedure is computationally heavy and is not feasible as a FDE procedure to combined GPS/Galileo navigation, since, e.g., in case of 18 available satellite signals and 4 unknowns, it would be necessary to assess over 254000 subsets in one epoch, which is the result of $\sum_{k=5}^{13} \frac{18!}{(18-k)!k!}$.

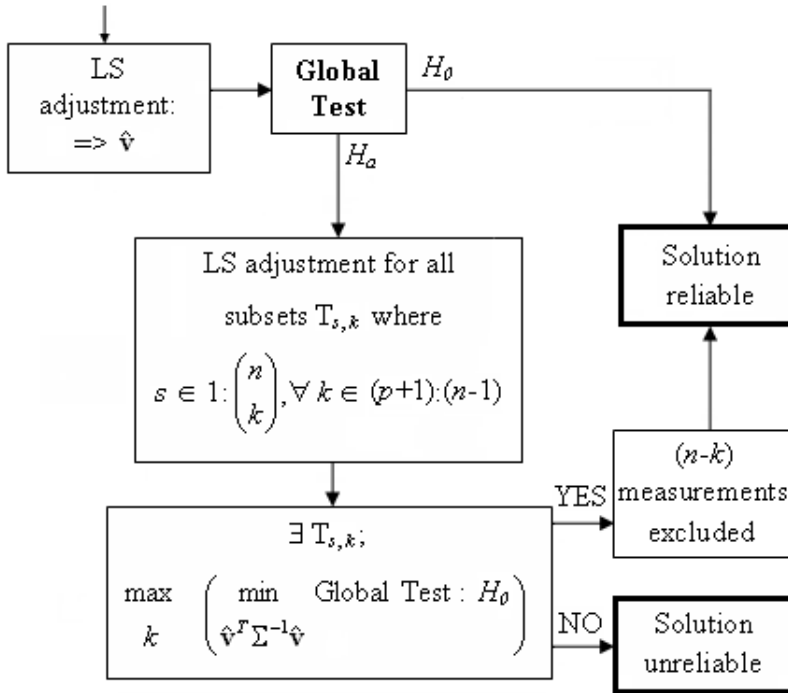


Fig. 23. FDE by Observation Subset Testing.

6.2.2 Forward-Backward FDE

If m outliers are suspected, a redundancy of at least $m + 1$ is needed in order to possibly identify them. However, due to the mutual influence of observations, i.e., an error of one observation is absorbed by the residuals of all observations, erroneous rejection of a good observation is possible, especially with large or multiple biases (Lu, 1991). In degraded signal-environments, the redundancy is generally poor and, thus, it is desired to keep as many observations as possible for obtaining an efficient estimate [P1, P3, P5]. Therefore, if more than one observation is being excluded, the

iterated reliability checking should include a reconsideration of an earlier rejected observation (Wieser, 2001).

The Forward-Backward FDE method includes using the global test to identify an inconsistent solution and performing the local test to identify and exclude the erroneous measurement. The exclusion is, however, not performed if there is another observation that is more influential than the one being subject to assessment. Thus, in the FDE execution, no influential observations may be tolerated. When pinpointing the observation i to be excluded, it should be excluded from the solution only if the i th redundancy number r_i follows the equation $r_i > |r_{ji}|$ ($j \neq i, j = 1 : n$). The global test and the local test with the additional influentiality check are performed recursively until no more erroneous measurements are found and the solution is flagged reliable or the solution is declared unreliable. In addition, the reconsideration of an earlier rejected observation is included in the Forward-Backward FDE scheme, as presented in Fig. 24. This is performed by reconsidering all the excluded measurements and performing global tests to find the measurements that can be implemented back to the solution computation. Thus, a measurement that has been excluded earlier is used again for the solution computation if the global test passes when tentatively including it into solution estimation. This is performed to ensure that the order of the excluded measurements does not cause an unnecessary exclusion. Due to the importance of the measurements to the geometry of the solution unnecessary exclusions are unwanted.

Taking into account the influentiality of the observation subject to exclusion could be implemented in all the discussed FDE methods, but, for comparison purposes, it is only taken into account in the Forward-Backward procedure.

6.2.3 Iterative Reweighted Estimation - The Danish Method

The Danish method (Jørgensen et al., 1985; Wieser, 2001) is an iteratively reweighted least squares algorithm which implements a robust estimator. It is very popular in geodetic applications. The Danish Method has received attention also in a few different fields: Leick talks about changing weights of observations in (Leick, 2004) in order to detect blunders and minimize or even eliminate their effect on the adjustment as well as Huber briefly mentions in (Huber, 1981) about modified weights in the computation of the regression estimate. The Danish Method aims at achieving con-

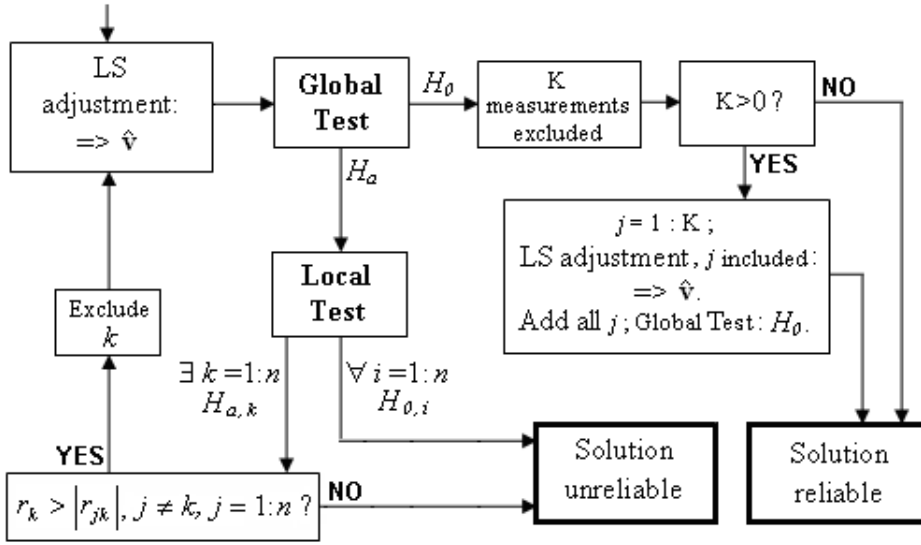


Fig. 24. Forward-Backward FDE Procedure.

sistency between the model and the observations by modifying the a priori weights of the few observations, which are not consistent with the majority of the observations. Iteratively reweighted least squares is, however, not based on rigorous statistical theory (Leick, 2004) but locates and potentially eliminates the blunders automatically while examining the residuals per iteration. If the magnitude of a residual is outside a defined range, the weight of the corresponding observation is reduced with the process of re-weighting and readjusting continuing until the solution converges and no weights are being changed (Leick, 2004). The Danish method has very similar performance as the FDE methods described earlier but it is computationally much more efficient. As any robust estimator and FDE scheme it has a breakdown point of 50%, i.e., it can only be successful if there are more good observations than outlying ones.

To incorporate the geometry of the satellite distribution and the different quality of the observations, a hint given in (Jørgensen et al., 1985) is followed and a re-weighting based on normalized residuals is here suggested. The variance for observation i in iteration $k + 1$ of an epoch, $\sigma_{i,k+1}^2$, can then be constructed as follows

$$\sigma_{i,k+1}^2 = \sigma_{i,0}^2 \cdot \begin{cases} e^{\frac{\bar{w}_{i,k}}{T}} & \bar{w}_{i,k} > T \\ 1 & \bar{w}_{i,k} \leq T \end{cases} \quad (75)$$

where

$$\begin{aligned}\bar{w}_{i,k} &= \left| \frac{\hat{v}_{i,k}}{\sqrt{(\mathbf{C}_{\hat{v}_{i,1}})_{ii}}} \right| \\ T &= \mathbf{n}_{1-\frac{\alpha_0}{2}}\end{aligned}\quad (76)$$

where $\sigma_{i,0}^2$ denotes the a priori variance of observation i . Such an 'a priori' variance can be obtained as an example from a C/N_0 -dependent variance model. If the i th normalized residual exceeds the critical value T computed from the normal distribution, the Danish method increases the variance exponentially. If the normalized residual of the i th observation, $\bar{w}_{i,k}$, is less than the threshold T , the a priori variance for that observation is maintained in the estimation procedure. Therefore, the prior values are lower bounds for the variances actually used. In each iteration, the estimated residuals are normalized using the standard deviations from the first iteration as seen in Eq. 76, and the variances of all observations are modified according to Eq. 75. Note that the values $\bar{w}_{i,k}$ are exactly the standardized residuals after the first iteration but not after subsequent ones. However, this standardization by a fixed quantity helps to isolate the inconsistent observations and allows for convergence at the same time (Kuusniemi et al., 2004). The variance covariance matrix in the k th iteration for n observations is hence constructed as follows

$$\Sigma_k = \begin{bmatrix} \sigma_{1,k}^2 & 0 & \cdots & 0 \\ 0 & \ddots & & \vdots \\ \vdots & & \ddots & 0 \\ 0 & \cdots & 0 & \sigma_{n,k}^2 \end{bmatrix}\quad (77)$$

The iterations in the modified Danish estimation method start with a traditional least squares estimation using the inverse of the variance covariance matrix of the observations as the weight matrix (Wieser, 2001). After this, in each iteration k , the normalized residuals for all observations are computed. Then, new variances are computed and least squares estimation iteration is conducted. When the variance of an observation grows exponentially, the weight of that observation decreases rapidly in the estimation and the observation can be regarded as being excluded. The iterations for an epoch are stopped when the variances no longer change significantly and the norm of the unknowns to be estimated is small enough for the solution to be accepted.

The Danish method is similar in its exclusion capability to the previous Forward-Backward FDE and Subset Testing but it is computationally more efficient. The ratio

of the processing times was about 1:50 for both the Subset Testing and Forward-Backward FDE when processing the data sets presented in the following chapter. Although the difference in the processing times might have been somewhat more balanced by optimizing the source code, the Danish method is, however, much lighter computationally. The major drawback of the Danish method is that it is an empirical procedure with no generally valid statistical explanation. The Danish method is, however, simple, computationally efficient, and has found to perform very well in practical applications, as will be demonstrated in the results section.

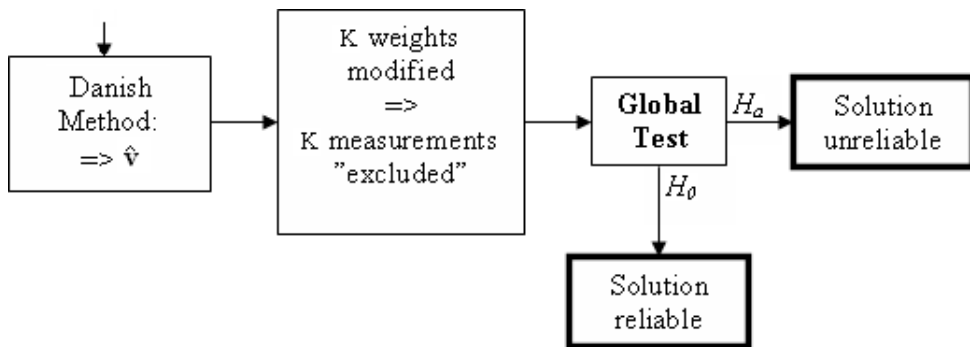


Fig. 25. FDE by the Danish Method.

6.3 Quality Control

The quality of the user position estimate depends not only on the quality of the range measurements but also on the user/satellite observation geometry. The dilution of precision (DOP) concept provides a simple quality measure of the geometry. The DOP values should not surpass a predetermined threshold even after rejection of outliers to ensure good user/satellite observation geometry. Bad geometry amplifies random errors and biases and, therefore, produce large position errors. The overall quality control procedure implemented in this thesis includes assessing the user redundancy, the consistency using FDE, and the geometry. For a user navigation solution to pass the quality control there should be enough redundancy to perform the reliability testing. In addition, no zero redundancy numbers of observations should be tolerated, since a zero redundancy implies an uncontrollable observation and any bias in that

observation cannot be identified. The quality control also includes the reliability monitoring itself in terms of executing the FDE procedures.

The overall quality control scheme is presented in Fig. 26. In the quality controlled results presented in the following section, a position DOP (PDOP) cut-off of 10 is employed that was regarded to represent an appropriate threshold for screening poor geometries in degraded signal environments. Naturally, the cut-off value is a flexible parameter that can be chosen as wanted depending on the application. A failure

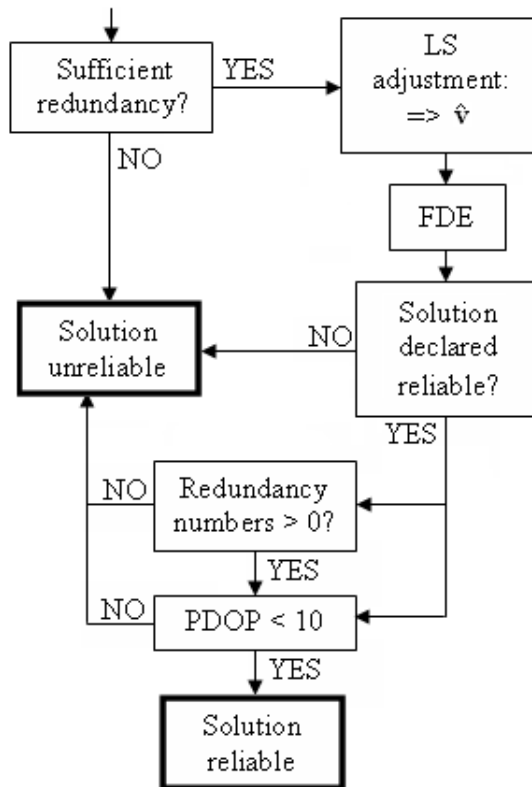


Fig. 26. Quality Control of a Navigation Solution.

detection and isolation method can be combined with geometry assessment also as is done in [P7], where FDI and certain KDOP analysis are done in parallel. KDOP denotes a geometric dilution of precision weighted by user equivalent range errors. The KDOP measure aims to combine geometrical integrity with signal condition estimates, and comparison of KDOP values of different satellite combinations may result

into a satellite isolation (Sairo et al., 2003).

6.4 Observation Weighting Based on Carrier-to-Noise Ratio

In general, an identity matrix is not a sufficient approximation for the weight matrix Σ^{-1} . It yields still an unbiased estimate, but causes erroneous accuracy estimates and misleading reliability analysis results (Kuusniemi et al., 2004). A more suitable variance model of the observations can be derived by investigating satellite data from real-world experiments. For this purpose, HSGPS data was collected using a SiRF *XTrac-LPTM* HSGPS receiver. The data is now analyzed in order to discover appropriate variance models for the pseudorange and pseudorange rate measurements dependent on the signal power for lightly and heavily degraded signal environments. The variance models for the observations that are discussed are only generally valid ideas and they are not trying to be optimum or universal weighting schemes. More specific models can be developed for definite data sets and equipment used but the objective here is to introduce more generally applicable models.

6.4.1 Variance Models for Lightly Degraded Signal Environments

First, lightly degraded data from an indoor HSGPS test of 12 hours is analyzed. The data is the same as discussed in Section 3.5.2. First pseudorange measurements are considered after which the pseudorange rate measurements are discussed.

Variance Model for Pseudorange Observations

In high-precision positioning, satellite elevation dependent weighting of the observations has been used successfully (Wang et al., 1998). The number and the impact of possible error sources increase with decreasing satellite elevation, but the elevation is not necessarily an indicator of the actual signal quality (Wieser, 2001). The carrier-to-noise ratio measured by the receiver is such an indicator. Fig. 27 shows the previous pseudorange errors of the garage experiment when satellite elevation and carrier-to-noise ratio, C/N_0 , are varied. It can be seen, as expected, that larger observation errors are obtained with low elevation satellites, but there is an even stronger correlation between the spread of the observation errors and the C/N_0 values. Thus,

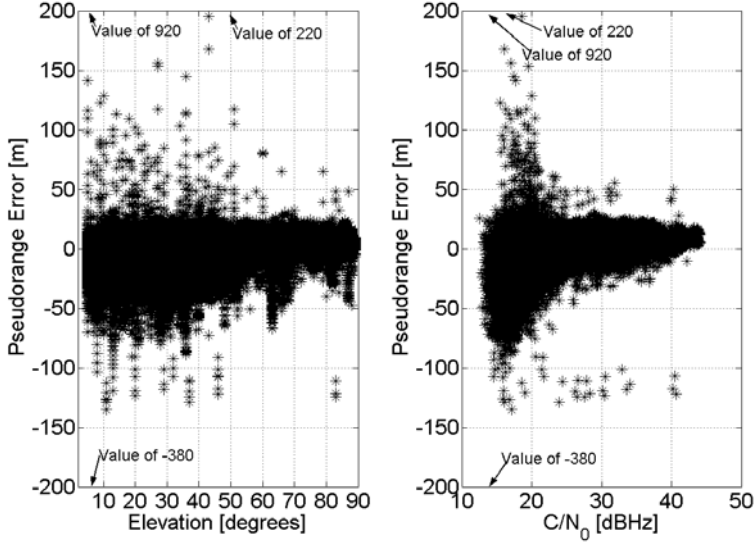


Fig. 27. Lightly Degraded Signal Environment: Pseudorange Error as a Function of Elevation and Carrier-to-Noise Ratio.

it is suggested that the C/N_0 is used as an input to a variance model for weighting the GNSS measurements, especially in obstructed line-of-sight conditions. An advantage of the C/N_0 weighting is that it performs as well as an elevation dependent in clear sky conditions but often better in poor signal-environments. A C/N_0 based variance covariance matrix of the observations can be constructed as follows

$$\Sigma = \text{diag}(s_1, s_2, \dots, s_n) \quad (78)$$

where

$$s_i = a + b * 10^{\frac{-C/N_0}{10}} \quad (79)$$

The constants a and b need to be chosen according to the environment and the user equipment. Here the following values have been used for the pseudorange measurements for lightly degraded signal conditions: $a = 10 \text{ m}^2$ and $b = 150^2 \text{ m}^2 \text{ Hz}$. The assumptions made in the new variance model include that the pseudorange measurements are uncorrelated and the errors are normally distributed with $\mathbf{N}(0, \Sigma_p)$. This model has been developed in (Hartinger and Brunner, 1999) for use with GPS carrier phase observations but it may be equally beneficial with pseudoranges as well as pseudorange rates, as discussed shortly. The resulting dependence of the modeled

standard deviation and the C/N_0 values is presented in Fig. 28. The standard devia-

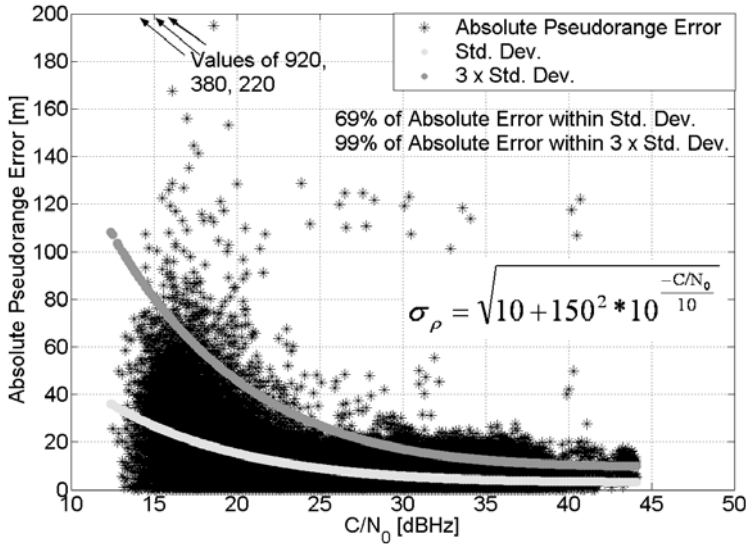


Fig. 28. Lightly Degraded Signal Environment: Absolute Pseudorange Error and the Standard Deviation of Pseudorange Error as a Function of Carrier-to-Noise Ratio.

tion, σ_ρ , as output by the variance model of Eq. 79 with $a = 10 \text{ m}^2$ and $b = 150^2 \text{ m}^2 \text{ Hz}$ has been plotted on top of the absolute pseudorange error data. 69% of the absolute pseudorange error is here within the standard deviation values from the variance model. In addition, the $3\sigma_\rho$ bound has been plotted, which roughly corresponds to a 99.7% confidence level for normally distributed data. The figure indicates that the overall fit is good, but a locally better fit could be obtained for this specific dataset with higher σ_ρ at medium to high C/N_0 and lower σ_ρ at low C/N_0 . However, the model as defined in Eq. 79 is simple and performs well with a variety of GPS data. Fig. 29 presents the normal probability plots for graphical normality testing of the true pseudorange errors normalized by their standard deviation from a constant variance model on the left hand side and from the new variance model on the right hand side. The pseudorange errors normalized with the standard deviation are denoted as misclosure data. The errors were obtained by fixing the user position coordinates to known values and removing them from the adjustment process leaving only the clock error to be estimated. The residuals from this process are regarded as unbiased estimates of the pseudorange errors. The standard deviation for the pseudorange er-

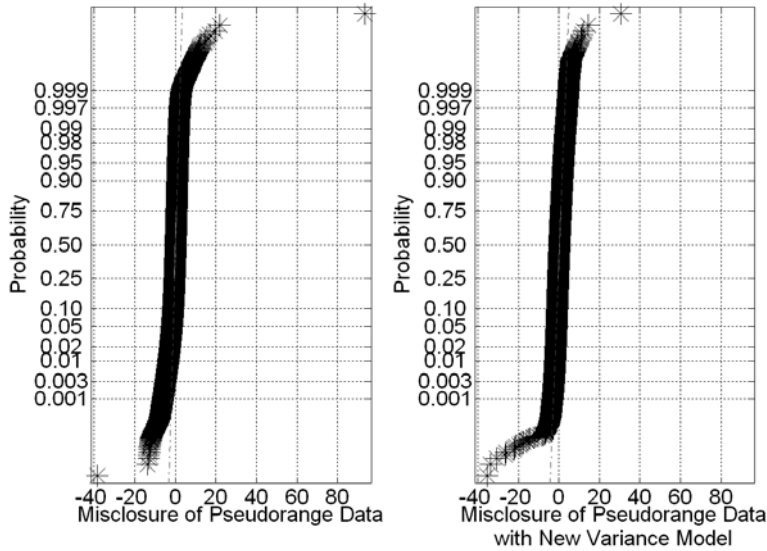


Fig. 29. *Lightly Degraded Signal Environment: Normal Probability Plots of Pseudorange Misclosure Data with a Constant Variance Model and the New Variance Model.*

rors from a constant variance model has been computed as sample standard deviation from the data ($\sigma_p = 10$ m), and the standard deviation from the new variance model has been computed from Eq. 79 and shown also in Fig. 28. In a normal probability plot, the plot is linear if the data comes from a normal distribution (DeVor et al., 1992). Superimposed on the plot is a line extrapolated out to the ends of the sample to help evaluate the linearity of the data. Thus, the left hand side of Fig. 29 shows that there are strong deviations from normality in the misclosure data when a constant variance is applied. The figure indicates that the central part of the data has significantly smaller standard deviation than the tails of the data set. Thus, using equal variances for observations in the estimation procedure is not a proper model and the new variance model is needed for providing an optimum estimate and a basis for subsequent statistical reliability testing (Kuusniemi et al., 2004). The normal probability plot of the misclosures of the pseudorange error normalized by their standard deviations from the new variance model in Eq. 79 is illustrated on the right hand side of Fig. 29. Clearly, this model matches the data much better than the equal-variance model. The remaining deviations towards the tails of the distribution indicate that there are outliers which cannot be covered by the variance model. They need to be

handled by the reliability monitoring (Wieser and Brunner, 2000).

Variance Model for Pseudorange Rate Observations

A similar analysis of a C/N_0 -dependent generally valid variance model of the form $a + b * 10^{\frac{-C/N_0}{10}}$ of Eq. 79 can be performed also for the pseudorange rate observations. As well as the spread of the pseudorange measurement errors is more correlated with the signal power than the signal elevation angle, also the pseudorange rate measurements are more clearly dependent on the carrier-to-noise ratios as presented in Fig. 30.

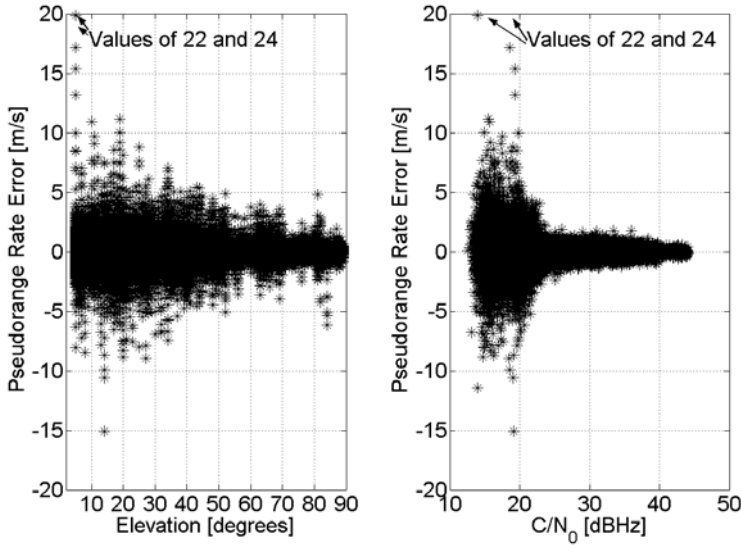


Fig. 30. Lightly Degraded Signal Environment: Pseudorange Rate Error as a Function of Elevation and Carrier-to-Noise Ratio.

The new variance model of Eq. 79 can thus also be applied for the pseudorange rate measurements, and the following values have been used for the pseudorange rate variance model: $a = 0.01 \frac{m^2}{s^2}$ and $b = 25 \frac{m^2}{s^2} Hz$. The assumptions made in the new variance model include that the pseudorange rate measurements are uncorrelated and the errors are normally distributed with $\mathbf{N}(0, \Sigma_{\dot{\rho}})$. The resulting dependence of the modeled standard deviation and the C/N_0 values is presented in Fig. 31. The standard deviation, $\sigma_{\dot{\rho}}$, as output by the variance model in Eq. 79 with $a = 0.01 \frac{m^2}{s^2}$

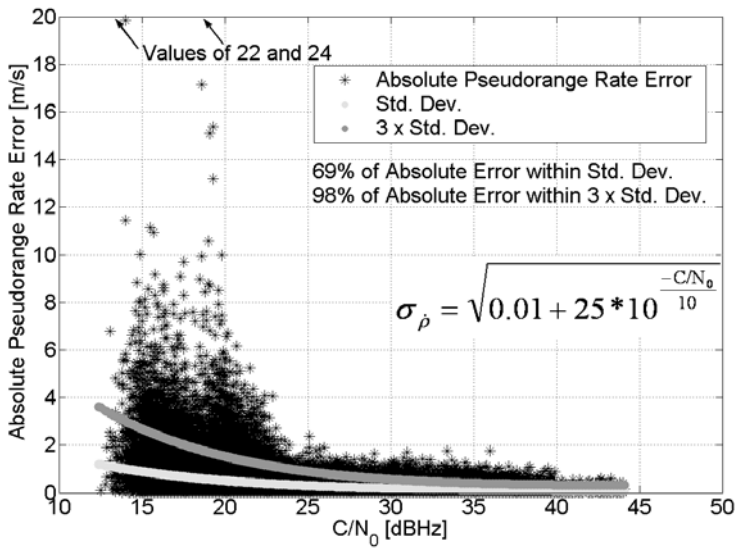


Fig. 31. Lightly Degraded Signal Environment: Absolute Pseudorange Rate Error and the Standard Deviation of Pseudorange Rate Error as a Function of Carrier-to-Noise Ratio.

and $b = 25 \frac{m^2}{s^2} Hz$ has been plotted on top of the absolute pseudorange error data. 69% of the absolute pseudorange rate error stays within the standard deviation values from the variance model. In addition, the $3\sigma_{\dot{\rho}}$ bound has been plotted, and 98% of the data is within this bound. The figure indicates as well that the overall fit is good, but a more complex, locally better fit could again be obtained for this specific dataset.

The left hand side of Fig. 32 presents a normal probability plot for graphical normality testing of the pseudorange rate errors normalized by their sample standard deviation which is denoted as misclosure data. A sample standard deviation of 0.5 m/s was applied in the constant variance model. The left hand side of the normal probability plots in Fig. 32 shows that there are strong deviations from normality in the misclosure data of the pseudorange rate observations when normalization with the equal variance model has been performed. The figure indicates that the central part of the data has significantly smaller standard deviation than the tails of the data set. Thus, using equal variances for observations in the estimation procedure is not a proper model. The normal probability plot of the misclosures of the pseudorange rate error normalized by their standard deviations from the new variance model in Eq. 79

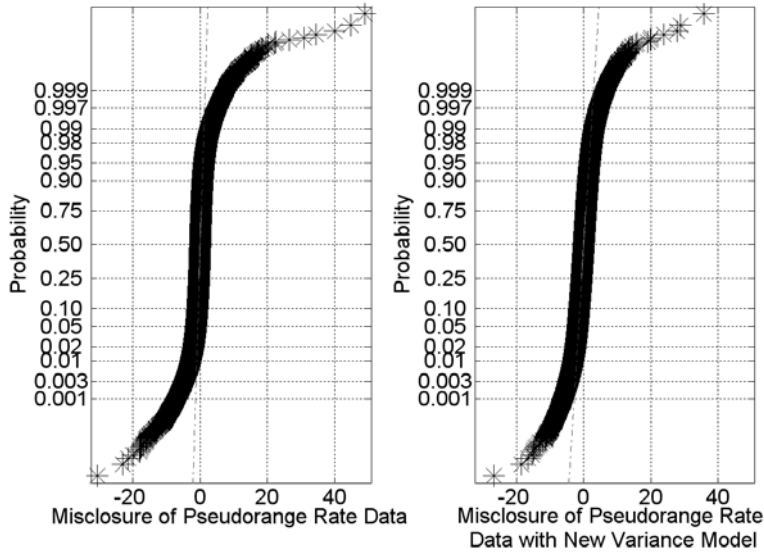


Fig. 32. Lightly Degraded Signal Environment: Normal Probability Plots of Pseudorange Rate Misclosure Data with a Constant Variance Model and the New Variance Model.

is illustrated on the right hand side of Fig. 32. There are only slight improvements in normality of the misclosure data with the new variance model, and the remaining deviations towards the tails of the distribution indicate that there are still a few outliers which cannot be covered by the variance model, and they need to be accounted for by reliability testing.

6.4.2 Variance Models for Heavily Degraded Signal Environments

The model as defined in Eq. 79 is simple and performs well with a variety of GPS data. However, the parameters a and b need to be derived differently for a heavily attenuated signal environment, since the a and b values introduced above for the pseudorange and pseudorange rate observations in lightly degraded signal environments are not suitable for a heavily attenuated signal environment with a higher level of overall signal degradation. Thus, similar figures as Fig. 28 and Fig. 31 will be shown for a 30-minute urban canyon experiment with a HSGPS receiver. This data experiment and the errors occurring were described also in Section 3.5.3. First, pseudorange measurements are considered after which the pseudorange rate measure-

ments are discussed in order to compose the variance models for the pseudorange and pseudorange rates in a heavily deteriorated signal environment.

Variance Model for Pseudorange Observations

The spread of the pseudorange measurement errors is more correlated with the signal power than the signal elevation angle also in a heavily deteriorated signal environment, as presented in Fig. 33. The figure shows, that at low carrier-to-noise ratios, however, the pseudorange errors seem to be shifted toward the negative side, most likely due to the multipath degradation and echo-only signal reception specific for this particular urban canyon environment.

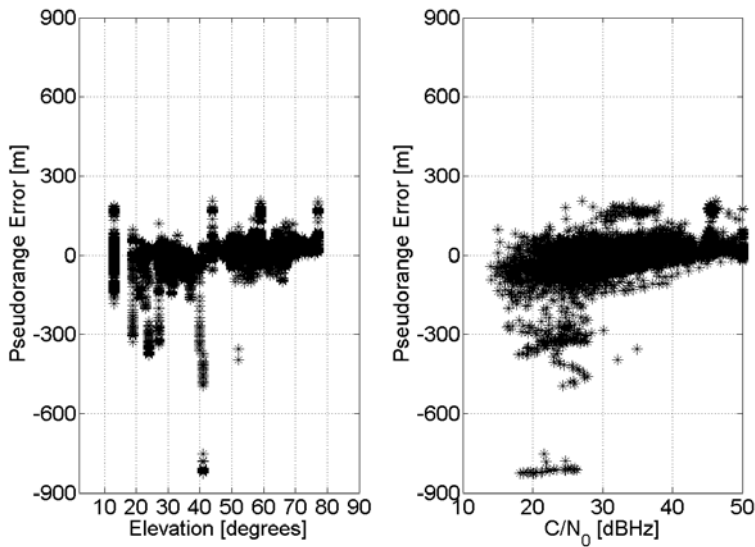


Fig. 33. Heavily Degraded Signal Environment: Pseudorange Error as a Function of Elevation and Carrier-to-Noise Ratio.

For the heavily degraded signal environment, a variance model with the parameters $a = 500 \text{ m}^2$ and $b = 10^6 \text{ m}^2 \text{ Hz}$ for the pseudorange case is now applied. The resulting dependence of the modeled standard deviation and the C/N_0 values is presented in Fig. 34. The standard deviation, σ_p , as output by the variance model in Eq. 79 with $a = 500 \text{ m}^2$ and $b = 10^6 \text{ m}^2 \text{ Hz}$ has been plotted on top of the absolute pseudorange error data. 69% of the absolute pseudorange error is within the standard deviation

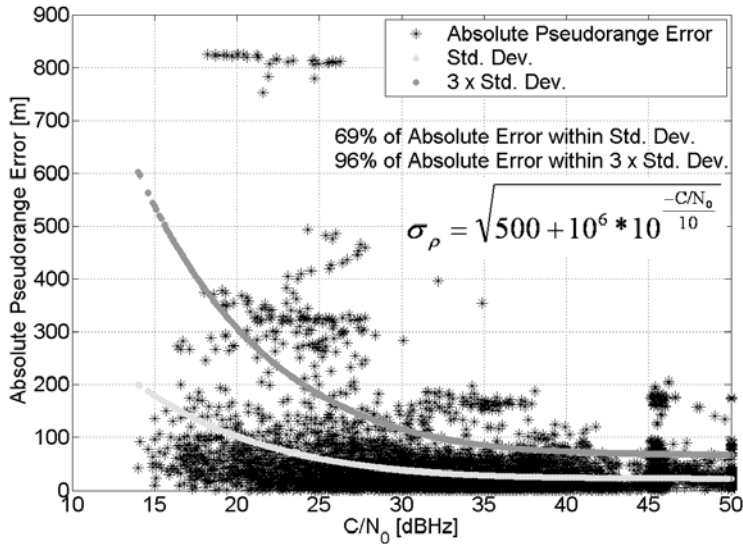


Fig. 34. Heavily Degraded Signal Environment: Absolute Pseudorange Error and the Standard Deviation of Pseudorange Error as a Function of Carrier-to-Noise Ratio.

values from the variance model. In addition, the $3\sigma_p$ bound has been plotted, which corresponds here to only a 96% of the error staying within that bound. The figure indicates that the overall fit is not very good, and locally better fit could be obtained. Fig. 35 presents the normal probability plots of the pseudorange data when a constant variance model has been applied with the variance composed from the sample standard deviation (69 m) and when the new proposed variance model of Eq. 79 has been applied with $a = 500 \text{ m}^2$ and $b = 10^6 \text{ m}^2\text{Hz}$. Fig. 35 implies that the new variance model is actually not much more suitable in a normality sense, and the misclosures with the new variance model do not follow a normal distribution better than the constant variance model. However, the errors are still modeled quite well with the new variance model since the results presented in the following chapter of the downtown parking lot experiment show that the new variance model is profitable.

Variance Model for Pseudorange Rate Observations

In addition, the pseudorange rate measurement errors are more correlated with the signal power than the signal elevation angle in the heavily deteriorated signal envi-

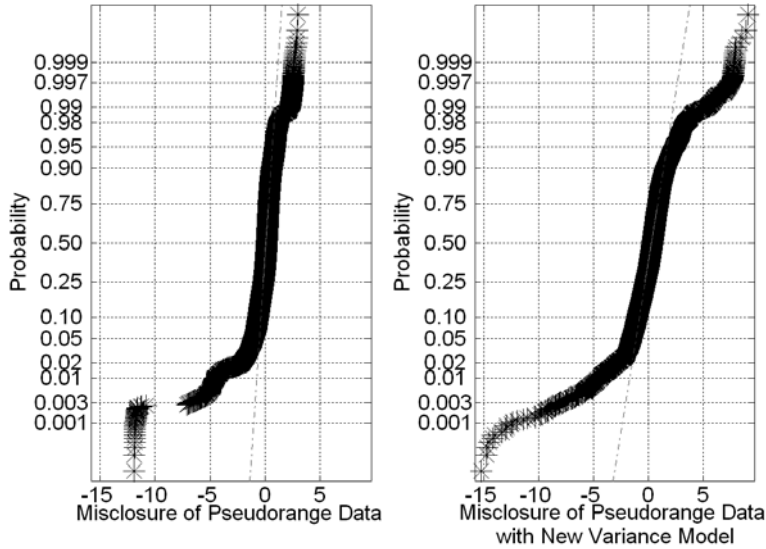


Fig. 35. Heavily Degraded Signal Environment: Normal Probability Plots of Pseudorange Misclosure Data with a Constant Variance Model and the Proposed Variance Model.

ronment of the urban canyon parking lot as presented in Fig. 36. The figure shows, that at low carrier-to-noise ratios, however, the pseudorange rate errors seem also to be shifted toward the negative side, most likely due to the signal degradations specific for this particular urban canyon environment.

For this heavily deteriorated signal environment, the new variance model of Eq. 79 is applied for the pseudorange rate measurements with the values $a = 0.001 \frac{m^2}{s^2}$ and $b = 40 \frac{m^2}{s^2} Hz$. The resulting dependence of the modeled standard deviation and the C/N_0 values is presented in Fig. 37. The standard deviation, σ_p , as output by the variance model in Eq. 79 with $a = 0.001 \frac{m^2}{s^2}$ and $b = 40 \frac{m^2}{s^2} Hz$ has been plotted on top of the absolute pseudorange error data. Even 71% of the absolute pseudorange rate error is within the standard deviation values from the variance model. In addition, the $3\sigma_p$ bound has been plotted, and only 93% of the data is within this bound. The figure indicates as well that the overall fit is not very good in this short test.

Fig. 38 presents the normal probability plots of the pseudorange rate data when a constant variance model has been applied with the variance composed from the sample standard deviation (0.5 m/s) and when the new proposed variance model of Eq. 79 has been applied with $a = 0.001 \frac{m^2}{s^2}$ and $b = 40 \frac{m^2}{s^2} Hz$. Fig. 38 implies that the

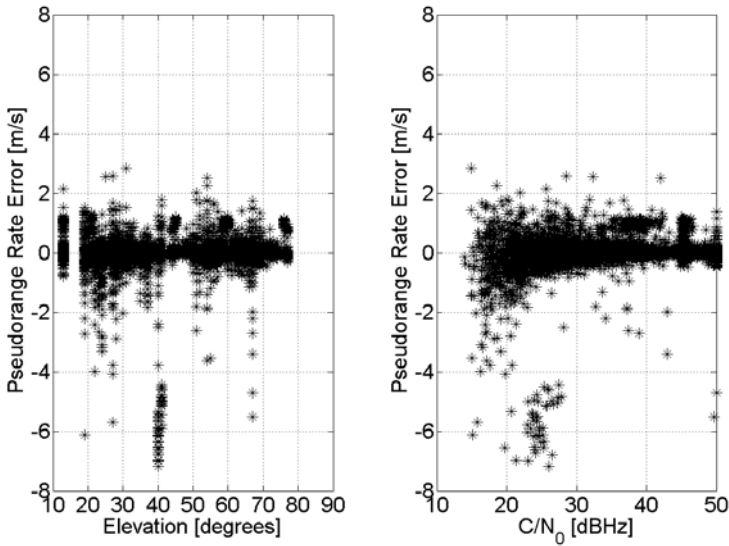


Fig. 36. Heavily Degraded Signal Environment: Pseudorange Rate Error as a Function of Elevation and Carrier-to-Noise Ratio.

misclosures with the new variance model do not follow a normal distribution as well as the pseudorange rate errors normalized with the constant variance derived from the sample. However, there is in percentage not a major difference, since still only about 3% of the misclosures deviate from normality when the new variance model is applied and they can be detected by reliability monitoring. The pseudorange rate errors of the downtown parking lot experiment are still modeled quite well with the new variance model, and the results of the downtown parking lot experiment will show, that the new variance model is profitable with respect to a constant variance model.

It is noted, that on occasions in urban and indoor environments, some strong echo-only signals that are significantly erroneous may still have a moderate signal power. In this case, the large observation error will not necessarily be reflected in the signal power, and thus, in the C/N_0 dependent weight model. These outliers are then left to reliability monitoring to be detected and excluded. On the average, however, a low power signal includes more noise and is more erroneous than a strong signal, and, thus, weighting based on the signal power level is justified.

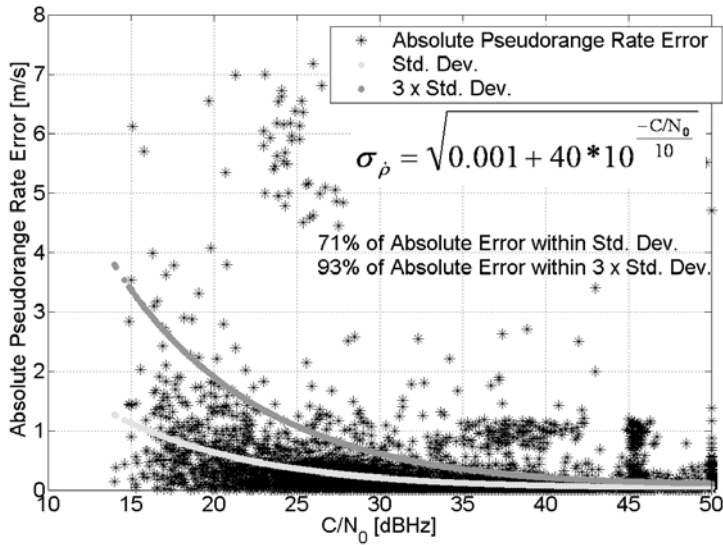


Fig. 37. Heavily Degraded Signal Environment: Absolute Pseudorange Rate Error and the Standard Deviation of Pseudorange Rate Error as a Function of Carrier-to-Noise Ratio.

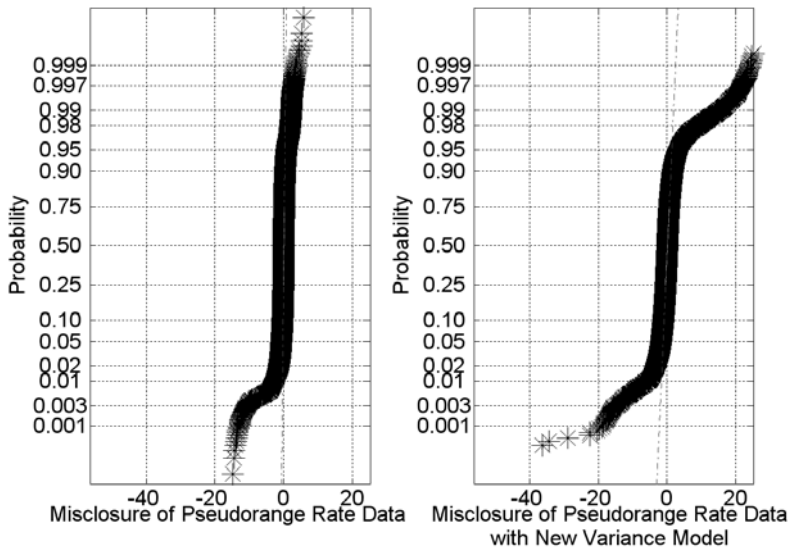


Fig. 38. Heavily Degraded Signal Environment: Normal Probability Plots of Pseudorange Rate Misclosure Data with a Constant Variance Model and the Proposed Variance Model.

7. RESULTS - TESTING AND ANALYSIS

The theory of HSGPS lies in the improved ability to acquire and track weak GPS signals. However, while the increased tracking capability of HSGPS is highly advantageous in terms of solution availability and improved redundancy, simultaneously, severe interference effects due to poor signal conditions lead to large measurement errors, and reliability monitoring becomes increasingly essential. Epoch-by-epoch least squares (LS) is used in the analysis of the developed reliability enhancement methods henceforth instead of more practical filtering approaches due to sensitivity analysis purposes.

7.1 *Real-Life High-Sensitivity GPS Tests and Reliability Analysis*

In this section, the results of real-life tests performed with a high sensitivity GPS receiver in different signal environments are presented. The HSGPS data sets are examined to assess the performance of the discussed quality monitoring methods. The test receiver used was a SiRF *XTrac* – LP^{TM} evaluation kit. The sensitivity of the receiver goes as low as -186 dBW, which corresponds to 25-30 dB fading of nominal line-of-sight GPS signal power.

7.1.1 *Static HSGPS Tests*

Two static HSGPS experiments will be analyzed; a static test inside a wooden, residential garage, and a static test in an urban canyon.

Indoor Residential Garage Test

Introduction to Procedure



Fig. 39. Residential Garage as the Setting of the Static Indoor HSGPS Test.

The experiment was carried out inside the residential garage of Fig. 39 over a time period of 12 hours in June 2003. The inside of the garage is shown on the right hand side of Fig. 39 and the left hand side shows the exterior. During the test, the wooden garage door was closed. The SiRF *XTrac* – LP^{TM} HSGPS receiver and a NovAtel 600 series antenna were used in the garage test, for both the initialization for 20 minutes outdoors in good line of sight conditions before the actual start of the experiments and in the indoor data collection. Only the indoor data is assessed here.

The analysis is focused on the effectiveness of the reliability testing schemes on position and velocity accuracy and reliability. In the least squares data processing, height constraining was used in order to have the best obtainable redundancy for reliability monitoring. The height of the static indoor test was known, as will often be the case in indoor applications, and this information was added to the estimation processes to gain the additional redundancy.

First, the availability conditions are discussed. The pseudorange and pseudorange rate, i.e., measured Doppler, errors as well as carrier-to-noise ratios of the available observations were presented in Section 3.5.2. Then, results of applying the new variance model, and the reliability enhancement methods and quality control to the indoor-experiment are shown and assessed in terms of error distributions. The uncertainty levels for the reliability monitoring were chosen as follows: the false alarm rate was set to $\alpha = 0.1\%$ and the probability of missed detection was set to $\beta = 10\%$, i.e., the power of the test was set to 90%. With different settings for the confidence

levels, also different reliability monitoring results would be obtained than presented herewith.

Fig. 40 presents the number of available satellites in the 12-hour indoor experiment. There is a surprisingly good availability in the indoor test, providing good reliability monitoring capability. However, the number of satellites varies strongly which is different from a typical outdoor situation in a favorable environment.

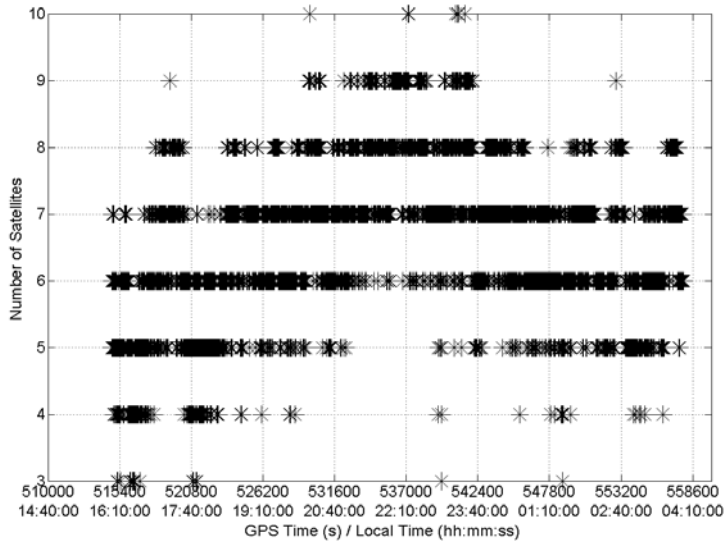


Fig. 40. Garage: Number of Available Satellites.

Position and Velocity Estimation

First, least squares is compared with weighted least squares with the new variance models, both in position domain in Fig. 41 and then in velocity domain in Fig. 42. The effect of applying the fault detection and exclusion methods, the Forward-Backward FDE of Fig. 24, the Danish Method of Fig. 25, and Subset Testing of Fig. 23, are then presented. First, the results are presented in position domain in Fig. 43, and then in velocity domain in Fig. 44. Table 5 summarizes the horizontal position errors and Table 6 summarizes the horizontal speed errors for the indoor garage experiment with HSGPS.

The results in Figures 41 and 42 show that weighting with the new variance models, $\sigma_p^2 = 10 + 150^2 * 10^{-\frac{C/N_0}{10}} m^2$ and $\sigma_v^2 = 0.01 + 25 * 10^{-\frac{C/N_0}{10}} m^2/s^2$, improve the standard

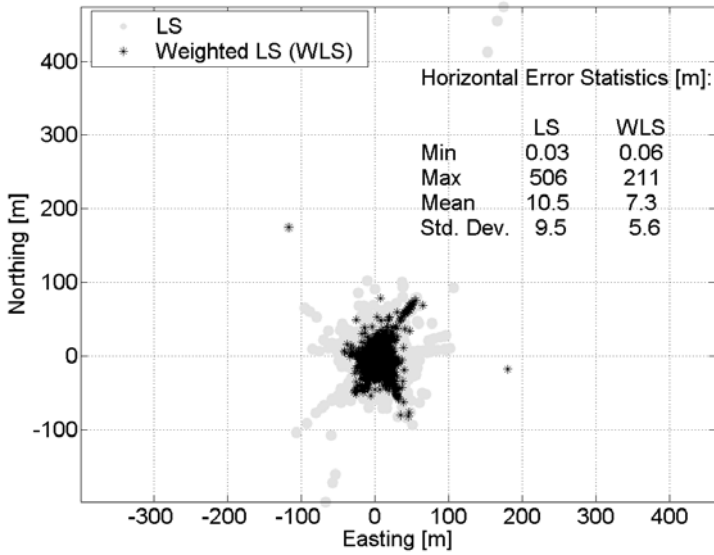


Fig. 41. Garage: Horizontal Position Errors with Unweighted and Weighted Least Squares.

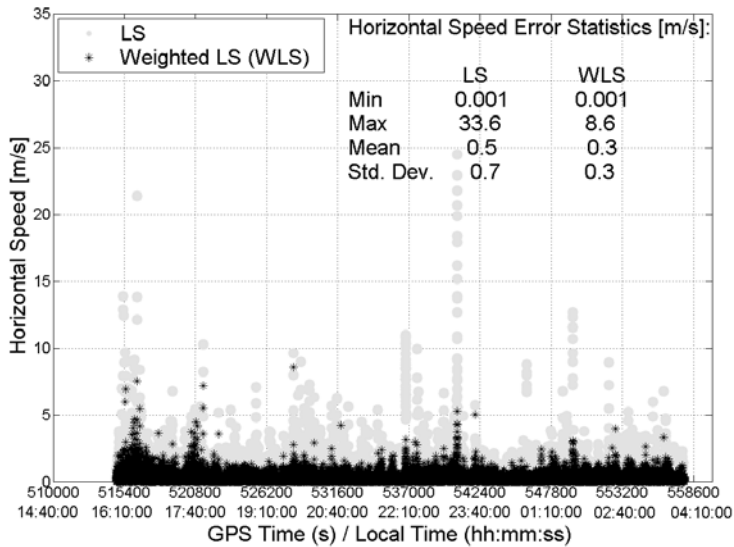


Fig. 42. Garage: Horizontal Speed Errors with Unweighted and Weighted Least Squares.

deviation of the error by about 40% in the horizontal position case and by about 60% in the horizontal speed case when compared to the unweighted least squares

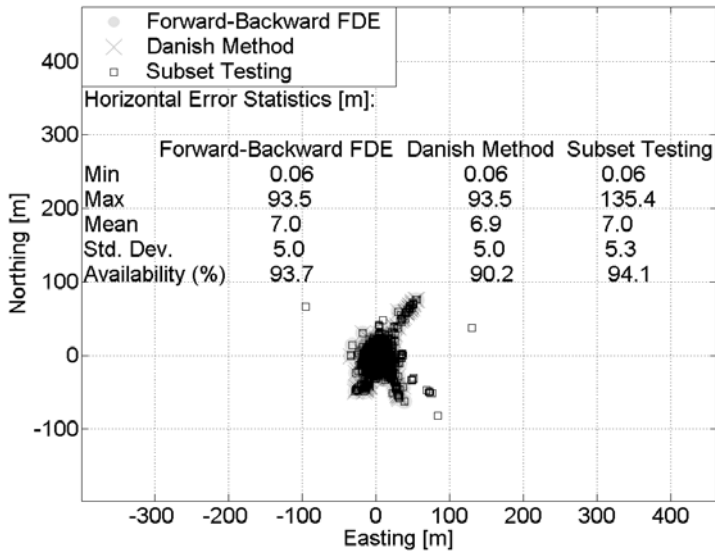


Fig. 43. Garage: Horizontal Position Errors when Three Different Fault Detection and Exclusion Methods Applied.

Table 5. Garage: Horizontal Position Errors and Availability Summarized.

	LS	WLS	F-B FDE	Danish Method	Subset Testing
Min (m)	0.03	0.06	0.06	0.06	0.06
Max (m)	506.0	211.0	93.5	93.5	135.4
Mean (m)	10.5	7.3	7.0	6.9	7.0
Std. Dev. (m)	9.5	5.6	5.0	5.0	5.3
Availability (%)	99.9	99.9	93.7	90.2	94.1

Table 6. Garage: Horizontal Speed Errors and Availability Summarized.

	LS	WLS	F-B FDE	Danish Method	Subset Testing
Min (m)	0.001	0.001	0.001	0.001	0.001
Max (m)	33.6	8.6	5.8	5.8	12.5
Mean (m)	0.5	0.3	0.3	0.3	0.3
Std. Dev. (m)	0.7	0.3	0.2	0.2	0.3
Availability (%)	99.9	99.9	93.3	88.9	94.1

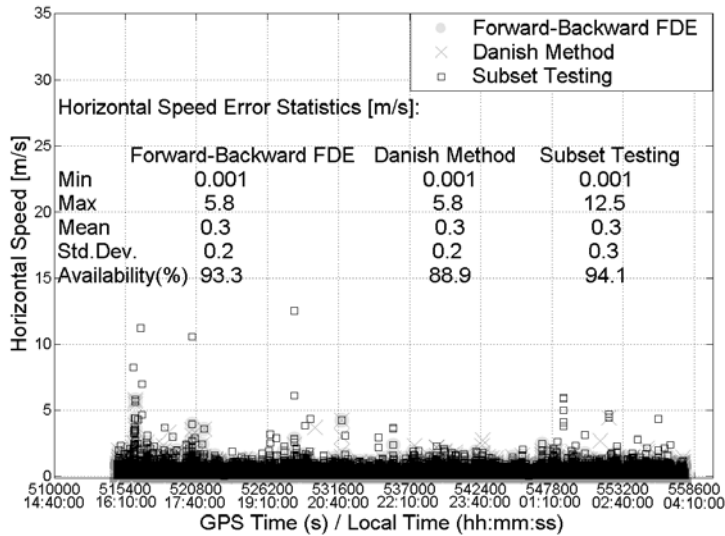


Fig. 44. Garage: Horizontal Speed Errors when Three Different Fault Detection and Exclusion Methods Applied.

computation with assumed equal variances of $\sigma_p^2 = 8^2 m^2$ and $\sigma_v^2 = 0.05^2 m^2/s^2$. In addition, with proper weighting, the maximum error goes even down from 500 to about 200 m in the horizontal position case and from 34 to about 9 m/s in the horizontal speed case. Availability of a LS and a WLS solution in time is 99.9% during the 12-hour indoor-experiment; only 0.1% of the time there were not enough satellites to compute a solution.

Overall, the availability of a position solution decreases to approximately 93% when applying the quality checks in the Forward-Backward FDE, the Danish Method, and the Subset Testing. However, this availability is still outstanding. Applying the reliability monitoring methods improve the results in the position and the velocity domains even further, as seen in Figures 43 and 44, and the Danish method and the Forward-Backward FDE method perform the best in this experiment, however, with lower availability of reliable flagged solutions than with the Subset Testing procedure. With the quality controlled Forward-Backward FDE applied, approximately 6.3% of the position solutions were excluded by the quality control of Fig. 26 including 5.6% of time epochs with observations with a zero redundancy number, 0.5% of time epochs of unsuccessful failure identification, i.e., final global test did not pass,

0.2% of time epochs with insufficient initial redundancy, and less than 0.1% due to a PDOP surpassing the threshold 10. In the epochs that passed the quality control, only about 2% required the exclusion of erroneous range observations. Only up to two exclusions were made to the pseudorange observations. With the proper C/N_0 -dependent variance models already applied, however, only few outliers remained that needed to be detected and excluded.

The accuracies of the position and velocity are indeed further improved when applying reliability monitoring and quality control methods. However, the Subset Testing performs here worst when without any reweighting or checking the influentiality of the measurements it lets some subsets with errors pass the global test due to the errors there canceling each other out. In addition, when excluding a measurement, the geometry degrades further and the errors remaining have more effect on the solution.

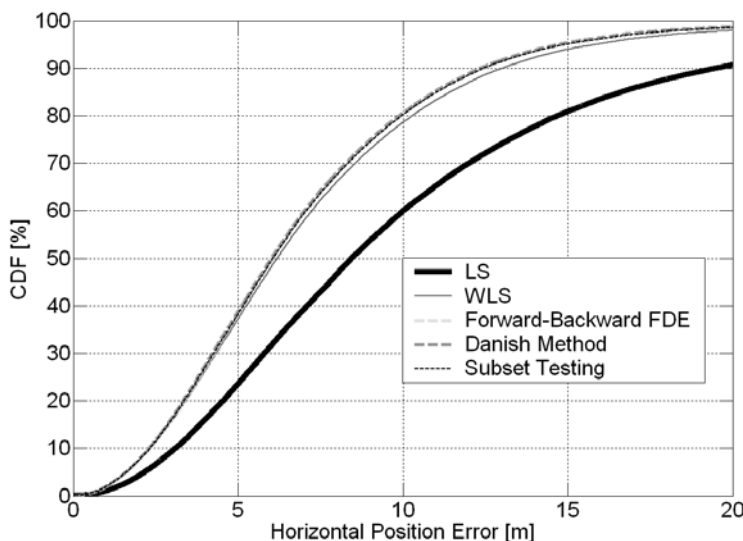


Fig. 45. Garage: Empirical Distribution Functions of Horizontal Position Errors.

Fig. 45 shows the empirical cumulative distribution functions of the horizontal position errors of the garage experiment when least squares, weighted least squares, least squares completed by Forward-Backward FDE, the Danish Method, and least squares completed by Subset Testing have been applied, respectively. This figure also

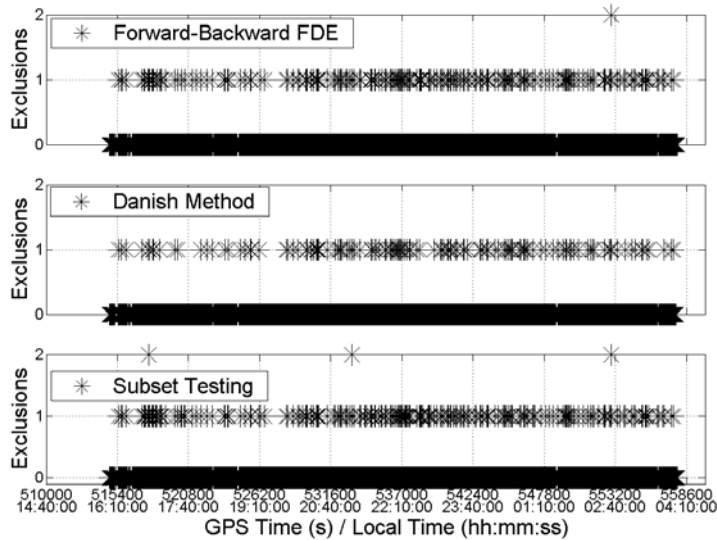


Fig. 46. Garage: Number of Exclusions of Pseudorange Observations.

suggests that the variance model has a significant impact, but the additional overall accuracy gain by the quality controlled reliability testing is small. This was to be expected; reliability testing is not about improving the precision, i.e., accuracy in the absence of biases, but about rejecting the usually few contaminated solutions. It is a security feature which only shows up in the maximum error and the absolute number of large errors.

Fig. 46 presents the number of exclusions of pseudorange observations performed in the position estimation. The global tests in the Subset Testing scheme allow for the most exclusions to be performed and in some of these cases excluding an erroneous measurement degraded the overall geometry making the result worse.

Fig. 47 shows the empirical cumulative distribution functions (CDF) of the horizontal speed errors of the garage experiment when least squares, weighted least squares, least squares completed by Forward-Backward FDE, the Danish Method, and least squares completed by Subset Testing have been applied respectively. Fig. 48 presents the number of exclusions of the pseudorange rate observations performed in the velocity estimation. With the quality controlled F-B FDE applied, approximately 6.7% of the velocity solutions were excluded by the quality control of Fig. 26 including

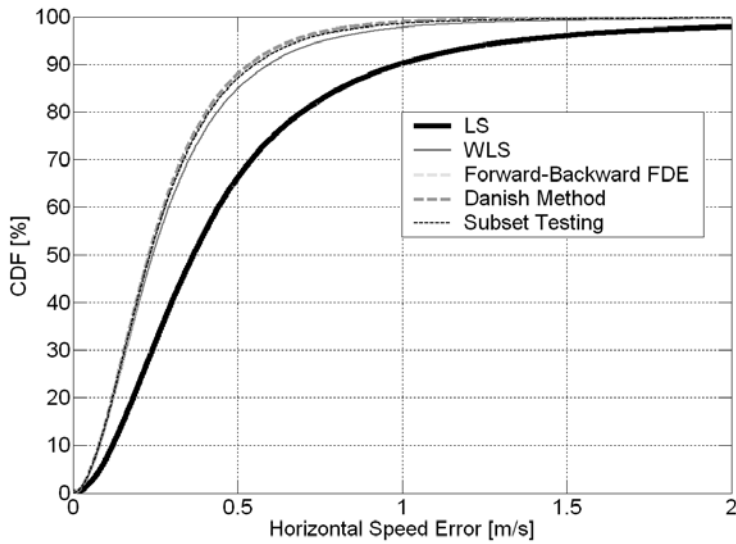


Fig. 47. Garage: Empirical Distribution Functions of Horizontal Speed Errors.

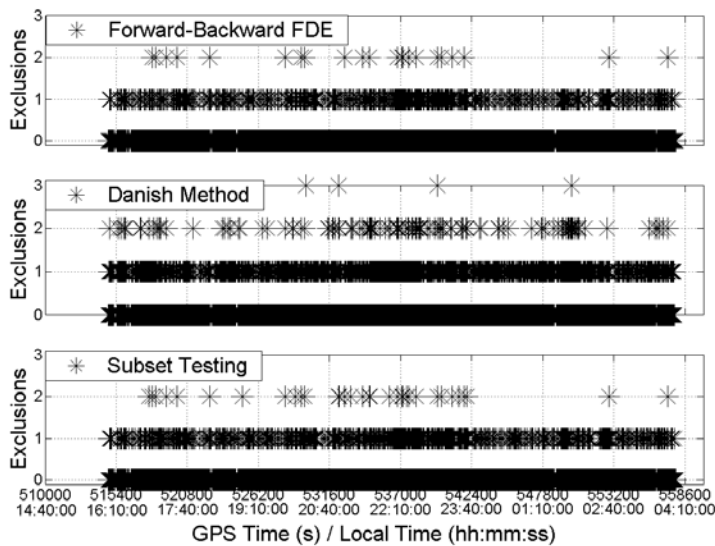


Fig. 48. Garage: Number of Exclusions of Pseudorange Rate Observations.

5.6% of time epochs with observations with a zero redundancy number, 0.9% of time epochs of unsuccessful failure identification, i.e., final global test did not pass in

the velocity computation, 0.2% of time epochs with insufficient initial redundancy, and less than 0.1% due to a PDOP surpassing the threshold 10. In the epochs that passed the quality control, only about 5% required the exclusion of erroneous range rate observations, i.e., the measured Doppler, as shown in Fig. 48. Here, the Danish Method shows most exclusions of observations by modifying the weights of the measured Doppler observations. In addition, the Forward-Backward FDE shows the least exclusions due to the feature in the procedure of not performing an exclusion if the observation to be excluded is not the most influential one. The Subset Testing slightly now fails to find the most suitable subset in its global testing since it results in a larger maximum horizontal speed error value than when applying only the weighted least squares without any quality control.

Reliability Boundaries

As the position solution is more meaningful to real-life navigation applications, the theoretical reliability levels and their relation with real-life errors are here assessed only in position domain.

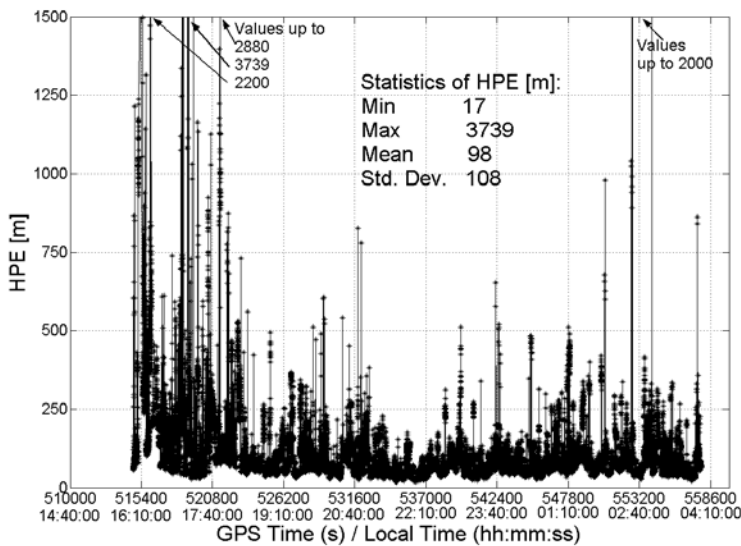


Fig. 49. Garage: HPE Values.

The theoretical reliability boundary, i.e., the horizontal protection limit, is discussed next with the external reliability measure, the Horizontal Positioning Error (HPE) of

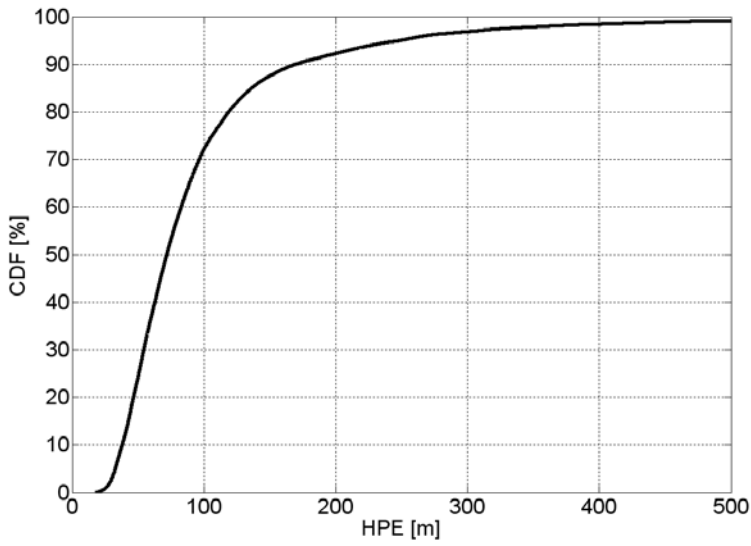


Fig. 50. Garage: Empirical Distribution of HPE.

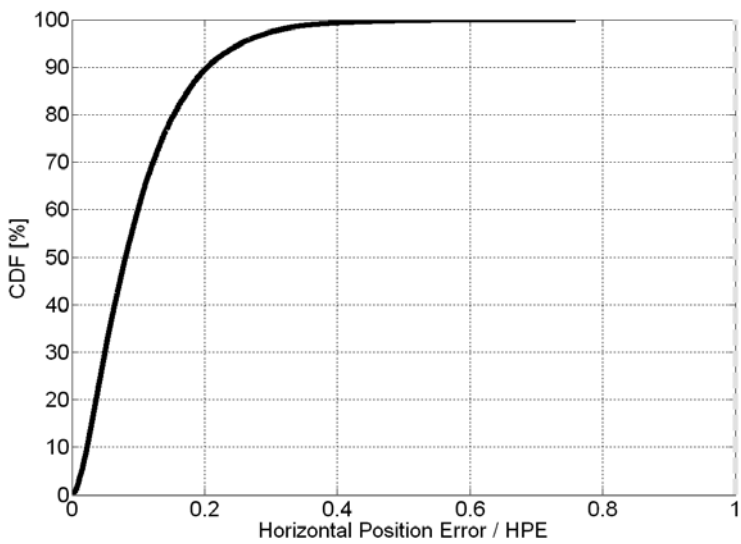


Fig. 51. Garage: Empirical Distribution of the Ratio Between Horizontal Position Error and HPE.

Eq. 69. Fig. 49 presents the maximum horizontal positioning error, HPE, predicted for each epoch in the garage test. The system can thus marginally be protected against this radial error when quality control and reliability testing are applied. Fig. 50 shows the empirical cumulative distribution function (CDF) of the HPE. We see that 72% of the time, the system is marginally protected against position errors of 100 m. Only about 1% of the time the HPE is larger than 500 m. Fig. 51 is used to compare the horizontal positioning error, HPE, against which the solution can be marginally protected, to the real quality controlled position error available from least squares completed with Forward-Backward FDE in this indoor experiment. The plot shows the empirical distribution of the actual 2-dimensional error of the quality controlled result scaled by the corresponding HPE. A value greater than 1 would indicate that the actual error surpasses the HPE, but this does not occur here. Given the probability β of missed detection, we might expect a few epochs, where this actually occurs. However, $\beta = 10\%$ only means that in 10% of the cases where an outlier of exactly the size of a minimum detectable blunder (MDB) actually occurs, this outlier will not be detected, and an error of size HPE results. In reality, only perhaps $P1 = 10\%$ outliers occur in the first place, and of those only a small percentage, say $P2$, will be close to the MDB (Kuusniemi et al., 2004). Most will be smaller and thus perhaps go unnoticed but certainly cause less error than the HPE, or larger and thus be easily detected (Kuusniemi et al., 2004). So, the probability of actually encountering an outlier of size MDB which is unnoticed is much smaller than β , namely about $P1 * P2 * \beta$.

Position Accuracy Estimation

Fig. 52 shows the horizontal position errors of the static indoor test and the respective DRMS accuracy estimates, D from Eq. 51, when the Forward-Backward FDE, the Danish Method and the Subset Testing were successively applied. The percentages of how often the actual errors are within the respective DRMS estimates are provided in the figure. The DRMS estimate provides here a reasonable estimation of the errors. The analysis is here concentrated only on the position accuracy due to the wider applicability of the position solution to real-life applications. In this test, the DRMS estimate does provide quite close to the 63.2% of probability it is supposed to if the assumptions are met. The noise assumptions of the new variance model $\sigma_p^2 = 10 + 150^2 * 10^{-\frac{C/N_0}{10}}$ do match the real errors well in this test, and the a posteriori variance factor reflects the true error conditions quite well.

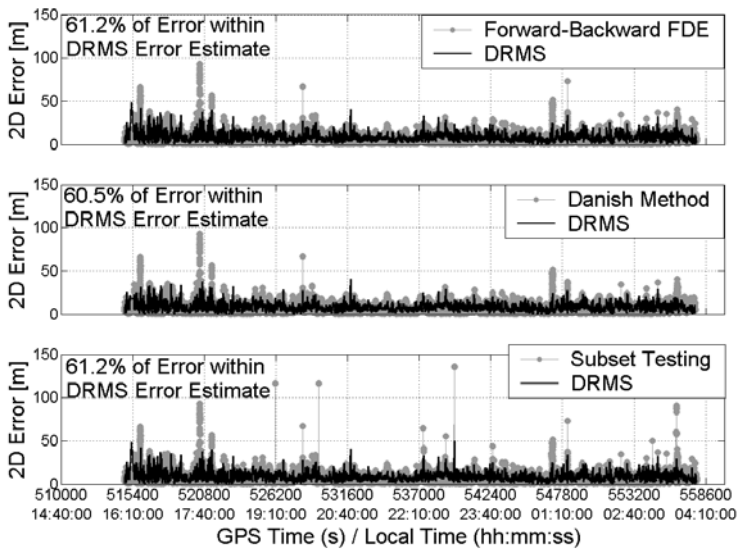


Fig. 52. Garage: Horizontal Position Errors and DRMS Error Estimates when Three Different Fault Detection and Exclusion Methods Applied.



Fig. 53. Garage: Empirical Distribution of the Ratio Between Horizontal Position Error and DRMS Error Estimate.

Fig. 53 presents a more detailed distribution of the ratio between the horizontal position errors of the quality controlled result with the Forward-Backward FDE applied and the corresponding DRMS error estimate. The figure shows that 61.2% of the error stay within the estimate, i.e., when the ratio equals 1, and the rest of the errors exceed the values of the estimate as expected.

Downtown Parking Lot Test

Introduction to Procedure



Fig. 54. Urban Environment Parking Lot as the Setting of the Static Outdoor HSGPS Test.

A test was carried out in a parking lot in an urban canyon over a time period of 35 minutes in February 2004 in downtown Calgary, Canada. The parking lot used in the experiment is shown in Fig. 54 where the parking lot is presented from both sides with the antenna of the experiment set on the roof of a test van. A SiRF *XTrac* – *LPTM* HSGPS receiver and a NovAtel 700 series antenna were used in the test. The reference for the experiment accurate to about a meter was obtained by averaging obtained reliable solutions and map-matching. Height constraining was used to have the best obtainable redundancy. The false alarm rate for the reliability processing was set to $\alpha = 0.1\%$ and the probability of missed detection was set to $\beta = 10\%$.

The analysis is here focused on accuracy and reliability and the effect of applying the reliability and quality monitoring procedures. First, Fig. 55 presents the number of available satellites in the parking lot experiment, and overall, quite good availability is obtained in this urban canyon. However, as shown in Section 3.5.3., which presented the pseudorange and pseudorange rate error with their respective carrier-to-noise ratios for this test, very low power, erroneous signals were obtained. There

are some greatly outlying observation errors present, both in range and range rate measurements, which are the result of severe multipath degradation, i.e., echo-only signal tracking. On occasions, the absolute value of the pseudorange errors reach around 800 m and the absolute value of the pseudorange rate errors reach around 7 m/s due to the multipath deteriorations caused by the nearby high buildings.

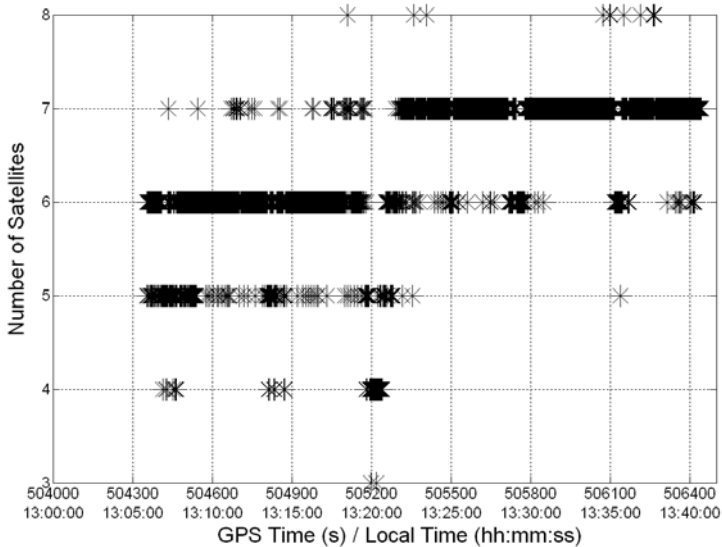


Fig. 55. Parking Lot: Number of Available Satellites.

Position and Velocity Estimation

Fig. 56 presents in a local level frame the horizontal position solution when unweighted and weighted least squares (LS) were applied. A variance of $\sigma_p^2 = 20^2 m^2$ was assumed for the equal variance unweighted LS, and for the weighted LS, the new variance model for heavily degraded signal conditions of $\sigma_p^2 = 500 + 10^6 * 10^{-\frac{C/N_0}{10}} m^2$ was applied. Fig. 56 shows the huge errors present due to the severely outlying observations. The standard deviation of the horizontal position error is still improved with just applying the new variance model from approximately 900 m to 500 m. There were a few positions, both with LS and weighted LS, that were off by hundreds of kilometers from the reference position, and these errors were here left out from the assessment due to their obvious faultiness. These deletions have reduced the availability to 96.4% and 97.4% with LS and weighted LS, respectively. The maximum

errors still obtained, however, are in the order of 10 kilometers.

Fig. 57 presents the horizontal speed error of the static test with LS and weighted LS. Here, a variance for the equal variance model of unweighted LS was assumed to be $\sigma_p^2 = 0.05^2 \text{ m}^2/\text{s}^2$, and for the weighted LS the new variance model for heavily degraded signal conditions of $\sigma_p^2 = 0.001 + 40 * 10^{-\frac{C/N_0}{10}} \text{ m}^2/\text{s}^2$. The standard deviation of horizontal speed error is reduced by almost 90% from 26 to 3 m/s when just applying the new C/N_0 based variance model.

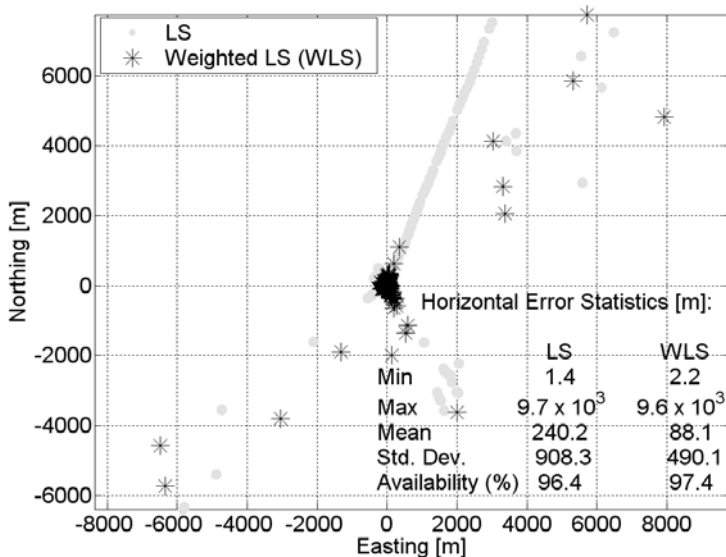


Fig. 56. *Parking Lot: Horizontal Position Errors with Unweighted and Weighted Least Squares.*

Fig. 58 presents the horizontal position errors in a local level frame around the reference position when the three FDE methods and quality control are applied. The error is reduced drastically with the availability still being fairly good, around 90%. As an elaboration on the reliability and quality monitoring, as an example, with Forward-Backward (F-B) FDE, around 9% of the time a solution is flagged as unreliable from quality control, including 6% of time instants, epochs, being flagged unreliable due to zero redundancy numbers, 2% due to a failed final global consistency check, and 1% flagged unreliable due to insufficient initial redundancy for reliability testing. In 18% of the reliably flagged solutions of F-B FDE accompanied by quality control, exclu-

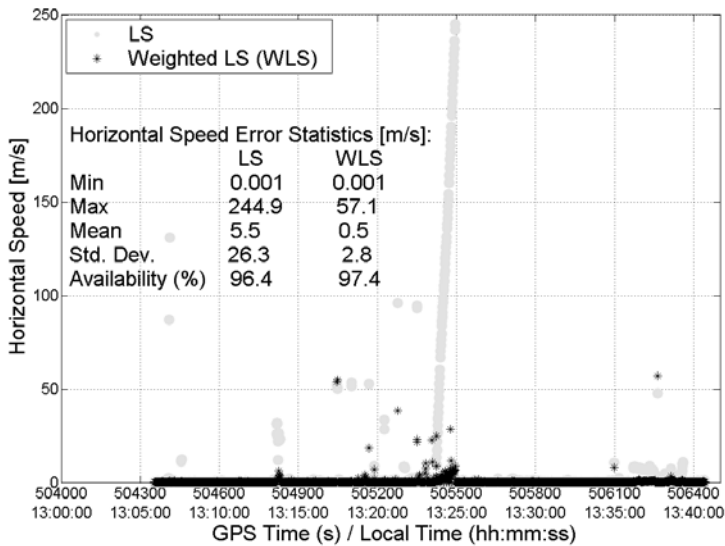


Fig. 57. Parking Lot: Horizontal Speed Errors with Unweighted and Weighted Least Squares.

sions have been made. Subset Testing performs here slightly worse than the F-B FDE and the Danish Method due to the global testing of all the subsets lets some faulty solutions pass the test, but, however, the Subset Testing has the highest availability.

Fig. 59 presents the horizontal speed error in the static downtown test when the FDE methods and quality control have been applied. Again, the F-B FDE and the Danish Method performs best with respect to accuracy resulting in standard deviations of 0.1 m/s. The Subset Testing results in a few erroneous speed results, however, having the highest availability. As an example, in the F-B FDE, a solution was declared unreliable 9.5% of the time by quality control, including 6% due to zero redundancy numbers, 2.5% due to final global test failure, and 1% due to insufficient initial redundancy. In none of the solutions did the PDOP exceed the predetermined threshold of 10. Overall, in the remaining solutions that passed the quality control, the F-B FDE performed exclusions 15% of the time.

Tables 7 and 8 summarizes the accuracy and availability of the parking lot experiment for position and velocity errors, respectively. Overall, the F-B FDE accompanied with quality control performs best in terms of considering both accuracy and availability.

Fig. 60 shows the empirical cumulative distribution functions (CDF) of the horizon-

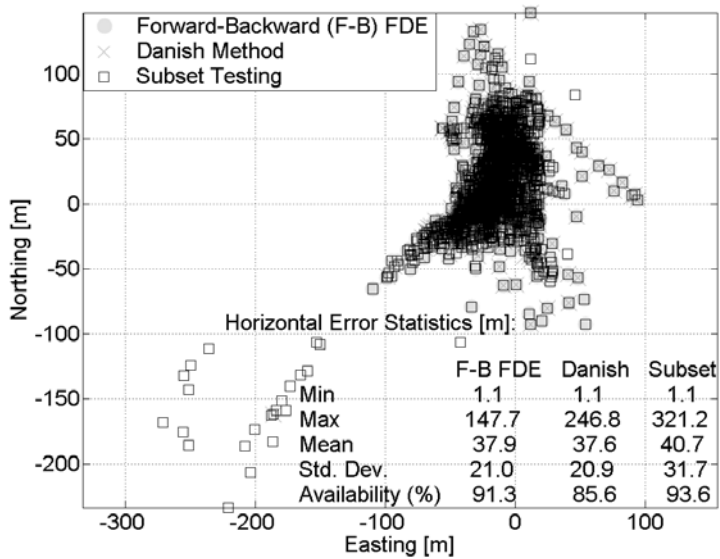


Fig. 58. Parking Lot: Horizontal Position Errors when Three Different Fault Detection and Exclusion Methods Applied.

Table 7. Parking Lot: Horizontal Position Errors and Availability Summarized.

	LS	WLS	F-B FDE	Danish	Subset Testing
Min (m)	1.4	2.2	1.1	1.1	1.1
Max (m)	9.7×10^3	9.6×10^3	147.7	246.8	321.2
Mean (m)	240.2	88.1	37.9	37.6	40.7
Std. Dev. (m)	908.3	490.1	21.0	20.9	31.7
Availability (%)	96.4	97.4	91.3	85.6	93.6

Table 8. Parking Lot: Horizontal Speed Errors and Availability Summarized.

	LS	WLS	F-B FDE	Danish	Subset Testing
Min (m)	0.001	0.001	0.001	0.001	0.001
Max (m)	244.9	57.1	3.4	1.5	54.2
Mean (m)	5.5	0.5	0.1	0.09	0.1
Std. Dev. (m)	26.3	2.8	0.1	0.1	1.2
Availability (%)	96.4	97.4	90.5	80.9	93.6

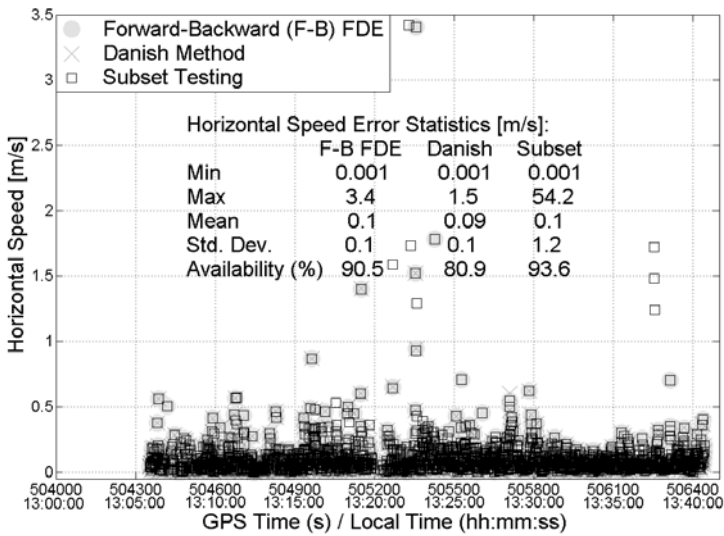


Fig. 59. Parking Lot: Horizontal Speed Errors when Three Different Fault Detection and Exclusion Methods Applied.

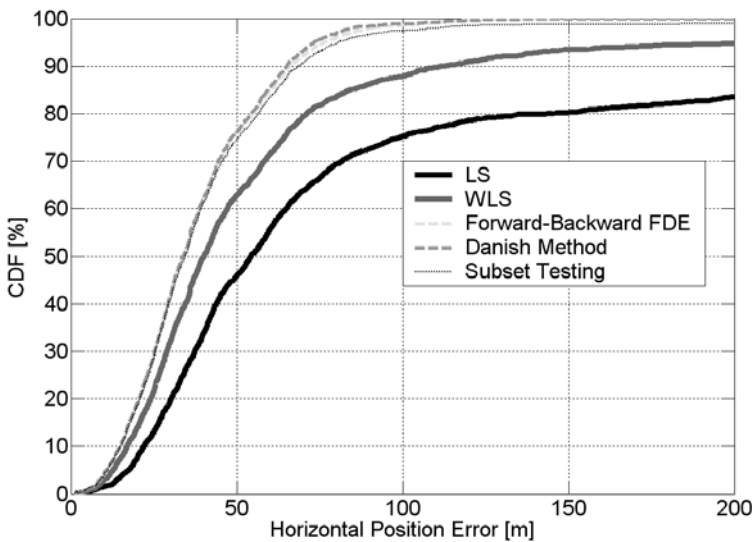


Fig. 60. Parking Lot: Empirical Distribution Functions of Horizontal Position Errors.

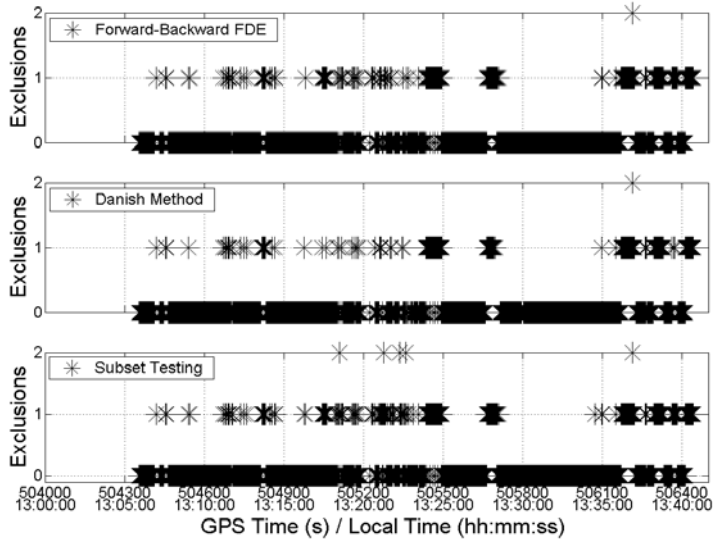


Fig. 61. Parking Lot: Number of Exclusions of Pseudorange Observations.

tal position errors of the parking lot experiment when least squares, weighted least squares, least squares completed by Forward-Backward FDE, the Danish Method, and least squares completed by Subset Testing have been applied, sequentially, giving hereby information on the distribution of the errors. With the FDE approaches and quality control applied, almost 80% of the solutions are within 50 meters from the reference. Fig. 61 presents the number of exclusions of pseudorange observations performed in the position estimation with the different FDE approaches showing that the Subset Testing allows for the most exclusions.

Fig. 62 shows the empirical cumulative distribution functions (CDF) of the horizontal speed errors of the static urban canyon experiment when least squares, weighted least squares, least squares completed by Forward-Backward FDE, the Danish Method, and least squares completed by Subset Testing have been applied, sequentially. With FDE and quality control, around 99% of the speed solutions are below 0.5 m/s. Fig. 63 presents the number of exclusions of pseudorange rate observations performed in the velocity estimation showing again the most exclusions performed by Subset Testing. At occasions, the pseudorange and pseudorange rate observations from the same satellite were excluded, but, however, not always. In addition, when resulting in a reliable flagged subset, the Subset Testing always resulted in a reliable subset for both

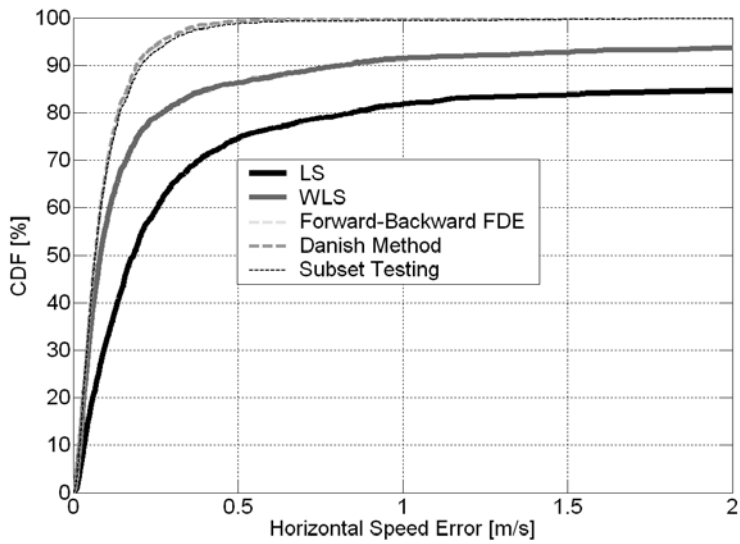


Fig. 62. Parking Lot: Empirical Distribution Functions of Horizontal Speed Errors.

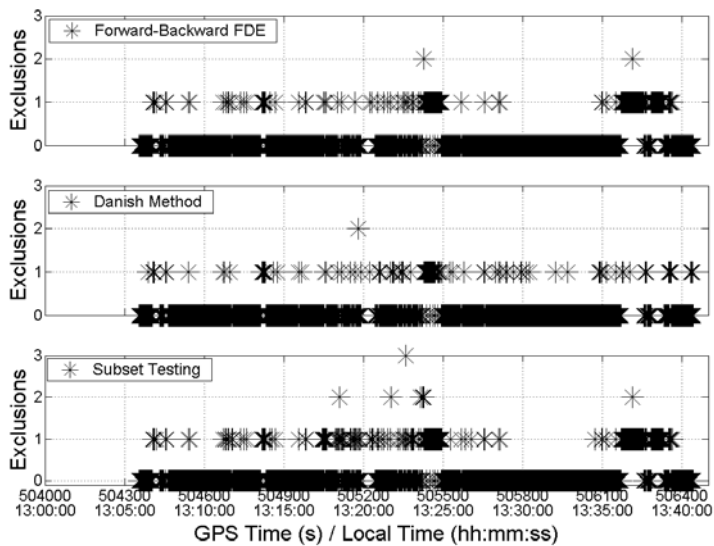


Fig. 63. Parking Lot: Number of Exclusions of Pseudorange Rate Observations.

the position and the velocity computation, though the subsets not always containing observations from the exactly same satellites. Generally, slightly more exclusions

were performed on the pseudorange rate measurements. Therefore, the Subset Testing results in an equal percentage of availability of a reliable flagged solution for both the position and speed solutions.

Position Reliability Boundaries

Next, the external reliability boundary, the HPE, is assessed as well as its relation with real errors in the static parking lot test. Fig. 64 presents the HPE values in time and statistics of the HPE in the parking lot experiment. A standard deviation of about 500 m is obtained in the HPE in this test. Fig. 65 provides information on the distribution of the HPE, and it shows that around 7% of the theoretical HPE boundary exceeds 1000 m. Fig. 66 presents the empirical distribution of the ratio between the real horizontal position error obtained by F-B FDE and quality control and the HPE boundary. It shows that none of the real errors reach the HPE boundary, since the HPE represents the worst case scenario that the system can be protected against if errors of the size of the MDB would occur.

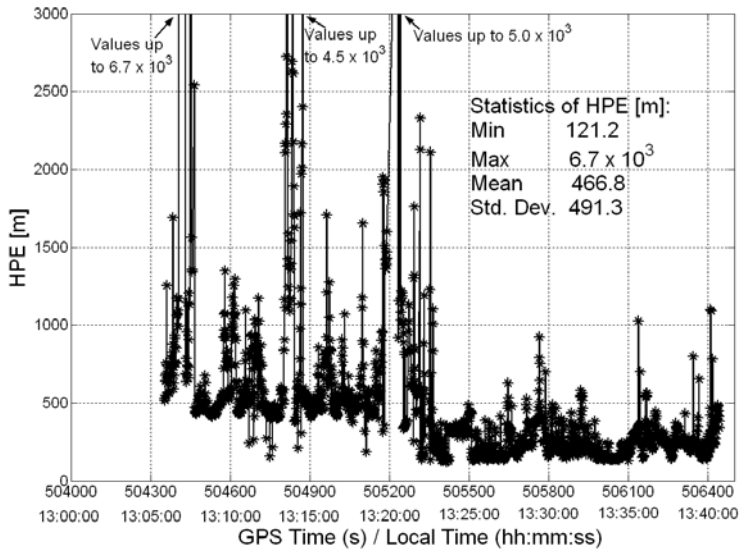


Fig. 64. Parking Lot: HPE Values.

Position Accuracy Estimation

The analysis is here concentrated only on the position accuracy due to the wider applicability of the position solution to real-life applications. Fig. 67 shows the hori-

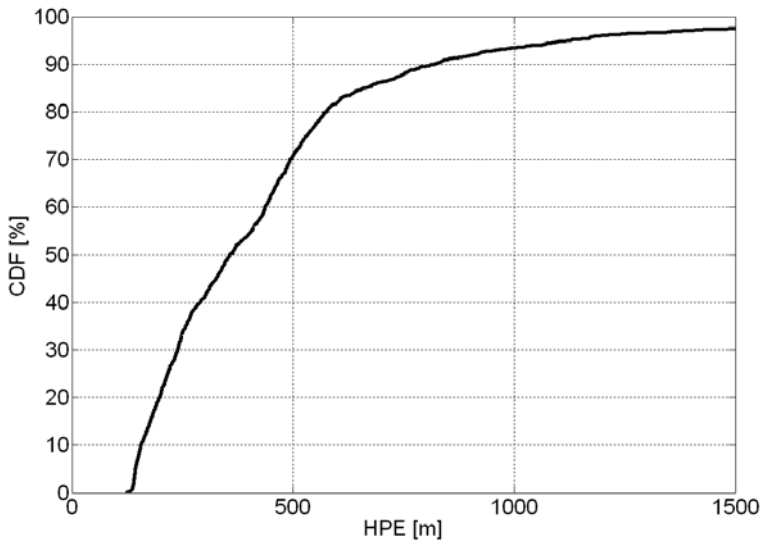


Fig. 65. Parking Lot: Empirical Distribution of HPE.

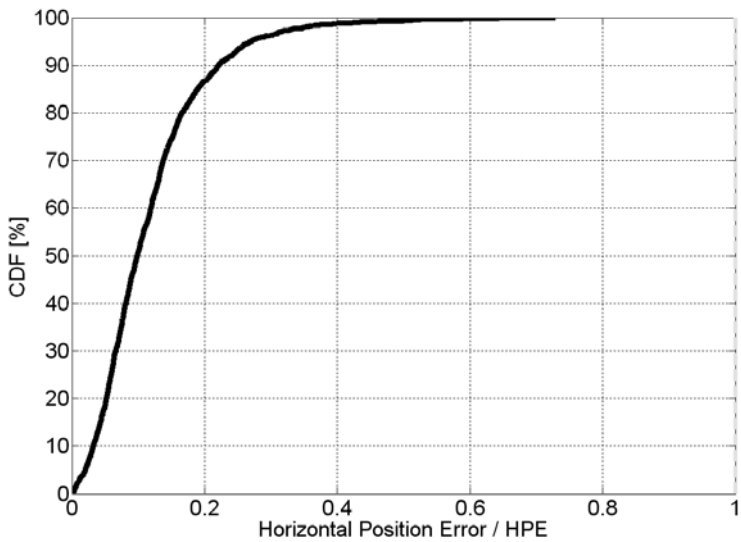


Fig. 66. Parking Lot: Empirical Distribution of the Ratio Between 2D Position Error and HPE.

horizontal position errors of the static parking lot test and the respective DRMS accuracy estimates, D of Eq. 51, when the Forward-Backward FDE, the Danish Method and the Subset Testing were successively applied. The percentages of how often the actual errors are within the respective DRMS estimates are provided in the figure, and in these three situations, only approximately around 30% of the actual horizontal errors are within the DRMS error estimate. The DRMS estimate provides still a quite reasonable estimation of the errors despite the noise assumptions of the new variance model $\sigma_p^2 = 500 + 10^6 * 10^{-\frac{C/N_0}{10}}$ not matching the real errors perfectly in this test. The a posteriori variance factor thus does not completely reflect the true error conditions but it still gives a reasonable indication.

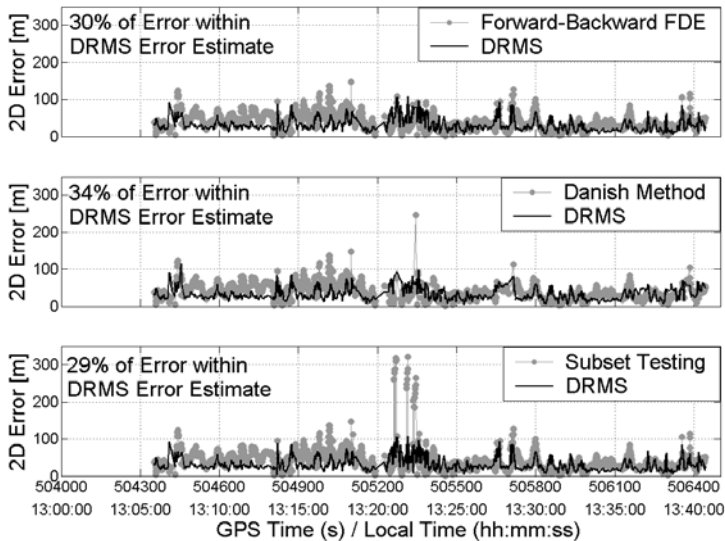


Fig. 67. Parking Lot: Horizontal Position Errors and DRMS Error Estimates when Three Different Fault Detection and Exclusion Methods Applied.

Fig. 68 presents the empirical distribution of the ratio between the horizontal position error of the quality controlled result with the Forward-Backward FDE applied and the DRMS error estimate. The figure shows the only 30% of the error staying within the estimate, i.e., when the ratio equals 1, and the rest of the errors exceed the values of the estimate.

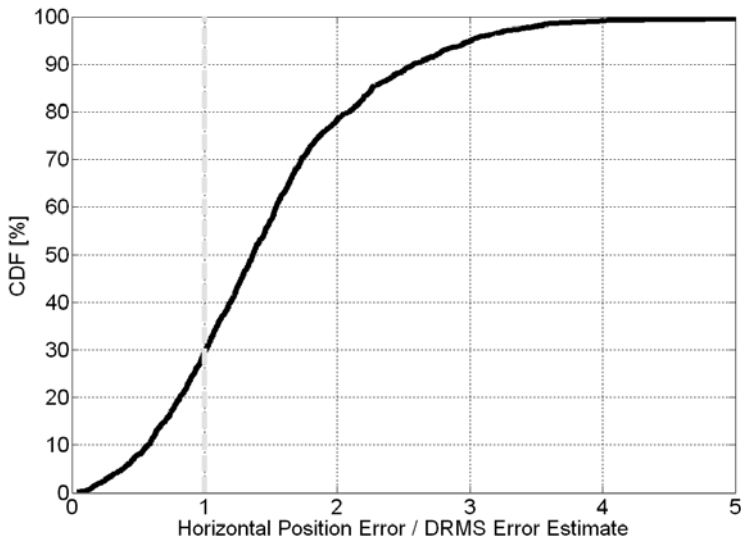


Fig. 68. *Parking Lot: Empirical Distribution of the Ratio Between Horizontal Position Error and DRMS Error Estimate.*

7.1.2 Kinematic HSGPS Tests

Two real-life kinematic HSGPS tests were performed in downtown Calgary, Canada, namely a pedestrian test and a vehicular test. The test trajectories of the two tests are shown in Fig. 69. In addition, pictures describing the test conditions in terms of the surrounding buildings causing blockages are provided. A picture showing the environment in the pedestrian test is provided in Fig. 70. Furthermore, a picture describing the test conditions in the vehicular test is provided in Fig. 71. As can be seen, there are high structures surrounding the streets in the experiments causing outlying observations due to multipath degradation. No definite reference could be obtained in the kinematic experiments and, thus, no absolute accuracy and reliability analysis will be given here, but rather just assessments comparing the results in the position domain to a map in a local level frame. The map includes the reference routes. The pedestrian test also included some static points when the pedestrian made stops on street corners, and in the vehicular test, an external velocity reference from an IMU/GPS (Integrated Measurement Unit/Global Positioning System) was available.

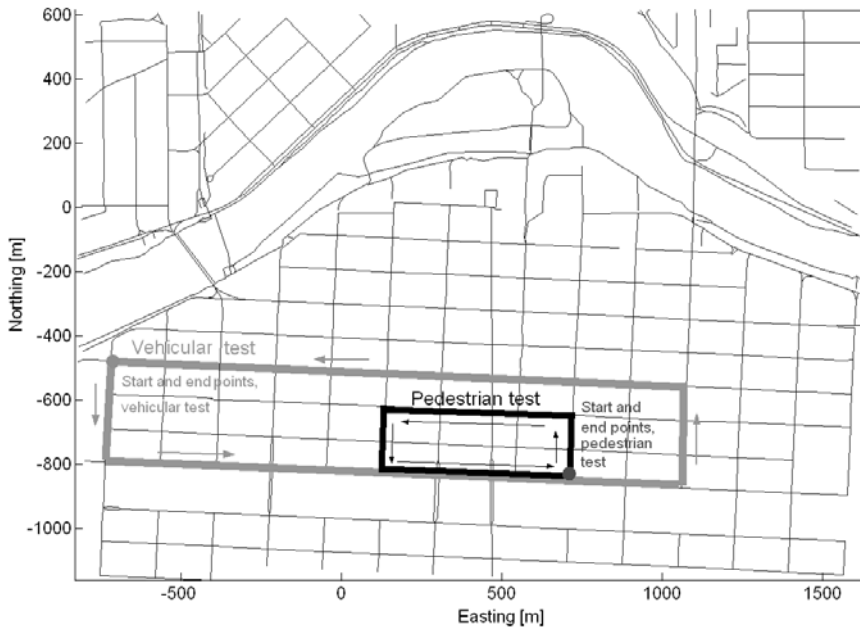


Fig. 69. Trajectories of the Urban Environment Kinematic HSGPS Tests.



Fig. 70. Surroundings of the Pedestrian HSGPS Experiment.



Fig. 71. Surroundings of the Vehicular HSGPS Experiment.

Downtown Pedestrian Test

Introduction to Procedure

First, the results for a 30-minute pedestrian test are presented and assessed. The test was carried out in an urban canyon downtown environment in December 2003 in Calgary, Canada. A SiRF *XTrac* – LP^{TM} HSGPS receiver and a NovAtel 700 series antenna were used in the pedestrian test with the antenna mounted on top of a backpack carried by the pedestrian. The pedestrian traveled the route shown in Fig. 69 making stops of few seconds in each street corner, which will be pointed out in the speed solution figures. Fig. 72 presents the number of available satellites and the corresponding carrier-to-noise ratios for the pedestrian experiment. Very low power signals were obtained, but, overall, availability is fairly good considering the surroundings. Height constraining was used to have the best obtainable redundancy. The false alarm rate for the reliability processing was set to $\alpha = 0.1\%$ and the probability of missed detection was set to $\beta = 10\%$.

Position and Velocity Estimation

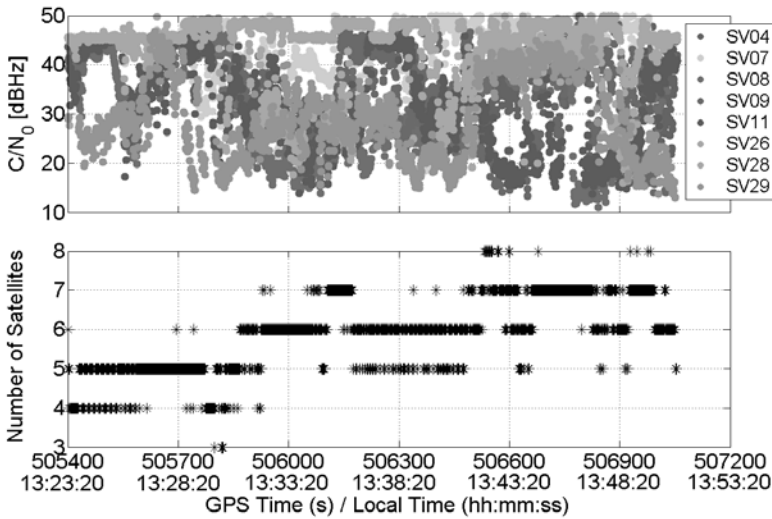


Fig. 72. Pedestrian Test: Available Satellites and Their C/N_0 Values.

Fig. 73 presents the position results for the pedestrian test with unweighted ($\sigma_p^2 = 20^2 m^2$) and weighted ($\sigma_p^2 = 500 + 10^6 * 10^{-\frac{C/N_0}{10}} m^2$) least squares (LS). It shows on a map the huge errors in order of kilometers that are obtained, and some of the errors are even outside of the scope of the map in the figure with the maximum errors being in the order of 80 kilometers. The new variance model reduces a few of the largest errors. The availability for LS and weighted LS is 100%.

Fig. 74 presents the horizontal speed of the pedestrian test with unweighted ($\sigma_p^2 = 0.05^2 m^2/s^2$) and weighted ($\sigma_p^2 = 0.001 + 40 * 10^{-\frac{C/N_0}{10}} m^2/s^2$) LS applied. Though there were no definite reference, the static periods are pointed out in the figure, and, generally, the speed of the pedestrian carrying a heavy backpack with the test equipment on the back does not exceed 3 to 4 m/s. Especially in the end of the test, where the environment was harsh in terms of high skyscrapers, huge errors in the horizontal speed solution of 200 to 300 m/s were obtained. More detailed statistics of the horizontal speed for unweighted and weighted LS is provided in the figure. Availability of a LS and weighted LS velocity solution was 100%.

Fig. 75 presents separately the horizontal positions of the pedestrian test in local level maps when the three FDE approaches accompanied with quality control were applied, respectively. The true route is also shown in the subfigures. The Danish

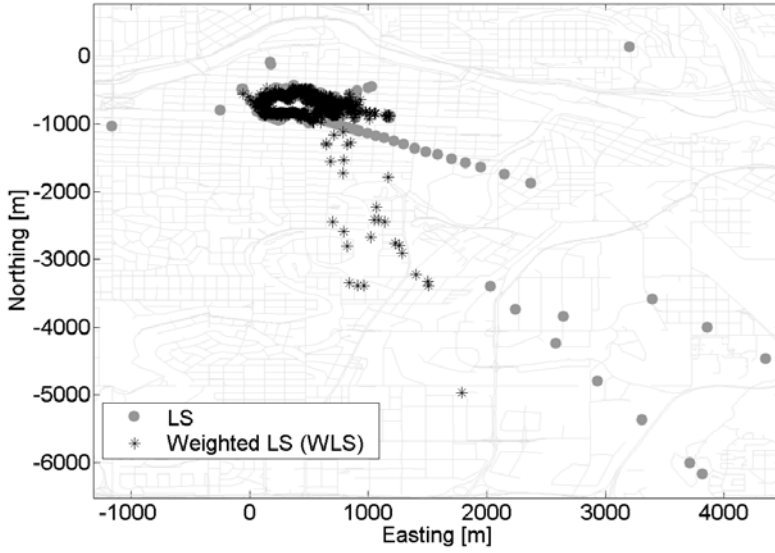


Fig. 73. Pedestrian Test: Horizontal Position with Unweighted and Weighted Least Squares.

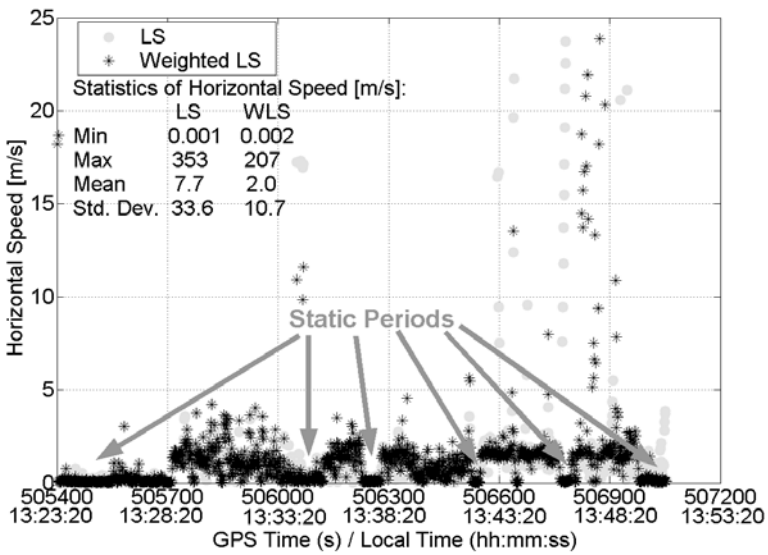


Fig. 74. Pedestrian Test: Horizontal Speed with Unweighted and Weighted Least Squares.

Method performs the best in terms of accuracy but it has the lowest availability of around 69%. The maximum errors when the FDE approaches are applied are now reduced to around 300 m, which is a major enhancement to the accuracy compared to when no reliability monitoring was applied in Fig. 73. Subset Testing resulted in the highest availability of approximately 77%. Table 9 summarizes the availabilities of a position solution in percentage with LS, weighted LS, F-B FDE, Danish Method, and Subset Testing.

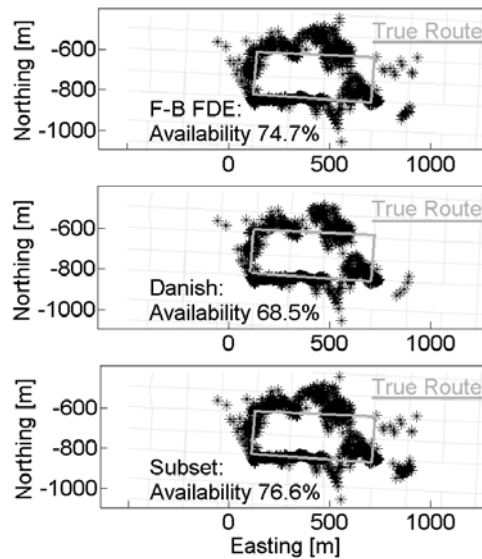


Fig. 75. Pedestrian Test: Horizontal Position when Three Different Fault Detection and Exclusion Methods Applied.

Table 9. Pedestrian Test: Availability Summarized of Position Solutions.

	LS	WLS	F-B FDE	Danish	Subset Testing
Availability (%)	100	100	74.7	68.5	76.6

Fig. 76 presents the exclusions performed by the FDE procedures to the range measurements. It shows that Subset Testing generally allows for the most exclusions. However, usually, only one exclusion of a range observation is made by the FDE approaches in this pedestrian test.

To elaborate in more detail on the reliability and quality control, in the Forward-Backward (F-B) FDE scheme, as an example of the FDE procedures, epochs were

flagged as unreliable around 25% of the time and these included 20% of epochs being flagged unreliable due to zero redundancy numbers, 4% of epochs failing the final global test, and 1% of epochs lacking the initial redundancy for reliability testing. No rejections due to the PDOP exceeding the threshold were necessary. Of the remaining reliable flagged epochs, in 11% of epochs, exclusion was performed.

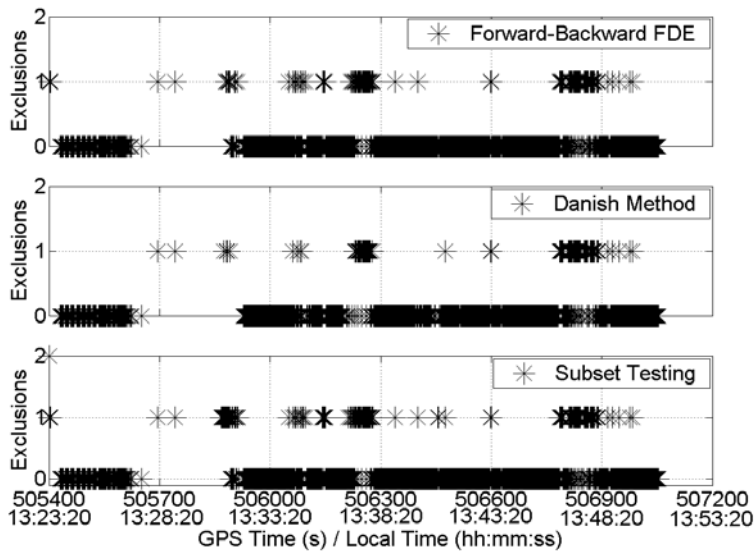


Fig. 76. *Pedestrian Test: Number of Exclusions of Pseudorange Observations.*

Fig. 77 presents the horizontal speed solutions when the FDE and quality control have been applied. The static periods are pointed out in the figure. There are still some major errors persisting, especially with the Subset Testing, whose global testing is sometimes letting the erroneous solutions pass the consistency check. However, overall, the maximum errors are reduced now significantly. Table 10 summarizes the availabilities of a horizontal speed solution in percentage with LS, weighted LS, F-B FDE, Danish Method, and Subset Testing. The Subset Testing always found simultaneously a reliable flagged solution also here for both position and velocity computation though performing different amounts of exclusions.

Fig. 78 presents the exclusions made by the FDE approaches on the range rate observations, i.e., the measured Doppler. The Subset Testing approach demonstrates the most exclusions. Again, as an example of the reliability and quality control operation, in the F-B FDE approach as much as 41% of the time epochs were flagged as

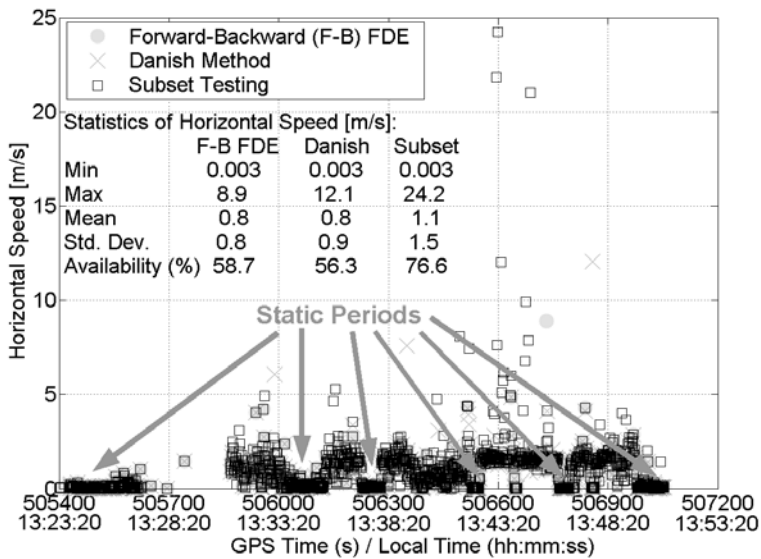


Fig. 77. Pedestrian Test: Horizontal Speed when Three Different Fault Detection and Exclusion Methods Applied.

unreliable by quality control. This includes having an observation with a zero redundancy number in 20% of epochs, a global consistency test failure in 20% of the time epochs, and not having enough initial redundancy to perform reliability testing in 1% of the time. Furthermore, on the remaining reliable flagged solutions by the quality control, exclusions of range rate observations were made by the F-B FDE scheme in 23% of the time epochs in the pedestrian test.

Position Reliability Boundaries

Next, the theoretical external reliability is briefly presented, i.e., the HPE values resulting in the pedestrian test. Fig. 79 presents the HPE values in time and elaborates on the statistics. The standard deviation of HPE in the pedestrian test is around 800 m, and the real-life errors obtained with the quality controlled FDE approaches are clearly less. Fig. 80 shows the distribution of the HPE values, where it can be seen

Table 10. Pedestrian Test: Availability Summarized of Speed Solutions.

	LS	WLS	F-B FDE	Danish	Subset Testing
Availability (%)	100	100	58.7	56.3	76.6

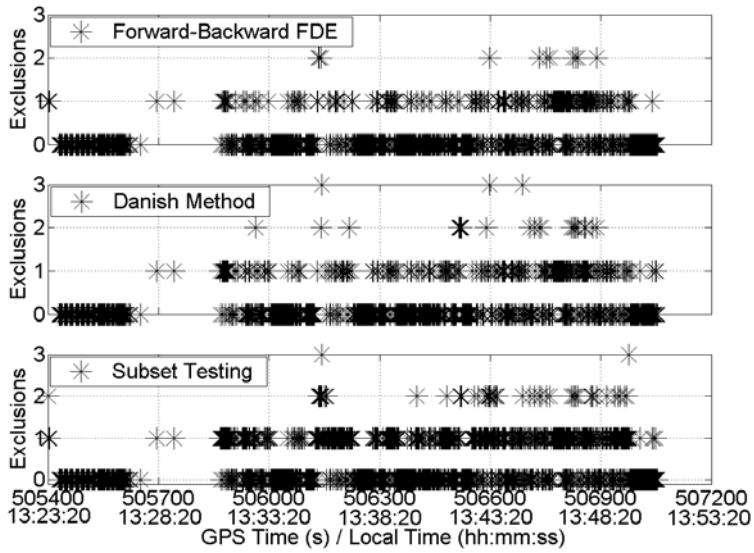


Fig. 78. Pedestrian Test: Number of Exclusions of Pseudorange Rate Observations.

that 5% of the theoretical HPE values are even over 2 kilometers.

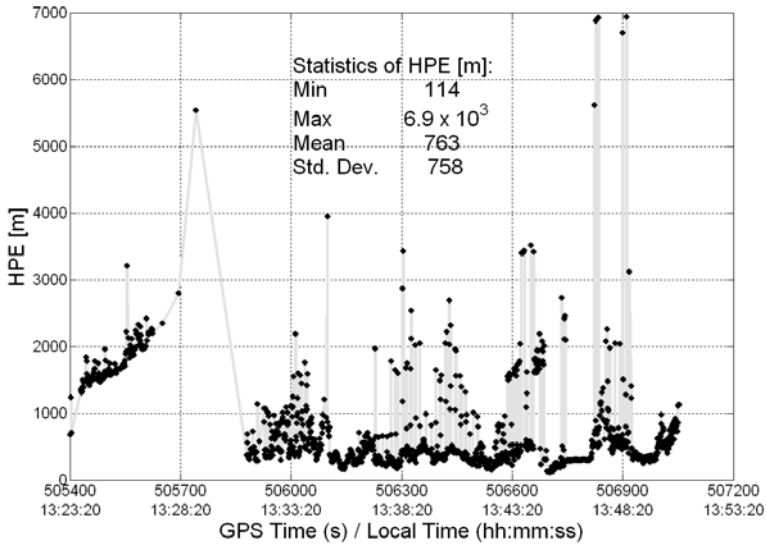


Fig. 79. Pedestrian Test: HPE Values.

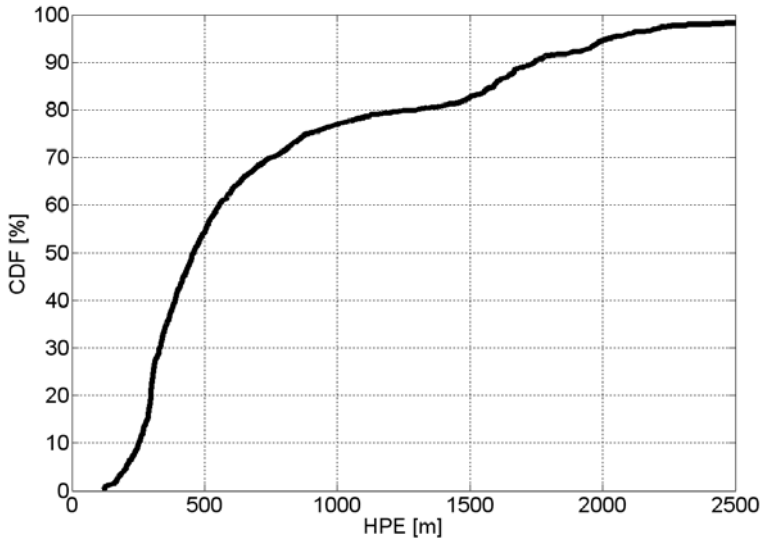


Fig. 80. Pedestrian Test: Empirical Distribution of HPE.

Position Accuracy Estimation

Due to not having a definite reference in the pedestrian test, the DRMS values when different FDE approaches are applied can only be roughly compared to the true errors visible on the maps in a local level frame in Fig. 75. Fig. 81 presents the DRMS horizontal accuracy estimates from the three FDE approaches, and it shows that the maximum DRMS error estimate is just under 400 m. This suits somewhat well the map displays of Fig. 75, and it can be roughly estimated that the true errors are within about 50% of the DRMS estimates giving thus a reasonable estimate of the position accuracy.

Downtown Vehicular Test

Introduction to Procedure

A vehicular test was carried out with a test van in an urban canyon downtown environment in February 2004 in Calgary, Canada. A SiRF *XTrac – LPTM* HSGPS receiver and a NovAtel 700 series antenna were used in the vehicular test with the antenna being placed on the roof of the van. Fig. 82 presents the number of available satel-

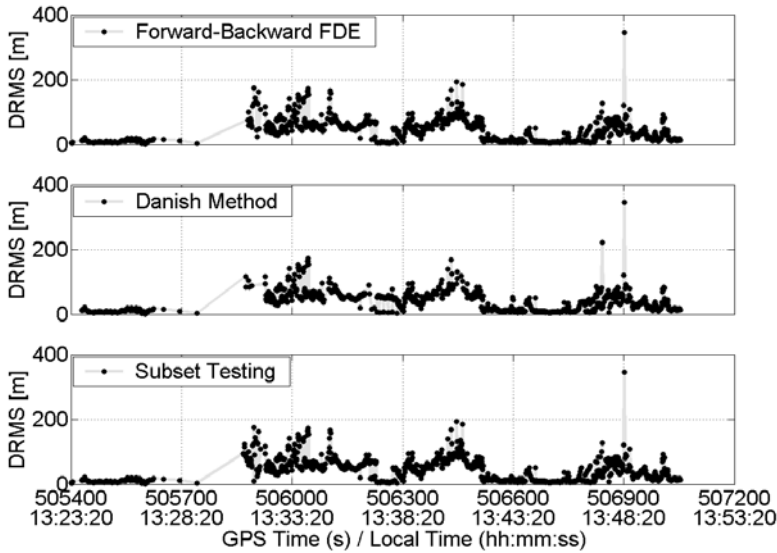


Fig. 81. Pedestrian Test: DRMS Error Estimates when Three Different Fault Detection and Exclusion Methods Applied.

lites and their corresponding carrier-to-noise ratio levels in the vehicular test. Very low power signals are also obtained due to the heavy obstructions of skyscrapers surrounding the route. Overall, a quite good signal availability is, however, obtained. Height constraining was again used to have the best obtainable redundancy. The false alarm rate for the reliability processing was set to $\alpha = 0.1\%$ and the probability of missed detection was set to $\beta = 10\%$.

Position and Velocity Estimation

Fig. 83 presents the unweighted ($\sigma_p^2 = 20^2 \text{ m}^2$) and weighted ($\sigma_p^2 = 500 + 10^6 * 10^{-\frac{C/N_0}{10}} \text{ m}^2$) LS position results of the vehicular test. Some severely outlying solutions were obtained, especially with the equal variance assumption of unweighted LS, and for both LS and weighted LS, solutions out of the scope of the map in Fig. 83 were also obtained having error in the order of hundreds of kilometers. Thus, reliability monitoring is essential.

Fig. 84 presents the horizontal speed solution of the vehicular test with unweighted ($\sigma_p^2 = 0.05^2 \text{ m}^2/\text{s}^2$) and weighted ($\sigma_p^2 = 0.001 + 40 * 10^{-\frac{C/N_0}{10}} \text{ m}^2/\text{s}^2$) LS applied. A reference of the horizontal speed is included in the figure. The reference speed was

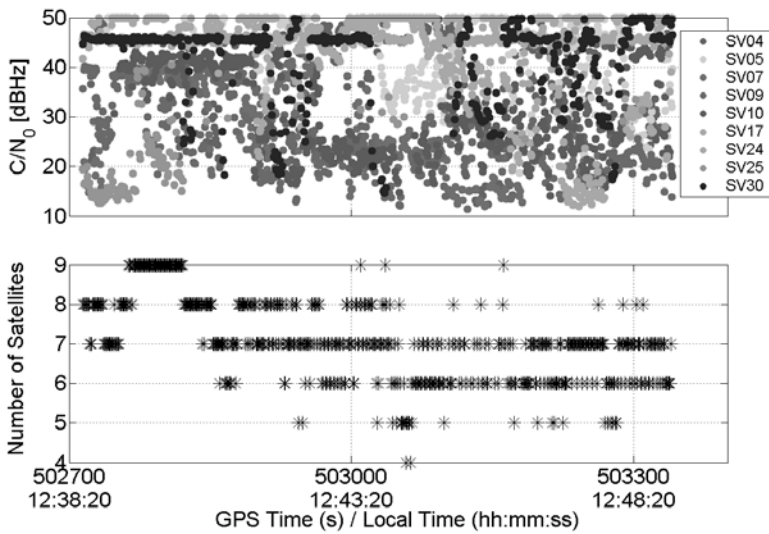


Fig. 82. Vehicular Test: Available Satellites and Their C/N_0 Values.

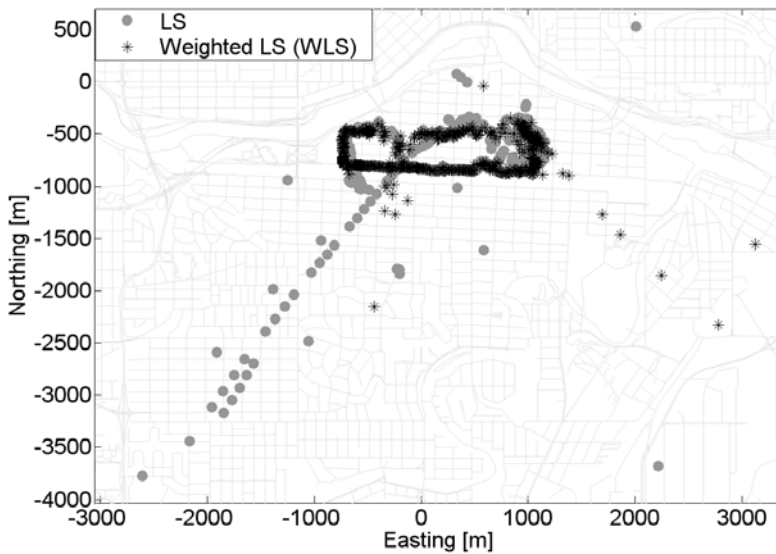


Fig. 83. Vehicular Test: Horizontal Position with Unweighted and Weighted Least Squares.

obtained from an integrated IMU/GPS system that was mounted to the test van to have a reference of the velocity of the vehicle. The IMU/GPS system used was a

Black Diamond System by NovAtel Inc. The unweighted LS demonstrates a few huge errors, up to almost 1300 m/s, and also the weighted LS demonstrates a maximum horizontal speed of over 1000 m/s as can be seen from the statistics displayed in Fig. 84. However, despite the few huge outliers, the weighted LS follows generally quite well the reference speed.

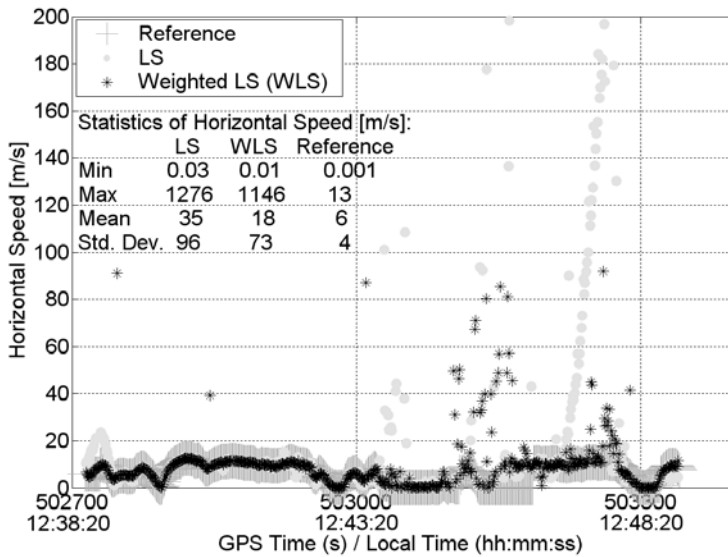


Fig. 84. Vehicular Test: Horizontal Speed with Unweighted and Weighted Least Squares. Reference Included in the Figure.

Fig. 85 shows the horizontal position results in a local level frame when applying the FDE approaches accompanied with quality control to the vehicular test. The true route is shown on the separate maps along with the point solutions. All the huge errors are now vanished, but there is in places error in the order of around 400 m, with all the FDE schemes. Overall, however, reasonably good accuracies and availabilities are obtained with all the reliability monitoring procedures considering the harsh environment. Subset Testing demonstrates again the best availability of a reliable flagged solution as a result of its global testing on all the subsets.

Fig. 86 presents the number of exclusions made by the FDE schemes to range measurements, and up to 3 exclusions were performed by all the procedures. Again, as an example of the operation of the reliability monitoring, in the F-B FDE, 6.5% of the solutions were flagged unreliable including 3.1% of time epochs having an ob-

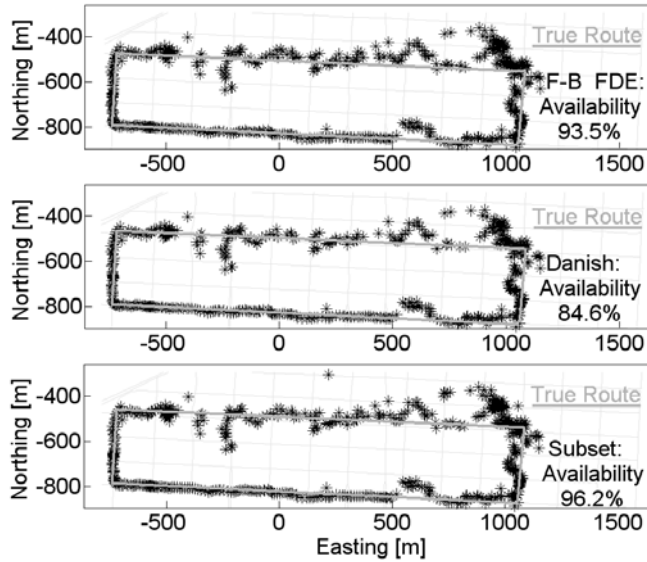


Fig. 85. Vehicular Test: Horizontal Position when Three Different Fault Detection and Exclusion Methods Applied.

servation with a zero redundancy number and 3.4% of epochs not passing the global consistency check. Of the remaining reliable flagged solutions, the F-B FDE performed exclusions to 23% of the epochs. Table 11 summarizes the availabilities of a horizontal position solution in percentage with LS, weighted LS, F-B FDE, Danish Method, and Subset Testing.

Table 11. Vehicular Test: Availability Summarized of Position Solutions.

	LS	WLS	F-B FDE	Danish	Subset Testing
Availability (%)	100	100	93.5	84.6	96.2

Fig. 87 presents the horizontal speed solutions of the vehicular test when FDE approaches and quality control were applied. The reference is included in the figure. The F-B FDE performs here the best of the three approaches compared to the reference speed. However, the Subset Testing has the highest availability of reliable flagged solutions, 96%. Table 12 summarizes the availabilities of a horizontal speed solution in percentage with LS, weighted LS, F-B FDE, Danish Method, and Subset Testing.

Fig. 88 presents the number of exclusions performed by the FDE procedures on the

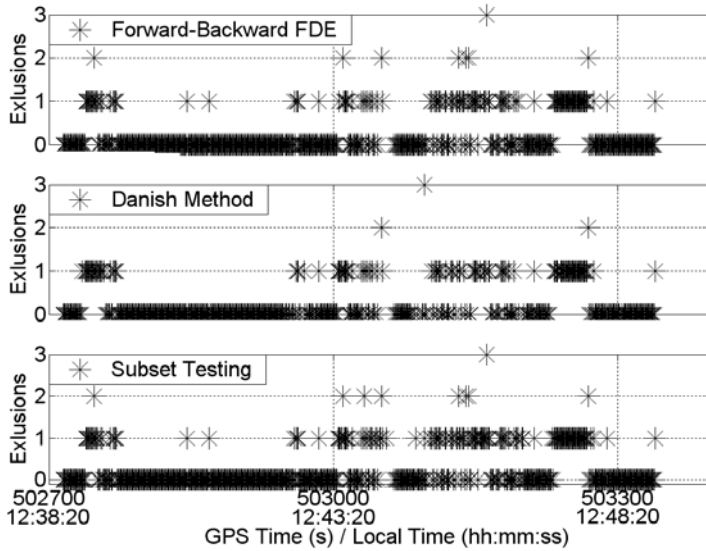


Fig. 86. Vehicular Test: Number of Exclusions of Pseudorange Observations.

range rate observations and up to 4 simultaneous exclusions were made at one single time instant. As an example in the velocity computation, the quality control in F-B FDE flagged around 25% of time epochs as unreliable including 3.1% of the time epochs containing a measurement with a zero redundancy number and 22% of the time epochs containing a solution that did not pass the final global test. Overall, on the remaining reliable flagged solutions, the F-B FDE performed exclusions on 53% of the epochs.

Position Reliability Boundaries

Figures 89 and 90 present the HPE values of the vehicular test with subject to the time of the experiment and as an experimental cumulative distribution function. Details of the statistics of the HPE are also provided. The theoretical horizontal positioning error boundary has in this test a standard deviation of approximately 450 meters, and

Table 12. Vehicular Test: Availability Summarized of Speed Solutions.

	LS	WLS	F-B FDE	Danish	Subset Testing
Availability (%)	100	100	75	74	96

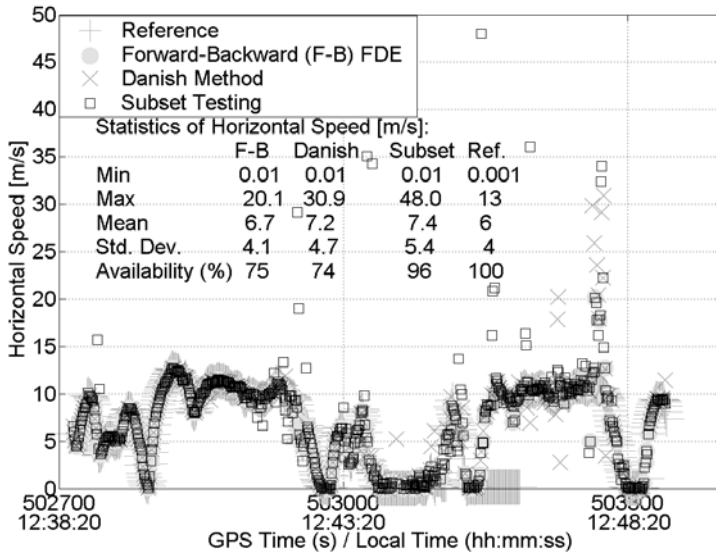


Fig. 87. Vehicular Test: Horizontal Speed when Three Different Fault Detection and Exclusion Methods Applied. Reference Included in the Figure.

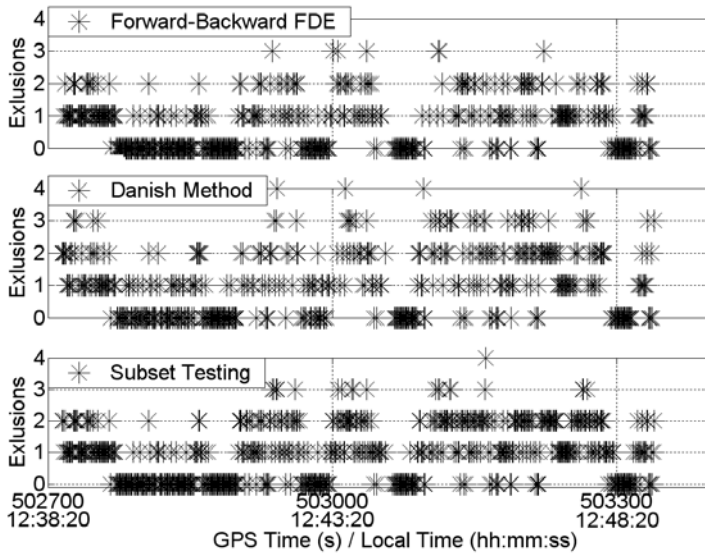


Fig. 88. Vehicular Test: Number of Exclusions of Pseudorange Rate Observations.

by comparing the obtained results to the reference route in the map of Fig. 85, the actual errors do not exceed the HPE.

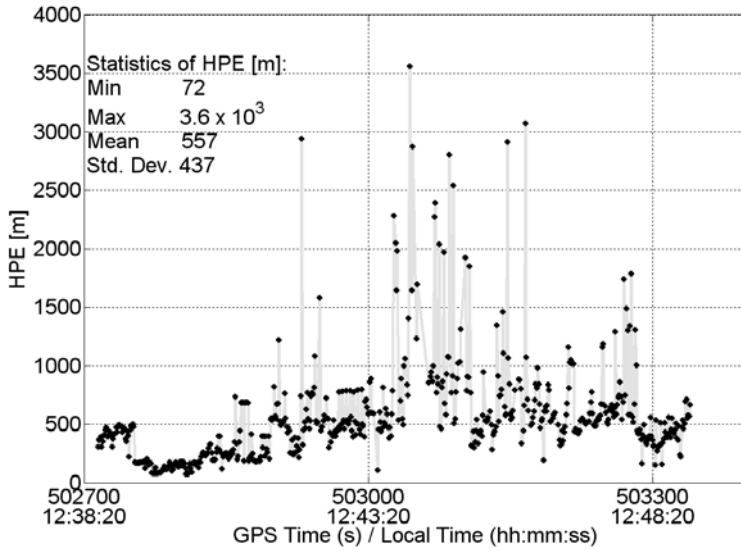


Fig. 89. Vehicular Test: HPE Values.

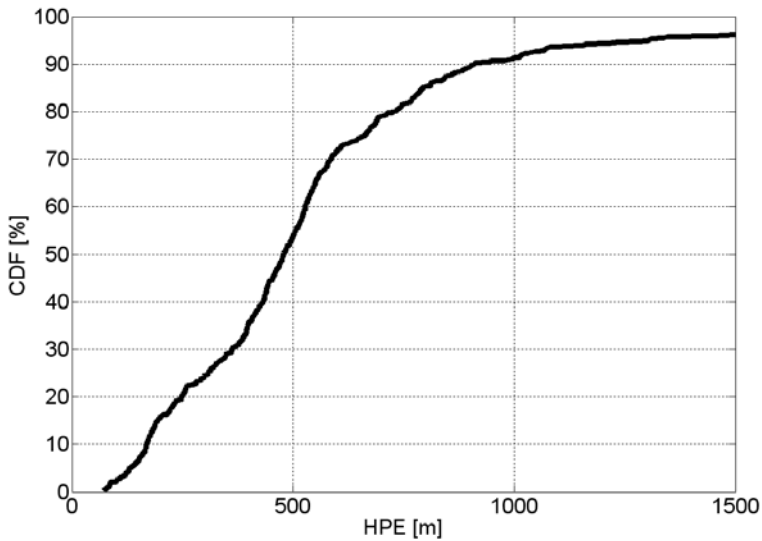


Fig. 90. Vehicular Test: Empirical Distribution of HPE.

Position Accuracy Estimation

Fig. 91 presents the DRMS horizontal position error estimate for the vehicular test with different FDE processing options. By examining Fig. 85, the real errors are on occasions slightly larger than the DRMS estimates of Fig. 91, but, overall, the horizontal accuracy estimate DRMS gives a reasonably good indication of the current error level also here.

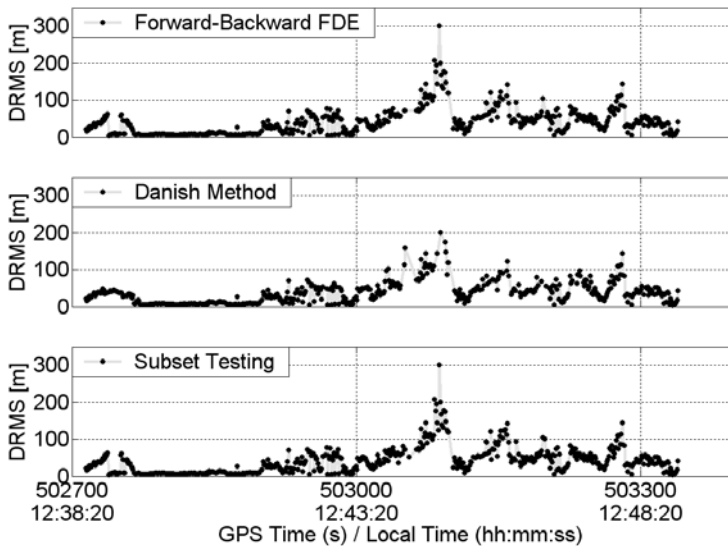


Fig. 91. Vehicular Test: DRMS Error Estimates when Three Different Fault Detection and Exclusion Methods Applied.

7.2 Integrated GPS/Galileo Simulation and Reliability Analysis

As seen in the previous real-life GPS experiments, standalone GPS, even if it is HS-GPS, does not provide throughout a sufficient amount of redundancy and available satellite signals to perform robust fault detection and exclusion. Standalone GPS is not necessarily sufficient if the aim is to ensure a desired level of accuracy of, e.g., the FCC E911 demands, in obstructed signal conditions of personal positioning environments. Future Galileo, combined with GPS, will provide twice the number of satellites above the horizon (Ryan and Lachapelle, 2000; Weber et al., 2001). Thus, better availability, accuracy, and reliability are expected even in extreme masking en-

vironments such as in urban canyons (O’Keefe, 2001; Malicorne et al., 2001), albeit still with a poor geometry. Furthermore, in harsh environments, all satellite signals are attenuated and, thus, erroneous, implying still a substantial need for reliability assessment.

Since no Galileo satellite signals are available yet, a software simulator is a valuable tool in evaluating the GPS/Galileo constellation and to check the usefulness of the discussed GNSS reliability testing methods for degraded signal environments. Thus, in addition to the real-life GPS tests, a GNSS software simulator, namely *SimGNSS2*, developed by the PLAN group (Position, Location And Navigation) of the Department of Geomatics Engineering, University of Calgary, is used here to produce data for testing purposes of the discussed reliability and quality monitoring schemes. In generating the GNSS measurements, the simulator first computes the true observables, the ranges and carrier phase, between the receiver and each GNSS satellite in-view. It then adds errors that affect the signals, with five different error factors being modeled: orbital uncertainties, ionospheric and tropospheric errors, as well as single-reflector multipath and receiver noise (Luo and Lachapelle, 2003). The assumed GPS/Galileo constellation shown in Fig. 92 consists of 24+5 GPS satellites on 22000-km-radius circular orbits with an inclination angle of 55 degrees, and 27+3 Galileo satellites on 29378-km-radius circular orbits with an inclination angle of 54 degrees (Alves, 2001).

7.2.1 Degraded Signal-Environment Simulation

Introduction to Procedure

A 6-hour data scenario of GPS/Galileo measurements with substantial errors in the range measurements was generated and the capability of detection and exclusion of erroneous pseudorange observations as well as the resulting accuracy is herewith assessed. Only position reliability and accuracy is of interest in this assessment and, thus, only pseudorange errors were concerned and assessed in the simulation. Two frequencies, L1 and E1, were considered in the simulation. Additional random pseudorange errors with a standard deviation of as high as 150 m were added to the simulation to represent the urban environment related substantial signal degradations of echo-only tracking, e.g., which the signal simulator is not equipped to produce. When processing the simulated GNSS data, the measurement variances were assumed equal

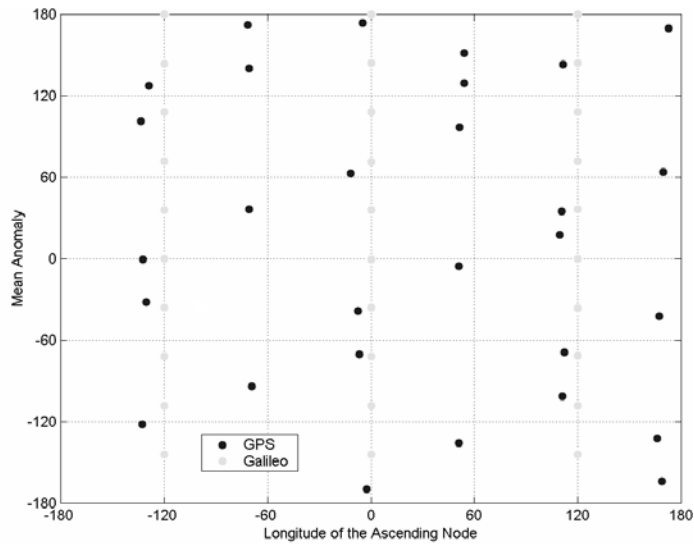


Fig. 92. Simulation: Simulated GPS/Galileo Constellation.

to GPS and Galileo signals (a one- σ_p value of 8 m), and height constraining was applied. No C/N_0 values were simulated and, thus, no C/N_0 dependent weighting, i.e., a variance model, was applied. The simulated 6-hour data set was set to Tampere coordinates (61.4498 degrees N, 23.8554 degrees E, 150 m height), Finland, with an elevation mask angle of 2 degrees at the beginning of GPS week 1321 (first week of May 2005). The false alarm rate for the reliability processing was set to $\alpha = 0.1\%$ and the probability of missed detection was set to $\beta = 10\%$.

As background information about the simulation, Fig. 93 presents the number of satellites in view for the GNSS simulation scenario. Fig. 94 presents the simulated pseudorange errors in this simulated data set by presenting the elevation angles for all available satellites versus their corresponding pseudorange error. Errors in this simulation include moderate ionosphere and troposphere errors, receiver noise, and orbital errors in all the observations, as inherent to the simulator data generation. In addition, randomly added errors were included that represented in-phase and out-of-phase multipath reaching up to hundreds of meters in six of the satellites in view, however not all simultaneously. Fig. 95 presents a histogram of the simulated errors including details of the statistics of the simulated range errors, and Fig. 96 presents an empirical cumulative distribution function of the simulated pseudorange errors. The statistics of the simulated errors reveal that the maximum absolute value of an

error simulated is 958 m and the standard deviation of all the errors equals 76.9 m. Fig. 97 presents the number of simulated outlying observations in time in the simulation. In one single time epoch, up to six simultaneous observation errors are present that are exceeding a maximum MDB of the corresponding time epoch in absolute value. Thus, if the error of an observation is exceeding the MDB value, it is identified here as being an outlier. 99.8% of the time epochs contained erroneous, outlying observations as shown in Fig. 97

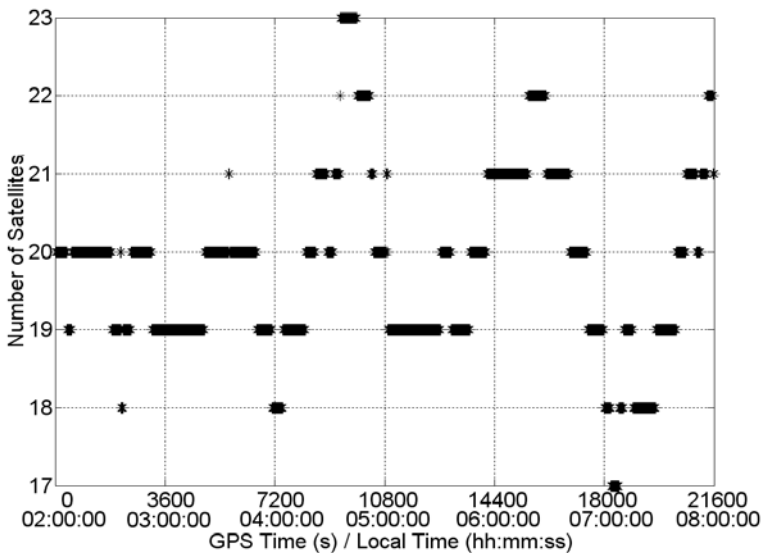


Fig. 93. Simulation: Available Satellites.

Position Estimation

Fig. 98 presents the horizontal position errors in a local level frame of the simulation test obtained by unweighted ($\sigma_p^2 = 8^2 m^2$) least squares (LS) estimation. The standard deviation of the LS horizontal position error is 19 meters without any reliability or quality monitoring applied.

Fig. 99 presents the horizontal position errors of the simulation test in a local level frame when quality control and the Forward-Backward (F-B) FDE and the Danish method have been applied to the simulation experiment data, respectively. The standard deviation of the horizontal position error when the F-B FDE has been applied is 2.3 meters and 1.9 meters when the Danish method has been applied. Subset testing

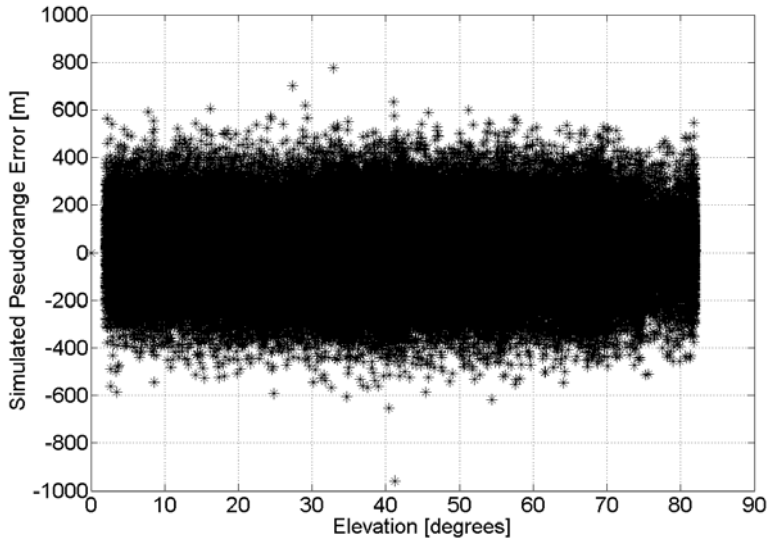


Fig. 94. Simulation: Simulated Pseudorange Errors vs. Elevations.

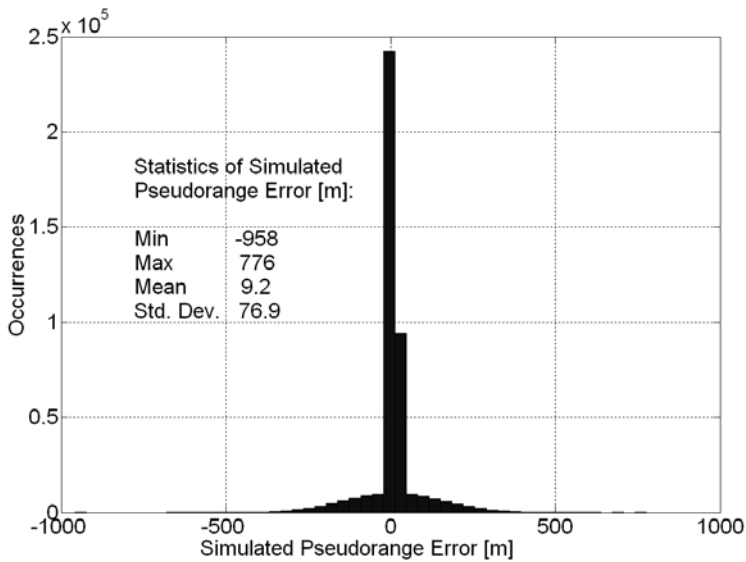


Fig. 95. Simulation: Histogram of Simulated Pseudorange Errors.

is not feasible to be applied to a GPS/Galileo situation due to the enormous amount of subsets to be assessed. The availability of a reliable flagged solution is 96.3% with

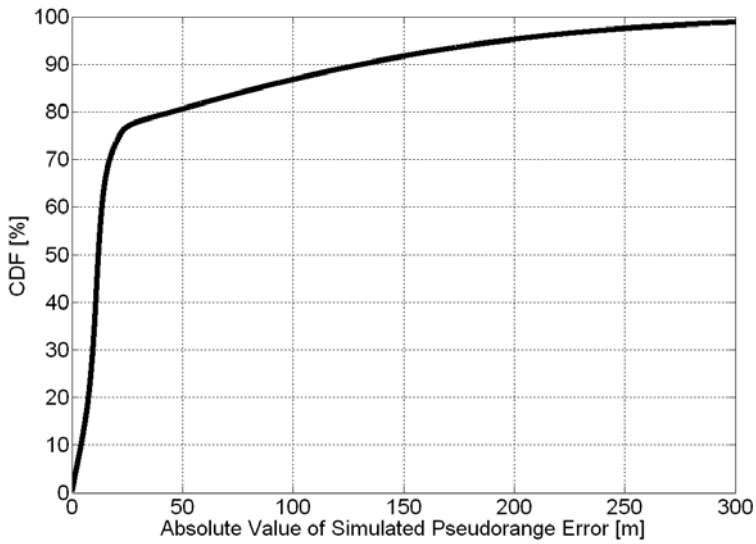


Fig. 96. Simulation: Empirical Cumulative Distribution Function of Simulated Pseudorange Errors.

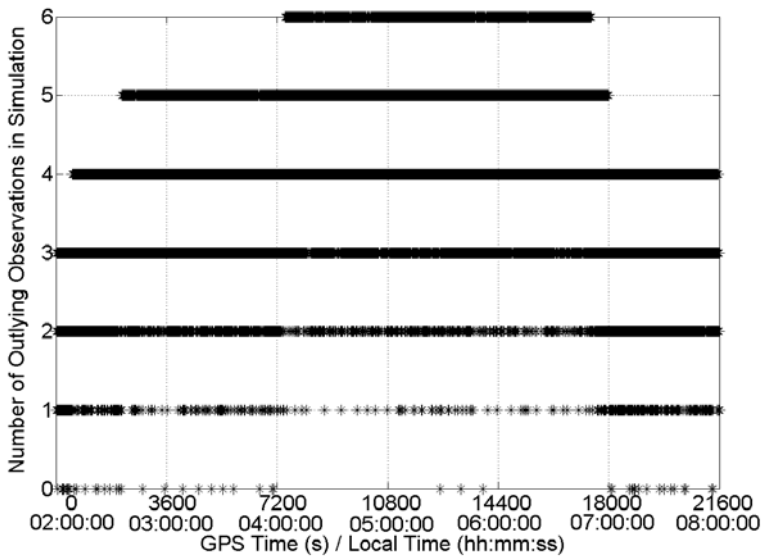


Fig. 97. Simulation: Number of Outlying Pseudorange Observation Errors.

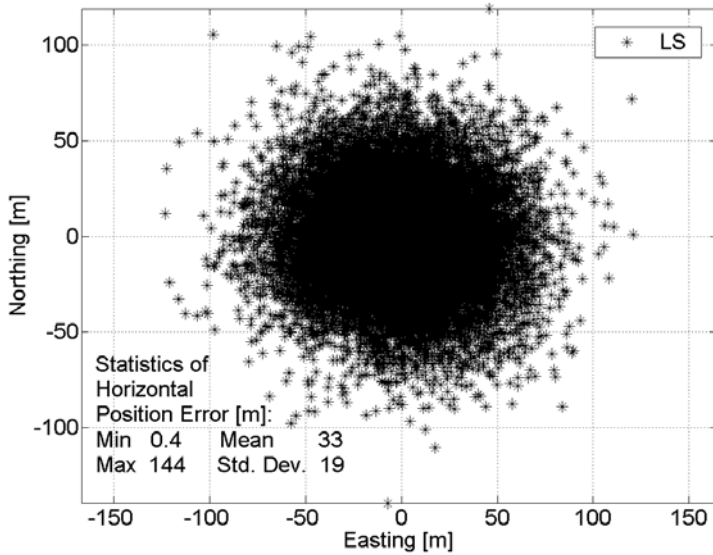


Fig. 98. Simulation: Horizontal Position with Unweighted Least Squares.

the F-B FDE, but the Danish Method suffers from the low assumed noise ($\sigma_p = 8$ m) of the observations whose weights are not being modified by the Danish re-weighting. The observations, whose weights are actually being modified in the Danish Method, are not, however, totally excluded from the estimation. Thus, the final global test has a higher failure rate, when the observations are not excluded but rather just down-weighted. This causes an unbalance between the observations with the unmodified and modified weights and the global test flags the solutions as inconsistent. The availability of a reliable flagged solution obtained with Danish estimation is therefore here only 42%.

Table 13. Simulation: Horizontal Position Errors and Availability Summarized.

	LS	F-B FDE	Danish
Min (m)	0.4	0.02	0.06
Max (m)	144	65	18
Mean (m)	33	4.0	3.6
Std. Dev. (m)	19	2.3	1.9
Availability (%)	100	96	42

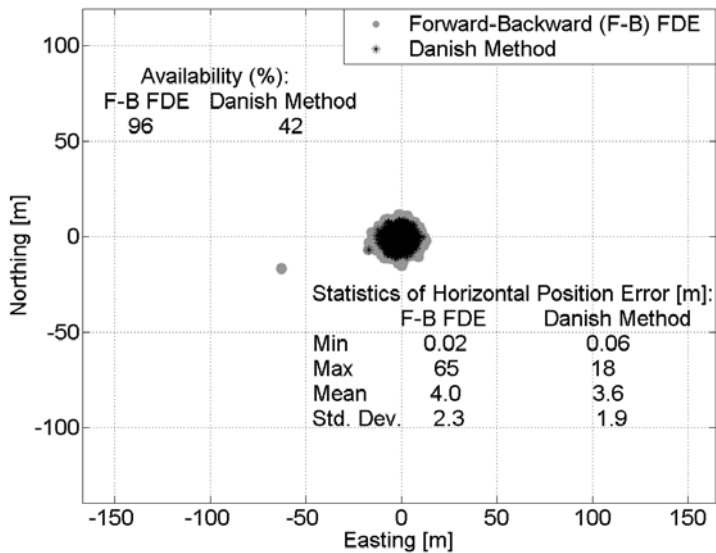


Fig. 99. Simulation: Horizontal Position with Forward-Backward FDE and the Danish Method.

Table 13 summarizes the horizontal position errors of the simulation experiment and presents the percentages of available solutions, i.e., reliable flagged solutions in the quality controlled Forward-backward FDE and the Danish Method cases. Fig. 100 presents the cumulative distribution functions of the horizontal errors of the results when least squares estimation, quality control and Forward-backward FDE, and quality control and the Danish Method are applied, respectively. The figures and the table show how accuracy is much improved when applying the FDE schemes, and there is no major difference in the resulting accuracy of the FDE schemes, except for the low availability resulting from the Danish Method and the one individual maximum error value resulting when applying the F-B FDE. The maximum error value of 65 m caused when applying the F-B FDE is obtained due to false exclusions. In that particular solution, 7 satellites were excluded, which is more than the three which were actually erroneous in that epoch. Moreover, totally false, not even erroneous satellites, were being excluded. The reason for this is the fact that the actual simulated errors canceled each other out in the extent that the exclusion procedure was fooled to excluded incorrectly. However, this was just one single epoch, and most of the time the exclusions were directed to the actually erroneous measurements.

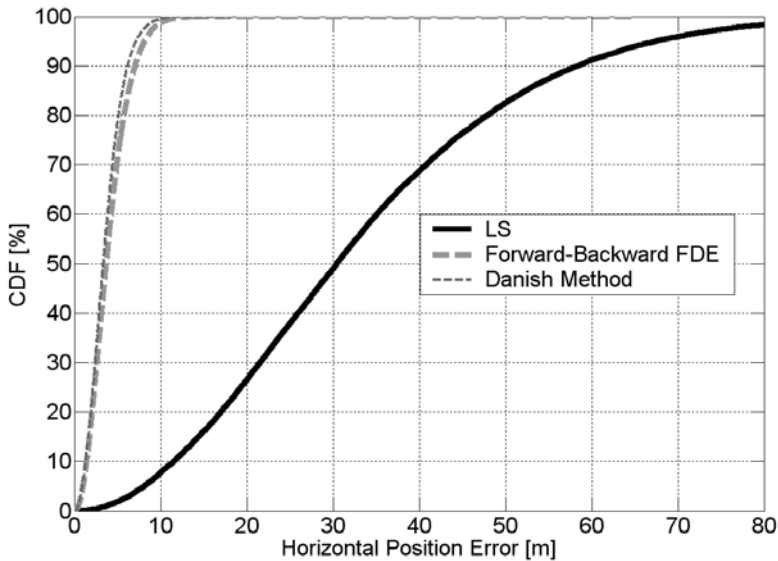


Fig. 100. Simulation: Empirical Distribution Functions of the Horizontal Position Errors with Least Squares Estimation, Forward-Backward FDE, and the Danish Method.

As a more detailed elaboration on the operation of the reliability and quality monitoring, in the F-B FDE, as an example, 4% of the time epochs were rejected due to being flagged unreliable because of a failed global consistency test. In 99.9% of the remaining reliable flagged solutions, exclusions were performed with the F-B FDE. Similar exclusion performance is obtained with the Danish Method, i.e., exclusions were performed in around 99.9% of the reliable flagged solutions, however, a much larger number of solutions, as much as 58%, were flagged as inconsistent by the final global test due to modifying of weights bringing about inconsistency. Overall, Fig. 101 presents the number of exclusions made by the Forward-Backward FDE procedure implemented within least squares estimation and by the Danish Method, respectively. Fig. 102 presents the values of the number of outlying simulated observations minus the exclusions performed by the F-B FDE and the Danish Method, respectively. The larger than zero values indicate that not all outlying observations were excluded and the smaller than zero values indicate that too many exclusions were performed subject to the number of outlying observations. However, the outlying observations were identified as only the ones with an error larger than the corresponding MDB, and, thus, also observations with smaller errors have been here excluded by

the FDE procedures. Moreover, F-B FDE performed the exclusions totally successfully 60% of the exclusions and the Danish Method performed successful exclusions 52% of the exclusions.

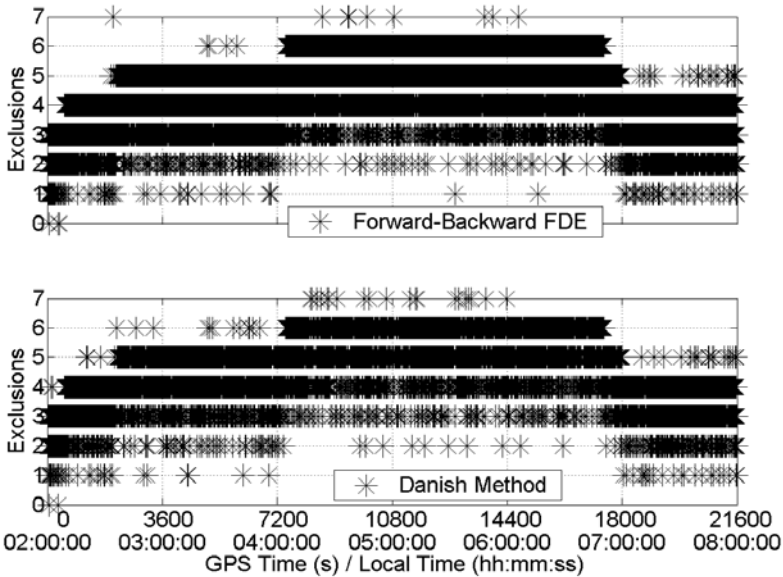


Fig. 101. Simulation: Exclusions Performed with Forward-Backward FDE and the Danish Method.

Position Reliability Boundaries

Figures 103 and 104 present the HPE values of the simulation experiment with subject to the time of the experiment and as an experimental cumulative distribution function. The standard deviation of the HPE values in the simulation test is as low as 1.8 meters due to the low assumption of $\sigma_p = 8$ m applied and not a more appropriate variance model. However, the HPE is still mostly quite close to what the system can be protected against by reliability monitoring of F-B FDE as shown in Fig. 99.

Fig. 105 presents the cumulative distribution function of the ratio between the horizontal position error obtained by the quality control and the Forward-Backward FDE and the HPE. There are under 3% of position errors obtained that exceed the theoretical HPE boundary.

Position Accuracy Estimation

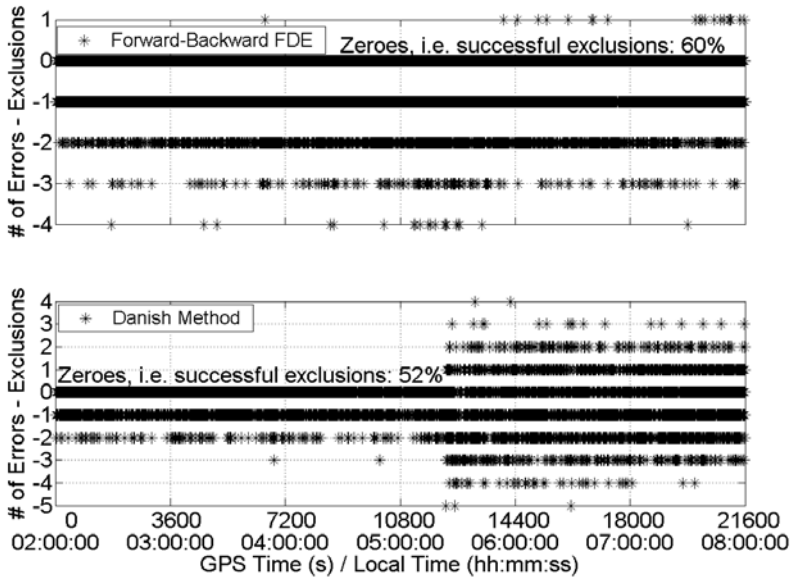


Fig. 102. Simulation: Number of Outlying Measurements Minus the Exclusions Performed with Forward-Backward FDE and the Danish Method.

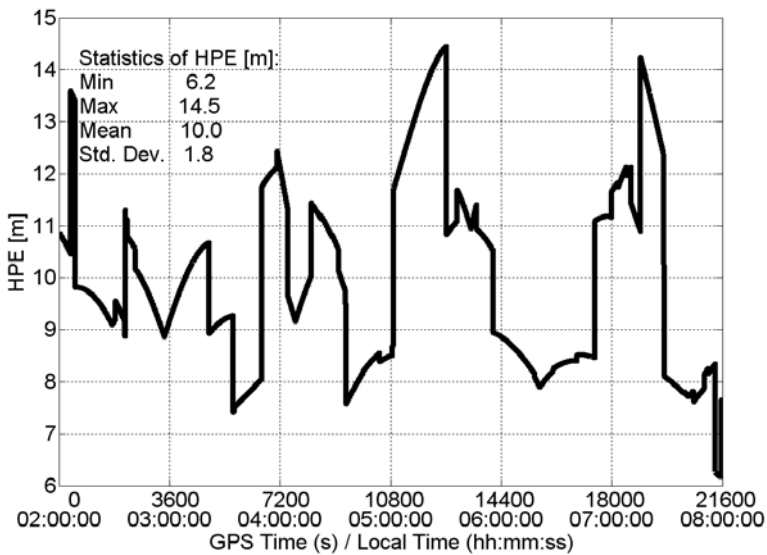


Fig. 103. Simulation: HPE Values.

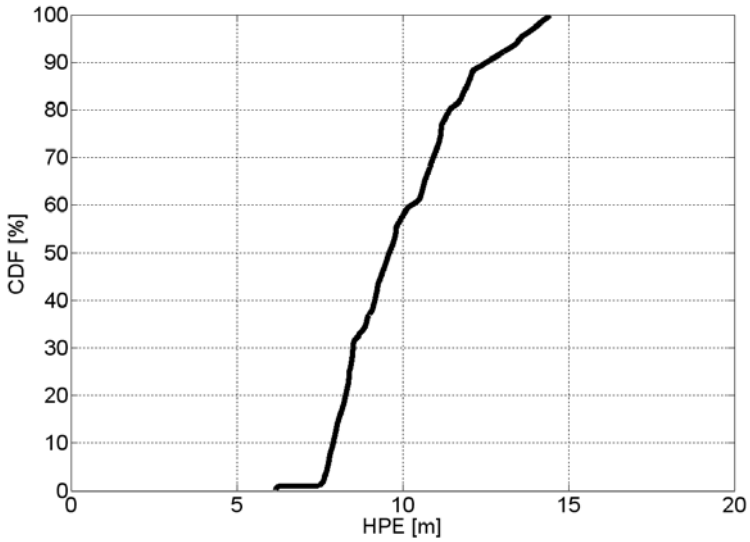


Fig. 104. Simulation: Empirical Distribution of HPE.

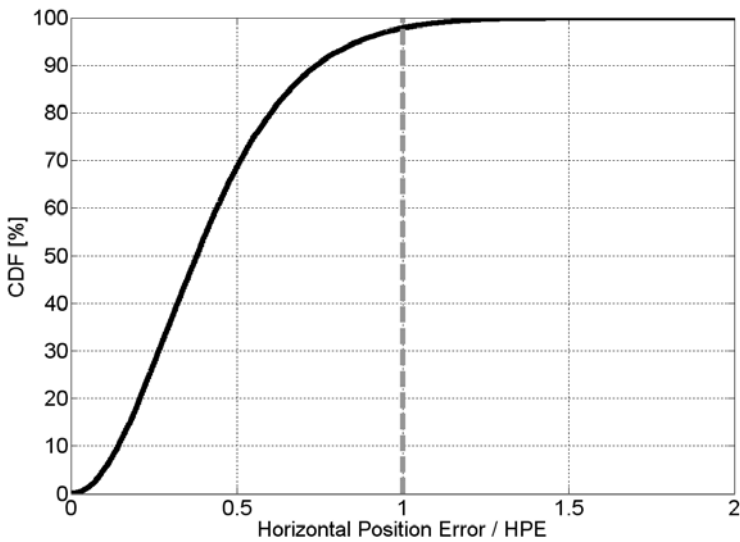


Fig. 105. Simulation: Empirical Distribution of the Ratio Between 2D Position Error and HPE.

Fig. 106 shows the horizontal position errors of the simulation when the Forward-Backward FDE and the Danish Method are successively applied as well as the respective DRMS accuracy estimates, the D of Eq. 51. The percentages of how often the actual errors are within the respective DRMS estimates are provided in the figure, and in these situations, 57% of the actual horizontal errors are within the DRMS error estimate with the Forward-Backward FDE case and 73% in the Danish Method case. The DRMS estimates provide thus a good estimation of the position errors, and the a posteriori variance factor does reflect the accuracy conditions.

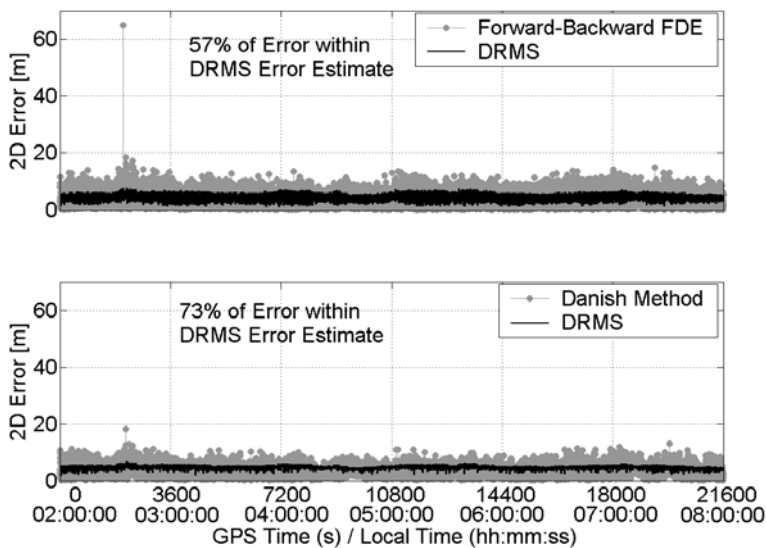


Fig. 106. Simulation: Horizontal Position Errors and DRMS Error Estimate when Two Different Fault Detection and Exclusion Methods Applied.

Fig. 107 presents the ratio between the horizontal position errors of the quality controlled result with the Forward-Backward FDE applied and the DRMS error estimate. The figure shows that as expected 57% of the error stay within the estimate, i.e., when the ratio equals 1, and the rest of the errors exceed the values of the estimate.

The performance enhancement of the quality and reliability monitoring with F-B FDE or the Danish Method is very distinct in the simulation experiment as seen from comparing Figures 98 and 99. The performance of reliability monitoring in the simulation is, however, somewhat inferior in relation to the demonstrated performance with HSGPS data due to the lack of signal quality indicators, i.e., the C/N_0 . The sig-

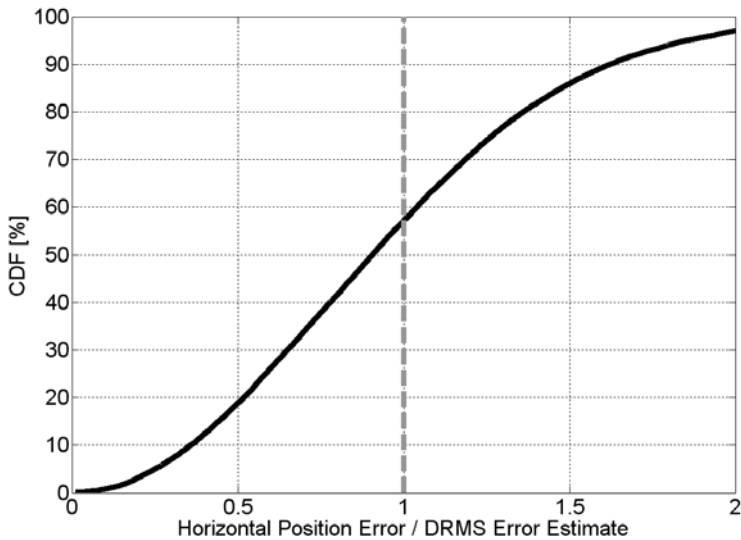


Fig. 107. Simulation: Empirical Distribution of the Ratio Between Horizontal Position Error of the Forward-Backward FDE and DRMS Error Estimate.

nal power was used successfully in the HSGPS tests to obtain an observation noise estimate and, thus, an equal variance had to be used for all the observations in the estimation schemes in the simulation experiment. Proper variance modeling is the key to successful and robust reliability testing as well as also accuracy estimation.

The problems of reliability monitoring, i.e., most importantly having the proper noise assumptions and a sufficient amount of redundancy to detect and isolate multiple errors, will not, however, be solved completely by the European Galileo system. Galileo will yield additional satellites and additional frequencies but is based on signals whose propagation is subject to the same restrictions and problems as currently with, e.g., GPS. In an open field, redundancy and precision will be enhanced by Galileo. However, indoors and in urban environment, the segments in the sky where a clean signal can go through are narrow, so the number of clearly tracked Galileo satellites will be near the number of GPS satellites with good signals. Therefore, Galileo will not improve the geometry in such environments; it mainly acts as if the GPS observations were more precise. Moreover, the Galileo satellites increase the number of observations but, in unfavorable environment, also the number of outliers. Therefore, Galileo will not improve the overall outlier detectability. The implicit

quality monitoring in Galileo will not help with the local user-surrounding problems and thus reliability monitoring remains important even in the future integrated GPS/Galileo environment (Kuusniemi et al., 2004).

8. CONCLUSIONS

Though reliability and quality monitoring is not always available in difficult signal environments due to the insufficient amount of observables, it is always when available essential in enhancing significantly the navigation reliability and accuracy and, therefore, constantly necessary.

This thesis discussed and gave insight to position and velocity FDE in personal satellite navigation. Indoor and urban canyon HSGPS data were analyzed in terms of observation errors and their distributions with respect to elevation and C/N_0 values. Variance models were proposed to be used in weighting attenuated GNSS measurements. It was shown that the C/N_0 based model can provide more realistic variances than the traditional elevation dependent approach, and much more realistic ones than the assumption of equal variance. Reliability theory in terms of reliability testing and statistical reliability conditions of a navigation system was discussed. The application of reliability theory in the failure detection and exclusion schemes developed was demonstrated using data from real-life HSGPS experiments and a GPS/Galileo simulation. The discussed reliability enhancement procedures, i.e., the Forward-Backward FDE reliability testing scheme, the robust Danish estimation method, and the Subset Testing, demonstrated significant reliability and accuracy improvements in degraded signal-environment navigation. The FDE schemes used the proposed variance models and they were combined with the additional quality control scheme taking into account measurement redundancy, consistency, and geometrical conditions.

The Danish Method is computationally more convenient than the Forward-Backward FDE and the Subset Testing mainly due to the fact that it operates on all the observations simultaneously. In some experiments, the Danish Method had slightly better results in terms of the maximum horizontal error but with the lowest availability of a reliable flagged solution. In general, the methods have no major differences in per-

formance. The Subset Testing is, however, not feasible for a combined GPS/Galileo situation with up to 24 satellites above the horizon. Moreover, the Forward-Backward FDE and the Subset Testing ultimately differ in the check for the influentiality of the observation subject to consideration whether to exclude it or not. In these particular test presented, the Forward-Backward FDE did not perform the re-implementation of an earlier rejected observation but the exclusion of a measurements was often reconsidered due to the influentiality assessment. Overall, using the proposed variance models, reliability monitoring, and quality control, the accuracy improvement was significant in all the conducted experiments compared to 'standard methods' based on equal weights with no FDE. Modifying the predetermined confidence levels of false alarms and missed detection in the reliability enhancement techniques would have resulted in slightly different results.

The lack of redundancy is the limiting factor of reliability enhancement. In addition, generally, if there are more erroneous observations than observations with acceptable quality, no reliability monitoring can enhance the results. The reliability monitoring can then, in the best case, only mark the result as unreliable. Unfortunately, GNSS in poor signal-environments usually provides only few surplus measurements and, therefore, the GNSS observations alone may not provide sufficient possibility for reliability monitoring. Therefore, additional information should be considered to assist in navigation and to also help the reliability assessment and enhancement. Such information could be obtained from digital television signals, cellular network time-of-arrival measurements, or additional sensors such as self-contained inertial sensors, which are independent of the GNSS signal propagation effects. The problem of sufficient redundancy will not be completely solved either by the European Galileo system, which will yield additional satellites and additional frequencies but is based on signals whose propagation is subject to the same restrictions and problems as currently with, e.g., GPS. In an open field, redundancy and precision will be, of course, enhanced by Galileo. However, indoors and in urban environment, the segments in the sky, where a clean signal can go through, are narrow. Therefore, the number of clearly tracked Galileo satellites will be near the number of GPS satellites with good signals. This implies that Galileo will not improve the geometry in such environments; it mainly acts as if the GPS observations were more precise. Galileo satellites increase the number of observations but, in unfavorable environment, also the number of outliers.

In this thesis, epoch-by-epoch least squares estimation was used for sensitivity analysis purposes to assess the implemented reliability enhancement methods. However, the ideas introduced are easily transferable and extendable to Kalman filtering and, thus, widely applicable.

8.1 *Main Results*

This thesis considered reliability and quality monitoring at the user-level for satellite-based personal navigation applications. Reliability monitoring was conducted on both position and velocity solutions. Failure detection and exclusion methods developed proved to be of great importance in degraded signal environments in order to ensure reliable and accurate user navigation solutions. Navigation error sources were discussed with real-life experiments in good, lightly attenuated, and heavily degraded signal conditions. The magnitudes of multipath, echo-only signal tracking, and noise induced errors in the satellite navigation observables are highly dependent of the environment where the navigation takes place and, thus, the chosen environments represented only a few typical cases of what can be realized. Accuracy prediction and reliability theory were presented including parameters for accuracy estimation, reliability testing procedures, and statistical reliability boundaries. Statistical reliability testing was briefly compared to traditional RAIM methods introduced in literature mainly for safety-critical applications. Three schemes to fault detection and exclusion for personal satellite navigation applications were developed: the observation Subset Testing scheme, the Forward-Backward FDE scheme, and the Danish estimation method. In addition, quality control and variance models for range and range rate measurements for lightly and heavily degraded signal environments were introduced.

The final section of the thesis presented results with data from static and kinematic real-life high sensitivity GPS experiments and from a GPS/Galileo simulation. The results suggest that the presented observation weighting, FDE, and quality control enhancement methods improve the navigation results significantly. In addition, based on the results of the experiments, the accuracy prediction parameter gives a good approximation of the position errors obtained and can thus be utilized in estimating the error conditions to the user. Though the Subset Testing is not feasible for GPS/Galileo due to the enormous amount of subsets to be assessed, the two other FDE methods and quality control improve substantially also the integrated GPS/Galileo navigation

solution reliability and accuracy. With GPS/Galileo, the availability and reliability will be improved especially in open line-of-sight conditions but reliability and quality monitoring are still essential, especially in heavily masked environments.

8.2 Future Development

The discussed reliability and quality monitoring results will be necessary to be transferred and extended to an extensively utilized Kalman filtering environment. Kalman filtering is widely accepted to provide optimal estimations of the navigation parameters of a dynamic platform, assuming the state and observation models are correct. In addition, computational and power requirements are essential to be accounted for when designing the reliability enhancement schemes. Power and memory consumptions are especially important design parameters for a portable wireless device, which is most likely the platform for the personal navigation applications of the degraded signal environments, where reliability enhancement need to be implemented.

Additional sensors, such as MEMS, DTV, and cellular network observables, are essential to be included in the user navigation solution estimation and reliability and quality assessment in order to reach sufficient availability of navigation capability in the urban and indoor areas. Integrating a satellite navigation receiver with a mobile phone and using AGPS will also enable hybrid navigation solutions with cellular network and satellite observations and, thereby, further improve availability. MEMS sensors have been successfully integrated with a satellite navigation receiver especially for pedestrian navigation applications. The advantage of MEMS integration lies essentially also in the increased availability of a navigation solution. Limitations of the MEMS sensors are, however, severe, and related to the drift of the sensor derived solution in time without calibration from an absolute navigation system, i.e., the GNSS. Research work with GNSS and MEMS integration as well as AGPS and hybrid solutions is still in progress.

It is likely that in the future there will exist personal navigators in which navigation capability from multiple sensor sources have been integrated and complex reliability enhancement techniques have been incorporated. These navigators would provide seamless navigation capability from outdoors to indoors with superior performance enabling a wide variety of navigation applications and added-value services.

BIBLIOGRAPHY

- N. Agarwal, J. Basch, P. Beckmann, P. Bharti, S. Bloebaum, S. Casadei, A. Chou, P. Enge, W. Fong, N. Hathi, W. Mann, A. Sahai, J. Stone, J. Tsitsiklis, and B. V. Roy. Algorithms for GPS operation indoors and downtown. *GPS Solutions*, 6(3): 149–160, Dec. 2002.
- P. Alves. The effect of Galileo on carrier phase ambiguity resolution. In *Proc. ION GPS 2001*, pages 2086–2095, Salt Lake City, UT, Sept. 11-14 2001. Institute of Navigation.
- W. Baarda. A testing procedure for use in geodetic networks. Netherlands Geodetic Commission, Publication on Geodesy, New Series 2. No. 5, Delft, Netherlands, 1968.
- V. Barnett and T. Lewis. *Outliers in Statistical Data*. John Wiley and Sons, Inc., New York, 1978.
- R. J. Beckman and R. D. Cook. Outlier.....s. *Technometrics*, 25(2):119–149, May 1983.
- J. W. Betz. The offset carrier modulation for GPS modernization. In *Proc. ION NTM 1999*, pages 639–648, San Diego, CA, Jan. 25-27 1999. Institute of Navigation.
- Å. Björck. *Numerical Methods for Least Squares Problems*. Society for Industrial and Applied Mathematics, Philadelphia, 1996.
- A. K. Brown. Receiver autonomous integrity monitoring using a 24-satellite GPS constellation. In *Proc. 1st Technical Meeting Satellite Division ION*, pages 21–33, Colorado Springs, CO, Sept. 21-25 1987. Institute of Navigation.
- A. K. Brown. Receiver autonomous integrity monitoring using a 24-satellite GPS constellation. *Papers published in NAVIGATION, Journal of The Institute of Navigation*, V:21–33, 1998. Red Book of RAIM.

- R. G. Brown. A baseline GPS RAIM scheme and a note on the equivalence of three RAIM methods. *NAVIGATION, Journal of The Institute of Navigation*, 39(3):101–116, Fall 1992.
- R. G. Brown and P. Y. C. Hwang. *Introduction to Random Signals and Applied Kalman Filtering*. John Wiley and Sons, Inc., New York, 3rd edition, 1997.
- W. Caspary. *Concepts of Network and Deformation Analysis*, volume 11 of *Monograph*. UNSW, School of Surveying, Sydney, Australia, 1988. pp. 1–183.
- CGALIES. C.G.A.L.I.E.S. - final report, 2002. URL <http://europa.eu.int/comm/environment/civil/pdfdocs/cgaliesfinalreportv1.0.pdf>. Report on implementation issues related to access to location information by emergency services E112 in EU.
- M. Chansarkar and L. J. Garin. Acquisition of GPS signals at very low signal to noise ratio. In *Proc. ION NTM 2000*, pages 731–737, Anaheim, CA, Jan. 2000. Institute of Navigation.
- G. Y. Chin, J. H. Kramer, and R. G. Brown. GPS RAIM: Screening out bad geometries under worst-case bias conditions. *NAVIGATION, Journal of The Institute of Navigation*, 39(4):117–137, Winter 1992.
- R. E. DeVor, T. Chang, and J. W. Sutherland. *Statistical Quality Design and Control, Contemporary Concepts and Methods*. Prentice Hall, 1992.
- S. Dinwiddy, E. Breeuwer, and J. Hahn. The Galileo system. In *Proc. ENC GNSS 2004, The European Navigation Conference*, Rotterdam, The Netherlands, May 16-19 2004. European Group of Institutes of Navigation.
- N. Draper and H. Smith. *Applied Regression Analysis*. John Wiley and Sons, Inc., New York, 2nd edition, 1981.
- L. Dutton, D. Rumens, W. Forrest, and L. Ruiz. Galileo's services. In *Proc. ION GPS 2002*, pages 249–257, Portland, OR, Sept. 24-27 2002. Institute of Navigation.
- E112. Enhanced 112, 2002. URL <http://europa.eu.int/comm/environment/civil/prote/112>.

- E911. Enhanced 911, November 2004. URL
<http://www.fcc.gov/911/enhanced/>.
- B. Eissfeller, G. Heinrichs, T. Pany, R. Weigel, H. Ehm, A. Schmid, A. Neubauer, G. Rohmer, and J.-A. Ávila Rodríguez. HIGAPS - a highly integrated Galileo/GPS chipset for consumer applications. *GPS World*, 15(9):38–47, May 2004.
- P. Enge. Local area augmentation of GPS for the precision approach of aircraft. *Proceedings of the IEEE*, 87(1):111–132, Jan. 1999.
- P. Enge, T. Walter, S. Pullen, C. Kee, Y.-C. Chao, and Y.-J. Tsai. Wide area augmentation of the Global Positioning System. *Proceedings of the IEEE*, 84(8):1063–1088, Aug. 1996.
- M. Fantino, F. Dosis, and J. Wang. Quality monitoring for multipath affected GPS signals. In *Proc. International Symposium on GNSS/GPS*, Sydney, Australia, Dec. 6-8 2004.
- J. L. Farrell and F. V. Graas. Statistical validation for GPS integrity test. *Papers published in NAVIGATION, Journal of The Institute of Navigation*, V:89–102, 1998. Red Book of RAIM.
- R. Fontana, W. Cheung, P. Novak, and T. Stansell. The new L2 civil signal. In *Proc. ION GPS 2001*, pages 617–631, Salt Lake City, UT, Sept. 11-14 2001. Institute of Navigation.
- R. Fontana and D. Latterman. GPS modernization and the future. In *Proc. IAIN World Congress, in association with ION AM 2000*, pages 222–231, San Diego, CA, Jun. 26-28 2000. Institute of Navigation.
- FRP. Federal radionavigation plan, 1999. URL
<http://avnwww.jccbi.gov/icas/doc/frp1999.pdf>.
- FRP. Federal radionavigation plan, 2001. URL
<http://www.navcen.uscg.gov/pubs/frp2001/FRP2001.pdf>.
- Galileo Brochure. Galileo, The European Programme for Global Navigation Services, March 2003. European Commission and European Space Agency.

- L. J. Garin, M. Chansarkar, S. Miocinovic, C. Norman, and D. Hilgenberg. Wireless assisted GPS-SiRF architecture and field test results. In *Proc. ION GPS 1999*, pages 489–497, Nashville, TN, Sept. 14-17 1999. Institute of Navigation.
- L. Gauthier, P. Michel, and J. Ventura-Traveset. EGNOS - the first European implementation of GNSS, programme development status overview. In *Proc. ENC GNSS 2003, The European Navigation Conference*, Graz, Austria, Apr. 22-25 2003. European Group of Institutes of Navigation.
- A. Gelb. *Applied Optimal Estimation*. The M.I.T. Press, Cambridge, Massachusetts, and London, England, 1974.
- R. Gold. Optimal binary sequences for spread spectrum multiplexing. *IEEE Trans. on Information Theory*, 13(4):619–621, Oct. 1967.
- F. R. Hampel, E. M. Ronchetti, P. J. Rousseeuw, and W. A. Stahel. *Robust Statistics, The Approach Based on Influence Functions*. John Wiley and Sons, Inc., New York, 1986.
- H. Hartinger and F. Brunner. Variances of GPS phase observations: the SIGMA- ϵ model. *GPS Solutions*, 2(4):35–43, Apr. 1999.
- R. Hatch, T. Sharpe, and Y. Yang. A simple RAIM and fault isolation scheme. In *Proc. ION GPS 2003*, pages 801–808, Portland, OR, Sept. 9-12 2003. Institute of Navigation.
- D. Hawkins. *Identification of Outliers*. Chapman and Hall, London/New York, 1980.
- G. Hein, M. Irsigler, J. Avila-Rodriguez, and T. Pany. Performance of Galileo L1 signal candidates. In *Proc. ENC GNSS 2004, The European Navigation Conference*, Rotterdam, The Netherlands, May 16-19 2004. European Group of Institutes of Navigation.
- G. W. Hein, J. Godet, J.-L. Issler, J. C. Martin, P. Erhard, R. Lucas-Rodriguez, and T. Pratt. Status of Galileo frequency and signal design. In *Proc. ION GPS 2002*, pages 266–277, Portland, OR, Sept. 24-27 2002. Institute of Navigation.
- S. Hewitson. GNSS receiver autonomous integrity monitoring: A separability analysis. In *Proc. ION GPS 2003*, pages 1502–1509, Portland, OR, Sept. 9-12 2003. Institute of Navigation.

- S. Hewitson and J. Wang. Impact of dynamic information on GNSS receiver integrity monitoring. In *Proc. International Symposium on GNSS/GPS*, Sydney, Australia, Dec. 6-8 2004.
- B. Hofmann-Wellenhof, H. Lichtenegger, and J. Collins. *Global Positioning System: Theory and Practice*. Springer-Verlag, Wien, Austria, 5th edition, March 2001.
- P. Huber. *Robust Statistics*. John Wiley and Sons, Inc., New York, 1981.
- ICD. GPS interface control document, IRN-200C-004, April 2000. URL <http://www.navcen.uscg.gov/pubs/gps/icd200/icd200cw1234.pdf>. US Coast Guard.
- P. C. Jørgensen, K. Kubik, P. Frederiksen, and W. Weng. Ah, robust estimation! *Aust J Geod Photogram Surv*, 42:19–32, June 1985.
- JPO. Navstar GPS fact sheet, May 2005. URL <http://gps.losangeles.af.mil/jpo/gpsoverview.htm>.
- E. D. Kaplan (Ed.). *Understanding GPS: Principles And Applications*. Artech House, Inc., Boston, London, 1996.
- S. Kay. *Fundamentals of Statistical Signal Processing: Estimation Theory*. Prentice Hall International, Inc., 1993.
- R. J. Kelly. The linear model, RNP, and the near-optimum fault detection and exclusion algorithm. *Papers published in NAVIGATION, Journal of The Institute of Navigation*, V:227–259, 1998. Red Book of RAIM.
- D. Kinkulkin. Fault detection, isolation and correction in GPS/GLONASS receivers. In *Proc. ION GPS 1997*, pages 459–464, Kansas City, MO, Sept. 16-19 1997. Institute of Navigation.
- R. Kirjner, A. Lyon, and J. Westbrook. Beyond the EGNOS system test bed providing EGNOS services. In *Proc. ION GPS 2003*, pages 2777–2782, Portland, OR, Sept. 9-12 2003. Institute of Navigation.
- J. Klobuchar. Ionospheric effects on GPS. in *Global Positioning System: Theory and Applications, Vol. I*, B. Parkinson and J. Spilker and P. Axelrad and P. Enge (Eds.), pages 485–515, 1996. American Institute of Aeronautics and Astronautics.

- K.-R. Koch. *Parameter Estimation and Hypothesis Testing in Linear Models*. Springer-Verlag, Berlin, Heidelberg, 1999.
- S. Kuang. *Geodetic Network Analysis and Optimal Design: Concepts and Applications*. Ann Arbor Press Inc., Chelsea, Michigan, 1996.
- H. Kuusniemi, A. Wieser, G. Lachapelle, and J. Takala. User-level reliability monitoring in urban personal satellite-navigation. *IEEE Trans. Aerospace and Electronic Systems*, 2004. Submitted.
- G. Lachapelle. Advanced GPS theory and applications. ENGO 625 Lecture Notes, University of Calgary, 2003.
- Y. C. Lee. Analysis of range and position comparison methods as a means to provide GPS integrity in the user receiver. *Papers published in NAVIGATION, Journal of The Institute of Navigation*, V:5–19, 1998. Red Book of RAIM.
- Y. C. Lee. Investigation of extending receiver autonomous integrity monitoring (RAIM) to combined use of Galileo and modernized GPS. In *Proc. ION GNSS 2004*, pages 1691–1698, Long Beach, CA, Sept. 21-24 2004. Institute of Navigation.
- A. Leick. *GPS Satellite Surveying*. John Wiley and Sons, Inc., Hoboken, New Jersey, 3rd edition, 2004.
- G. Lu. Quality control for differential kinematic GPS positioning. MSc thesis, Department of Geomatics Engineering, The University of Calgary, Calgary, Canada, 1991.
- O. Luba, L. Boyd, A. Gover, and J. Crum. GPS III system operations concepts. In *Proc. IEEE Position, Location, and Navigation Symposium*, pages 380–388, Monterey, CA, Apr. 26-29 2004. IEEE.
- D. J. Lucia and J. M. Anderson. Analysis and recommendation for the reuse of the L1 and L2 GPS spectrum. In *Proc. ION GPS 1998*, pages 1877–1886, Nashville, TN, Sept. 15-18 1998. Institute of Navigation.
- N. Luo and G. Lachapelle. Relative positioning of multiple moving platforms using GPS. *IEEE Trans. Aerospace and Electronic Systems*, 39(3):936–948, July 2003.

- C. Macabiau, B. Gerfault, I. Nikiforov, L. Fillatre, B. Roturier, E. Chatre, M. Raimondi, and A. Escher. RAIM performance in presence of multiple range failures. In *Proc. ION NTM 2005*, pages 779–791, San Diego, CA, Jan. 24-26 2005. Institute of Navigation.
- G. MacGougan. High sensitivity GPS performance analysis in degraded signal environments. MSc thesis, Department of Geomatics Engineering, The University of Calgary, Calgary, Canada, 2003.
- G. MacGougan, G. Lachapelle, R. Klukas, K. Siu, L. Garin, J. Shewfelt, and G. Cox. Performance analysis of a stand-alone high sensitivity receiver. *GPS Solutions*, 6(3):179–195, 2002. Springer Verlag.
- G. MacGougan and J. Liu. Fault detection methods and testing for marine GPS receivers. In *Proc. ION GPS 2002*, pages 2668–2678, Portland, OR, Sept. 24-27 2002. Institute of Navigation.
- M. Malicorne, M. Bousquet, and V. Calmettes. Galileo performance improvement for urban users. In *Proc. ION GPS 2001*, pages 2105–2113, Salt Lake City, UT, Sept. 11-14 2001. Institute of Navigation.
- P. Mattos. Acquiring sensitivity - to bring new signals indoors. *GPS World*, 15(5): 28–33, May 2004.
- K. McDonald and C. Hegarty. Post-modernization performance capabilities. In *Proc. ION AM 2000*, 2000.
- O. Mezentsev. *Sensor Aiding of HSGPS Pedestrian Navigation*. PhD thesis, Department of Geomatics Engineering, The University of Calgary, Calgary, Canada, 2005.
- P. Misra and S. Bednarz. Navigation for precision approaches: Robust integrity monitoring using GPS+Galileo. *GPS World*, 15(4):42–49, Apr. 2004.
- P. Misra and P. Enge. *Global Positioning System: Signals, Measurements and Performance*. Ganga-Jamuna Press, 2001.
- H. Miyashita. *Outliers in a Linear Regression Model*. PhD thesis, University of Illinois at Urbana-Champaign, Urbana, Illinois, 1982.

- M. Moeglein and N. Krasner. An introduction to SnapTrack server-aided GPS technology. In *Proc. ION GPS 1998*, pages 333–342, Nashville, TN, Sept. 1998. Institute of Navigation.
- J. Neter, M. Kutner, C. Nachtsheim, and W. Wasserman. *Applied Linear Statistical Models*. WCB/McGraw-Hill, 4th edition, 1996.
- P. Ober. *Integrity Prediction and Monitoring of Navigation Systems*. PhD thesis, Delft University of Technology, Delft, The Netherlands, 2003.
- K. O’Keefe. Availability and reliability advantages of GPS/Galileo integration. In *Proc. ION GPS 2001*, pages 2096–2105, Salt Lake City, UT, Sept. 11-14 2001. Institute of Navigation.
- O. Onidi. GALILEO is launched. In *Proc. ION GPS 2002*, pages 245–248, Portland, OR, Sept. 24-27 2002. Institute of Navigation.
- B. Parkinson and J. Spilker. *Global Positioning System: Theory And Applications, Volumes 1 and 2*. American Institute of Aeronautics and Astronautics, Inc., Washington, DC, 1996.
- B. W. Parkinson and P. Axelrad. Autonomous GPS integrity monitoring using the pseudorange residual. *NAVIGATION, Journal of The Institute of Navigation*, 35 (2):49–68, Summer 1988.
- B. S. Pervan, D. G. Lawrence, and B. W. Parkinson. Autonomous fault detection and removal using GPS carrier phase. *IEEE Trans. Aerospace and Electronic Systems*, 34(3):897–906, July 1998.
- B. Peterson, D. Bruckner, and S. Heye. Measuring GPS signals indoors. In *Proc. ION GPS 1997*, pages 615–624, Kansas City, MO, Sept. 16-19 1997. Institute of Navigation.
- M. Petovello. *Real-Time Integration of a Tactical-Grade IMU and GPS for High-Accuracy Positioning and Navigation*. PhD thesis, Department of Geomatics Engineering, The University of Calgary, Calgary, Canada, 2003.
- M. Poutanen. *GPS-paikanmääritys*. Tähtitieteellinen yhdistys Ursa, Helsinki, 1999.
- M. Powe and J. Owen. A flexible RAIM algorithm. In *Proc. ION GPS 1997*, pages 439–449, Kansas City, MO, Sept. 16-19 1997. Institute of Navigation.

- M. Rabinowitz and J. J. Spilker. Augmenting GPS with television signals for reliable indoor positioning. *NAVIGATION, Journal of the Institute of Navigation*, 51(4): 269–282, Winter 2004.
- J. Ray. *Mitigation of GPS Code and Carrier Phase Multipath Effects Using a Multi-antenna System*. PhD thesis, Department of Geomatics Engineering, The University of Calgary, Calgary, Canada, 2000.
- J. Ray. Advanced GPS receiver technology. ENGO 699.73 Lecture Notes, University of Calgary, May 2003.
- J. A. A. Rodriguez, M. Irsigler, G. W. Hein, and T. Pany. Combined Galileo/GPS frequency and signal performance analysis. In *Proc. ION GNSS 2004*, pages 632–649, Long Beach, CA, Sept. 21-24 2004. Institute of Navigation.
- P. Rousseeuw and A. Leroy. *Robust Regression and Outlier Detection*. John Wiley and Sons, Inc., New York, 1987.
- S. Ryan. *Augmentation of DGPS for Marine Navigation*. PhD thesis, Department of Geomatics Engineering, The University of Calgary, Calgary, Canada, 2002.
- S. Ryan and G. Lachapelle. Augmentation of DGNSS with dynamic constraints for marine navigation. In *Proc. ION GPS 1999*, pages 1303–1314, Nashville, TN, Sept. 14-17 1999. Institute of Navigation.
- S. Ryan and G. Lachapelle. Impact of GPS/Galileo integration on marine navigation. In *Proc. ION AM 2000*, pages 721–732, San Diego, CA, June 26-28 2000. Institute of Navigation.
- J. Saastamoinen. Atmospheric correction for the troposphere and stratosphere in radio ranging of satellites. *Geophysical Monograph 17, American Geophysical Union*, 1972.
- H. Sairo, D. Akopian, and J. Takala. Weighted dilution of precision as quality measure in satellite positioning. *IEE Proc. in Radar, Sonar, and Navigation*, 150(6): 430–436, Dec. 2003.
- K. Sandhoo and D. T. M. Shaw. Modernization of the Global Positioning System. In *Proc. ION GPS 2000*, pages 2175–2183, Salt Lake City, UT, Sept. 19-22 2000. Institute of Navigation.

- B. Schaffrin. Reliability measures for correlated observations. *Journal of Surveying Engineering*, 123(3):126–137, Aug. 1997.
- A. Sisodia, J. Hota, N. Vora, A. Siddiqui, H. Sanandiya, and S. Bera. Indian plan for satellite-based navigation systems for civil aviation. In *Proc. ION GPS 2003*, pages 2795–2811, Portland, OR, Sept. 9–12 2003. Institute of Navigation.
- S. Skone, V. Hoyle, and A. Coster. WAAS performance under increased ionospheric conditions. In *Proc. ENC GNSS 2004, The European Navigation Conference*, Rotterdam, The Netherlands, May 16–19 2004. European Group of Institutes of Navigation.
- S. Soley, R. Farnworth, A. van den Berg, R. Kremers, J. Sanz, C. Macabiau, and A. Fonseca. The data collection network: EGNOS revealed. In *Proc. ENC GNSS 2004, The European Navigation Conference*, Rotterdam, The Netherlands, May 16–19 2004. European Group of Institutes of Navigation.
- Special ION Publication on RAIM. *Global Positioning System, Paper Published in NAVIGATION*, volume V. Institute of Navigation, Alexandria, VA, 1998. Redbook of RAIM.
- J. Spilker. Tropospheric effects on GPS. in *Global Positioning System: Theory and Applications, Vol. I*, B. Parkinson and J. Spilker and P. Axelrad and P. Enge (Eds.), pages 517–546, 1996. American Institute of Aeronautics and Astronautics.
- SPS. GPS SPS performance standard, 2001.
URL <http://www.navcen.uscg.gov/gps/geninfo/2001SPSPerformanceStandardFINAL.pdf>.
- G. Strang and K. Borre. *Linear Algebra, Geodesy, and GPS*. Wellesley-Cambridge Press, Wellesley, MA, 1997.
- M. A. Sturza. Navigation system integrity monitoring using redundant measurements. *NAVIGATION, Journal of the Intitute of Navigation*, 35(4):69–87, Winter 1988.
- J. Syrjärinne. *Studies of Modern Techniques for Personal Positioning*. PhD thesis, Tampere University of Technology, Tampere, Finland, 2001.

- P. J. G. Teunissen. Quality control in integrated navigation systems. In *Proc. IEEE Position, Location and Navigation Symposium*, pages 158–165, Las Vegas, UT, March 20-23 1990. IEEE.
- P. J. G. Teunissen. Quality control and GPS. in *GPS for Geodesy, 2nd Edition.*, P.J.G. Teunissen and A. Kleusberg, Eds., Springer, New York, NY, pages 271–318, 1998.
- C. C. J. M. Tiberius. Quality control in positioning. *Hydrographic Journal*, 90(10): 3–8, Oct. 1998.
- H. Tomita, M. Harigae, and K. Hoshinoo. Flight evaluation of GPS-aided inertial navigation avionics with MSAS augmentation (MSAS-GAIA). In *Proc. ION GPS 2003*, pages 2819–2827, Portland, OR, Sept. 9-12 2003. Institute of Navigation.
- US Naval Observatory. Current GPS constellation, Oct. 2004. URL <http://tycho.usno.navy.mil/gpscurre.html>.
- A. J. van Dierendonck, P. Fenton, and T. Ford. Theory and performance of narrow correlator spacing in a GPS receiver. *NAVIGATION, Journal of The Institute of Navigation*, 39(3):265–283, Fall 1992.
- F. van Diggelen. GPS accuracy: Lies, damn lies, and statistics. *GPS World*, pages 41–45, Jan. 1998.
- F. van Diggelen. Indoor GPS: Wireless aiding and low signal strength detection. NAVTECH Seminar Course Notes, San Diego, CA, March 2001.
- F. van Diggelen. Indoor GPS theory and implementation. In *Proc. IEEE Position, Location, and Navigation Symposium*, pages 240–247, Palm Springs, CA, Apr. 15-18 2002. IEEE.
- F. van Diggelen and C. Abraham. Indoor GPS, the no-chip challenge. *GPS World*, 12(9):50–58, Sept. 2001.
- T. Walter and P. Enge. Weighted RAIM for precision approach. In *Proc. ION GPS 1995*, pages 1995–2004, Palm Springs, CA, Sept. 12-15 1995. The Institute of Navigation.
- J. Wang, M. P. Stewart, and M. Tsakiri. Stochastic modeling for static GPS baseline data processing. *Journal Surv. Eng.*, 124:171–181, Nov. 1998.

- T. Weber, H. Trautenberg, and C. Schäfer. GALILEO system architecture status and concepts. In *Proc. ION GPS 2001*, pages 1264–1273, Salt Lake City, UT, Sept. 11-14 2001. Institute of Navigation.
- D. Wells, N. Beck, D. Delikaraoglou, A. Kleusberg, E. Krakiwsky, G. Lachapelle, R. Langley, M. Nakiboglu, K.-P. Schwarz, J. Tranquilla, and P. Vanicek. *Guide to GPS Positioning*. Canadian GPS Associates, May 1987.
- A. Wieser. *Robust and Fuzzy Techniques for Parameter Estimation and Quality Assessment in GPS*. PhD thesis, Graz University of Technology, Graz, Austria, 2001.
- A. Wieser and F. K. Brunner. An extended weight model for GPS phase observations. *Earth Planets Space*, 52(10):777–782, 2000.
- A. Wieser, M. Petovello, and G. Lachapelle. Failure scenarios to be considered with kinematic high precision relative GNSS positioning. In *Proc. ION GNSS 2004*, pages 1448–1459, Long Beach, CA, USA, Sept. 21-24 2004. The Institute of Navigation.
- T. Zink, B. Eissfeller, E. Löhnert, and R. Wolf. Analyses of integrity monitoring techniques for a Global Navigation Satellite System (GNSS-2). In *Proc. ION AM 2000*, pages 117–127, San Diego, CA, June 26-28 2000. The Institute of Navigation.